AUTOMATIC TARGET DETECTION IN HYPERSPECTRAL IMAGES USING LEVEL SETS

by

Andres Alarcon Ramirez

A thesis submitted in partial fulfillment of the requirements for the degree of

MASTER OF SCIENCE
in
COMPUTER ENGINEERING

UNIVERSITY OF PUERTO RICO
MAYAGÜEZ CAMPUS
2009

Approved by:

_____	_____
Miguel A. Vélez Reyes , PhD Member, Graduate Committee	Date
_____	_____
Domingo Rodriguez, PhD Member, Graduate Committee	Date
_____	_____
Vidya Manian, PhD President, Graduate Committee	Date
_____	_____
Dorothy Bollman, PhD Representative of Graduate Studies	Date
_____	_____
Isidoro Couvertier Reyes, PhD Chairperson of the Department	Date

Abstract of Dissertation Presented to the Graduate School
of the University of Puerto Rico in Partial Fulfillment of the
Requirements for the Degree of Master of Science

AUTOMATIC TARGET DETECTION IN HYPERSPECTRAL IMAGES USING LEVEL SETS

By

Andres Alarcon Ramirez

July 2009

Chair: Vidya Manian

Major Department: Electrical and Computer Engineering

A novel variational method using level sets that incorporate spectral angle distance in the model for automatic target detection is presented. Algorithms are presented for detecting both spatial and pixel targets. The new method is tested in tasks of unsupervised target detection in hyperspectral images with more than 100 bands, and the results are compared with a widely used region-based level sets algorithm. In addition Texture and spectral information are incorporated into level set equation for extracting large targets placed on images The proposed method is also adapted for supervised target detection and its performance is compared with traditional orthogonal subspace projection and constrained

signal detector for the detection of pixel targets. The method is evaluated with different complexity such as noise levels and target sizes.

Resumen de disertación a la Escuela Graduada
de la Universidad de Puerto Rico como requisito parcial de los
Requerimientos del grado para Maestría en Ciencias

AUTOMATIC TARGET DETECTION IN HYPERSPECTRAL IMAGES USING LEVEL SETS

Por

Andres Alarcon Ramirez

Julio 2009

Consejero: Vidya Manian

Departamento: Ingeniería Eléctrica y de Computadores

Un novedoso método que utiliza Level set y que incorpora distancia espectral angular en la detección automática de objetivos es presentado. Distintos algoritmos fueron desarrollados para la detección de objetivos que tienen tamaño de pocos pixeles y otros de mayor tamaño. El nuevo método es probado en tareas de detección de objetivos no-supervisados en imágenes hiperespectrales con más de 100 bandas, y los resultados son comparados con otras técnicas de level set basadas en regiones que han sido ampliamente utilizadas. Adicionalmente información espectral y de textura es incorporada en la ecuación de level set para la extracción de objetos grandes situados en una imagen. El método propuesto es también adaptado para la detección supervisada de objetivos, y su rendimiento es comparado

con algoritmos de proyección del sub-espacio ortogonal y detección de señales restringidas para la detección de objetivos de pocos pixeles. El método es evaluado con diferentes niveles de ruido y tamaño de objetos.

To God
To the memory of my mother, you will always be in my heart
To my grandmother Carmen Rosa Ramírez
To my father Hernando Alarcon, for your support, friendship and love
To my family, the best gift that God gave me

ACKNOLEDGMENTS

I want to thank my advisor Dr. Vidya Manian for her support during my graduates studies. I would like to thank to the members of my graduate committee: Dr. Miguel Velez, Dr. Domingo Rodriguez. Thanks to the representative of graduate studies: Dr. Dorothy Bollman for her comments of thesis. Thanks to Samuel to went as substitute of Dr. Miguel Velez during my thesis defense.

I would like to thank Ms. Sandy Montalvo, you are a great woman, Thanks to the LARSIP and IRISE staff: Ms. Marie Ayala, Mr. Samuel Rosario, Mr. Victor Asencio, Ms. Maribel Feliciano, and Mrs. Vanessa Gutierrez. Also, I will like to thank all my friends (Andrés Velasco, Mariana Mendoza, John Sanabria, David Ortiz, Roberto Nuñez, Miguel Goenaga, Leidy Dorado and Nicolas Rey) and persons that were directly or indirectly involved in my life during the last 2 years.

Thanks to my family: my grandmother Carmen Rosa Ramirez, my father Hernando Alarcon, my brother John A. Ramírez, my aunts Luz Dary Alarcon and Noemí Ramírez for their support during the last 2 years.

This research work reported herein was funded primarily by the Bernard M. Gordon Center for Subsurface Sensing and Imaging Systems, under the Engineering Research Centers Program of the National Science Foundation (Award Number EEC-9986821).

Table of Contents

Table List

Tables **Page**

Figure List

Figures **Page**

List of Abbreviations

HSI	Hyperspectral Imagery
HYDICE	Hyperspectral Digital Imagery Collection Experiment
PCA	Principal Component Analysis
LARSIP	Laboratory for Applied Remote Sensing and Image Processing
SAD	Spectral Angle Distance
ROC	Receiver Operating Characteristic
OSP	Orthogonal Subspace Projection
ICA	Independent Component Analysis
CSD	Constrained Signal Detector
CMK	Constrained Kurtosis Maximization
CLS	Constrained Least Squares

List of Symbols

m	meters
nm	nanometers

1 INTRODUCTION

Hyperspectral images are characterized by hundreds of narrow and contiguous spectral bands; they have been successfully used for tasks of material identification, material mapping and target detection, mainly because they provide information necessary for more detailed image analysis. Automatic Target Detection/Recognition (ATR/D) algorithms try to locate both known and unknown objects in an image. Generally the sizes of the targets are considerably less than the background. ATR/D methods are applied in the areas of defense, security, sensing, biomedical and surveillance.

Three different approaches for target detection are defined in [20]. In the first, the spectral composition of the observed pixels (full pixels or mixed pixels) is taken into account; the second approach involves mainly adaptive matched filters which locate spectral targets by modeling scene background as either structured (geometric) with a set of end members (basis vectors) or as unstructured (stochastic) with a covariance or correlation matrix; the algorithms that belong to the last approach uses the available a priori information about target or background classes. Some of them are based on projection pursuit methodologies [19] to determine automatically the low-dimensional projections of such data sets that best highlight the interested target in an image.

Level set is a relatively new technique used widely for segmentation of both gray scale and color images. In [1] level set is used together with best band analysis (BBA) to classify hyperspectral

images of urban and rural nature. In [2] a semi-automated supervised hyperspectral image segmentation algorithm using level set is presented. However, this method has not been applied for target detection.

The classic models for level sets have been focused on either region-based approaches or edge-based approaches. This work explores both spatial and spectral information for target detection in hyperspectral images.

The proposed algorithm for target detection could have a wide use in defense due it can be applied for detecting military targets remotely. Additionally the proposed algorithm can be easily adapted for anomalies detection in biomedical images, which is very useful in an early diagnosis of several types of cancer.

1.1 Objectives

The main objectives of this work are as follows:

- Adapt the technique of level set for detection of both small and large targets.
- Detection of multiple targets in an image.
- Incorporate spectral angel distance (SAD) to the level set evolution equation to couple the spectral information presents in hyperspectral images. Use other spatial information such as texture for eliminating false alarms and increasing detection rate.
- Validate the algorithm in both synthetic and remote sensing images.
- Compare the performance of the proposed algorithm with other techniques used for target detection.

1.2 Contributions of this work

The main contribution of this work can be viewed as the following:

- A modified level set model which can be used in hyperspectral images by using both spectral and texture information for target detection task.
- A supervised and unsupervised method for target detection in hyperspectral image which incorporates level set.
- An evaluation of the proposed algorithm with different target/background image scenarios.

1.3 Thesis Overview

This Thesis is organized as follow, Chapter II presents the state of the art of target detection algorithms and a level sets approach, Chapter III describes both the algorithm for large target detection using spectral and texture information and the algorithm for small target detection. In addition an unsupervised target detection methodology for detecting multiple targets by using level sets and texture features is presented, Chapter IV presents results and their discussion, finally Chapter V presents conclusions and future work.

2 LITERATURE REVIEW

2.1 Hyperspectral Images

In recent years the capability of generating hyperspectral images with several spectral bands has increased. In addition hyperspectral imagers offer high spectral resolution that allows recovering important characteristics of distinct objects placed on the scene of interest. The basic principle is that objects reflect, absorb, and emit electromagnetic radiation in ways characteristic of their molecular composition and shape. The spatially and spectrally sampled information is typically visualized as a cube, whose face is a function of the spatial coordinates and whose depth is a function of spectral band (See Fig. 2.1).

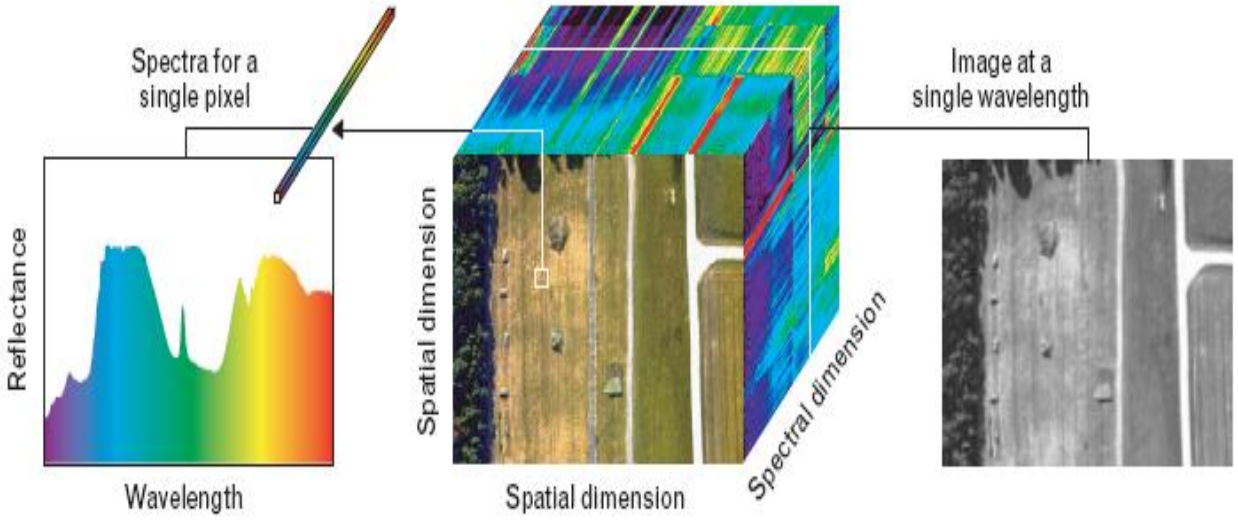

Figure 2.1 Characteristics of Hyperspectral Image. Image Courtesy [20].

In the wavelength dimension, each image pixel is a vector that provides a spectrum characterizing the materials within the pixel. Conversely, the data in each band corresponds to a narrow band image of the surface covered by the field of view of the sensor. This has lead to numerous applications, especially in the recognition of materials spread out over the Earth's surface and target detection.

2.2 Target Detection

Target detection can be studied from two different ways: unsupervised and supervised target detection, the first one is known as well as anomaly detection and it refers to extract pixels in the image that are different from all other pixels. Supervised target detection attempts to locate pixels containing a material of known spectral composition. Target detection has many applications, including military reconnaissance and environmental studies. Searching for the presence of a specific material over a large area poses many practical difficulties. The prospect of using remotely sensed HSI to perform this task in an accurate and timely manner has driven the research community to generate many different types of target detection algorithms.

2.3 Target detection algorithms

In [3] Shao-Shan and Chein have proposed an unsupervised method using Projection Pursuit, in which the original data is projected to another space conserving its most important characteristics. The target is viewed as an "outlier" of the background distribution due to the fact that small objects in a background can be regarded as anomalies in an image. The third and fourth moments (Skewness and Kurtosis) are used for the projection due to their ability to measure outliers. Similar

approximation was done by Robila and Varshney [4], using Independent Component Analysis (ICA) instead of Projection Pursuit. It transforms the mixed signals into components that are mutually independent that allow to recover a target from the background. A Faster algorithm (FastICA) was proposed in [27], which results in better results in terms of accuracy and computational complexity.

Traditional supervised subspace projection methods use the concept of mixed pixels in hyperspectral images, where the spectral signature of materials that constitute both the target and the background are defined beforehand. Orthogonal Subspace Projection (OSP) is one of the first techniques that could separate the desired target signature from the undesired background signature by a linear model [5] that define a pixel r according to the following equation,

$$r=d\alpha_p+U\gamma+n \qquad (2.1)$$

where *d* is the target material spectrum of *L* dimensions, *U* is a matrix of size *LxP* which represents the background spectrum of *P* materials present in it, n is the stochastic noise vector; α_p is the proportion of the target material that is present in the pixel r, in the same way γ is a vector which have the contributions of different materials that constitute the background. The terms α_p are determined by the following equation,

$$\alpha_p = \frac{d^T * P_U^\Gamma * r}{d^T * P_U^\Gamma * d} \qquad (2.2)$$

Where P_U^Γ is defined as,

$$P_U^{\Gamma} = I - U\left(U^T U\right)^{-1} U^T \tag{2.3}$$

A threshold is used to determine the amount of material in a pixel (abundance), based on which the target class is assigned to that pixel. Another method called Constrained Signal Detector (CSD) has been used in target detection and abundance estimation, mainly when there is a background with only one type of material. Gaussian noise is assumed here as in OSP, but CSD is derived using CLS (Constrained Least Squares) or constrained maximum-likelihood estimates of the target abundance [6] in the generalized likelihood ratio test. The factor α_p that determine the abundance of a material is defined by the following equation,

$$\alpha_p = \frac{Cu^T * Cu * d^T * P_U^{\Gamma} * r * \left(1 - Cu^T * d\right) * \left(1 - Cu^T * r\right)}{Cu^T * Cu * d^T * P_U^{\Gamma} * d + \left(1 - Cu^T * d\right)^2} \tag{2.4}$$

Where the term P_U is determined by the Equation (2.3) and C_U is given by,

$$C_U = U(U^T U)^{-1} 1 \tag{2.5}$$

In [25] constrained kurtosis maximization (CMK) is used for automatic target detection in hyperspectral images. The background is modeled as Gaussian distribution and targets correspond to the deviation of the distribution by using an optimization technique based in the fourth central moment that measures the flatness of a distribution and modeling the targets as anomalies that

commonly have a small size and occupies only a few pixels. The CMK is compared with unconstrained kurtosis maximization algorithm and the first one result in a higher detection rate and can recover smaller targets.

In [28] a hybrid method for target detection is used, when the target size is smaller than a pixel; the authors present a technique that is based on spectral information using statistical and physics-based approaches.

Spectral Matched filters are introduced in [31] for target detection in hyperspectral imagery by using target signature and background clutter covariance matrix. The goal is to design a linear filter with coefficients that minimizes the filter output energy subject to constraints.

The idea of kernel-based learning and matched subspace detection filters are combined in [13][30] to develop a new nonlinear subpixel target detection method for hyperspectral imagery . They use the fact that performing matched filtering in a non-linear feature space of high dimensionality increases the probability of getting better results.

The idea of regularization is incorporated in matched filters for target detection in hyperspectral imagery in [29]. The regularization smoothes the coefficient of the filter and forces it to become more stable and have better performance than non-regularized adaptive spectral matched filters.

2.4 Variational Level Set methods

Level set was used in images for first time by Malladi [10] to solve the problem of shape recovery; it places a closed, hypersurface inside (or outside) of the object of interest. The hypersurface is defined as.

$$\phi(x,y)=\begin{Bmatrix} 0 & (x,y)\in S \\ -D(x,y,S) & (x,y)\in R_1 \\ D(x,y,S) & (x,y)\in R_2 \end{Bmatrix} \tag{2.6}$$

Where *D((x, y), S)* computes the minimum Euclidean distance between the grid pixel *(x, y)* and the shape contour *S*, R_1 and R_2 are the region inside and outside of the shape contour respectively. The shape contour S is represented generally by circles; however other geometric shapes can be used (rectangles, triangles, etc). The graphical representation of ϕ(x, *y*) is showed in the following Figure.

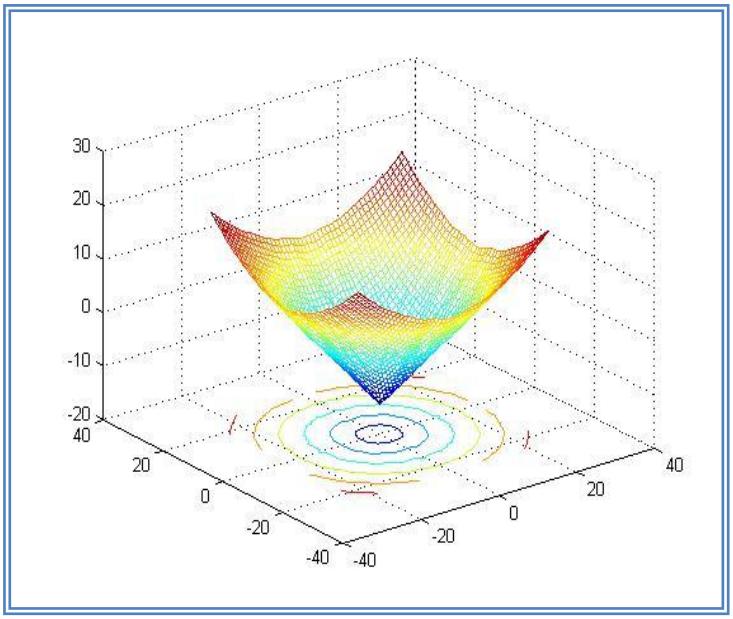

Figure 2.2 Level Set Surface

The surface ϕ (x, y) follows an equation of difference that is defined as.

$$\frac{\partial \phi(x,y)}{\partial t} = \left\{ \left(k(\phi(x,y)) + \nu \right) * g(I(x,y)) * \left| \nabla \phi(x,y) \right| \right\} \tag{2.7}$$

Where ν is a constant used to accelerate the evolution speed, g is a unique parameter that depends on the image itself, in addition it denotes a stopping function, i.e. a positive and decreasing function of the image gradient and is given by the following equation.

$$g(I)(x,y) = \frac{1}{1 + \left| \nabla G_{\sigma} * I(x,y) \right|^{d}} \tag{2.8}$$

The term $\nabla G_{\sigma} * I(x,y)$ is the gradient applied to the smoothed image with a Gaussian filter of standard deviation σ. $K(\cdot)$ denotes the mean curvature of the level set function $\phi(x,y)$ and is given by,

$$K(\phi(x,y)) = div\left(\frac{\nabla \phi(x,y)}{\left| \nabla \phi(x,y) \right|} \right) \tag{2.9}$$

The curvature term k (·) maintains the regularity of the contours, while the constant term v accelerates and keeps the contour evolution by minimizing the enclosed area. The hypersurface is updated according to the following equation,

$$\phi = \phi + \Delta t * \frac{\partial \phi}{\partial t} \tag{2.10}$$

The procedure described above is repeated many times until an object is encircled. The boundary at any time is located at $\phi(x, y) = 0$.

This hypersurface flows along its gradient field with a speed *F (K),* where *K* is the curvature of the hypersurface. Unknown shapes are recovered by making the front adhere to the object boundaries.

The use of Level Set in multi-spectral images has been investigated by Sarpio [9], where the function *g(I (x,y))* is replaced for the following one:

$$g\left(I(x, y)\right) = \frac{1}{1 + \left(\lambda_{+} - \lambda_{-}\right)} \tag{2.11}$$

λ_{+} and λ_{-} are the matrixes with the maximum and minimum *eigenvalues* respectively, calculated by the following expression:

$$\begin{bmatrix} g_{11} & g_{12} \\ g_{21} & g_{22} \end{bmatrix} = \sum_{b} \begin{bmatrix} \left(\frac{\partial I_b}{\partial x}\right)^2 & \left(\frac{\partial I_b}{\partial y} * \frac{\partial I_b}{\partial x}\right) \\ \left(\frac{\partial I_b}{\partial x} * \frac{\partial I_b}{\partial y}\right) & \left(\frac{\partial I_b}{\partial y}\right)^2 \end{bmatrix} \tag{2.12}$$

where I_b denotes the *b-th* band of the multispectral image *I(x, y)*. In the case of gray scale images, $\lambda_+ = |\nabla I|$ and $\lambda_- = 0$, so the stopping function shown in Equation (2.11) become identical to Equation (2.8).

Other modifications to the original evolution equation were presented by Chunming [10] as follows.

$$\frac{\partial \phi}{\partial t} = \left\{ \mu \left[\Delta\phi - div\left(\frac{\nabla \phi}{|\nabla \phi|} \right) \right] + \lambda * \delta(\phi) * div\left(g * \frac{\nabla \phi}{|\nabla \phi|} \right) + \nu * g * \delta(\phi) \right\} \tag{2.13}$$

Where $\Delta\phi$ is the Laplacian operator , and μ, λ, ν; are constants. $\delta(\phi)$ Is the Dirac function given by the following equation.

$$\delta(x) = \begin{Bmatrix} 0, & if & |x| \rangle \varepsilon \\ \frac{1}{\varepsilon}\left[1 + \cos\left(\frac{\pi x}{\varepsilon} \right) \right], & if & |x| \le \varepsilon \end{Bmatrix} \tag{2.14}$$

In Equation (2.13) the second and third terms are responsible for bringing the level set surface towards the object's borders whereas the first one determines the shape the surface takes.

Aiming to use image texture information, *Chan* and *Vese* [14] proposed a piecewise-constant technique that moves deformable contours presented in the level set surface by minimizing the energy function instead of searching for edges. The energy function measures the difference between

the piecewise-constant and the actual image intensity at every image pixel. The level set evolution equation is given by,

$$\frac{\partial \phi}{\partial t} = \{\delta_\varepsilon(\phi(x,y))[\nu * K(\phi(x,y)) - \{(I(x,y)-\mu_1)^2 - (I(x,y)-\mu_2)^2\}]\} \quad (2.15)$$

where μ_0 and μ_1 respectively denote the mean of the image intensity within the two subsets, i.e. the outside and inside of contours.

In [15] a level set model minimizing an energy criterion involving both region and boundary functional is proposed. These functionals are derived through a shape derivative approach instead of classical calculus of variation.

Other techniques use probability in the evolution function of level set [16][17], as the following equation shows,

$$\frac{\partial \phi}{\partial t} = \left\{\delta_\varepsilon(\phi(x,y))\left[\nu * div\left(\frac{\nabla \phi}{|\nabla \phi|}\right) + \log\left(\frac{p_1(I(x,y)\mid\{\mu_1,\Sigma_1\})}{p_2(I(x,y)\mid\{\mu_2,\Sigma_2\})}\right)\right]\right\} \quad (2.16)$$

where $p_1(u(x,y)|\{\mu_1,\Sigma_1\})$ and $p_2(u(x,y)|\{\mu_2,\Sigma_2\})$ are the probability density function that a pixel placed location (x,y) is inside or outside the border respectively.

The probability density function is a multidimensional Gaussian normal density with mean *u* and covariance σ. To apply this technique to multiband images, we assume independence between every band such that.

$$p_i\left(u\left(x,y\right)\right)=\prod_{b=1}^{B}p_{b,i}\left(u_b\left(x,y\right)\right) \tag{2.17}$$

where B represents the number of bands that constitute the image.

Applying logarithm to the probabilities in Equation (2.16) gives,

$$e_i\left(x,y\right)=-\log\left(p_i\left(u(x,y)\mid\{\mu_i,\Sigma_i\}\right)\right)\approx\log\left(\Sigma_i\right)+\left(u\left(x,y\right)-\mu_i\right)^Y\Sigma_i^{-1}\left(u\left(x,y\right)-\mu_i\right) \tag{2.18}$$

This represents the Mahalanobis distance, which can be replaced in Equation (2.16) as shown below,

$$\frac{\partial\phi}{\partial t}=\left\{\delta_\varepsilon\left(\phi(x,y)\right)\left[\nu*div\left(\frac{\nabla\phi}{|\nabla\phi|}\right)-\{e_2(x,y)-e_1(x,y)\}\right]\right\} \tag{2.19}$$

Level set has been used successful in both de-noising and segmentation of gray and color images [7][8][9], there are a few works that have been made use of it in hyperspectral images. [33] Presents a supervised hyperspectral classification procedure that applies Distance-Based Segmentation along with Best-Band Analysis (BBA) to subsequently use level set in order to smooth a surface of

classification and make it more homogenous. Two hyperspecteral images of urban and rural environments are used for classification.

In [23] both Level Set and Gabor filter are used for textures segmentation, the Gabor filter is applied to the image to transform it into a new space and then level set is applied to extract object placed into images. In addition several scales and orientations are used for Gabor filter; the results show that combining boundary and region information yields more robust and accurate texture segmentation results.

Level Set have been used with others techniques for image classification task [32]. For instance Wavelet transform and level set are used for supervised classification of grayscale images. The Wavelet transform is used to characterize texture. Then the level set uses this information to encircle the object to be classified.

The Kullback-Leibler divergence which is a similarity measure between distributions was used instead of Euclidean distance in the level set equation [24]. This approximation was applied for unsupervised texture segmentation in gray scale images.

This work involves modification of Equation (2.19) and adapting it for unsupervised and supervised target detection in hyperspectral images incorporating spatial and spectral information.

3 Automatic Target Detection Methods

3.1 Hyperspectral Data

The problem of target detection is treated from two perspectives: supervised and unsupervised target detection. In the first case a set of images captured by SOC700-VS camera with a spectral resolution of 2nm for a wavelength range from 400 nm to 1000 nm is used. The sizes of the images are of 97 by 183 pixels and 120 bands. The image is composed of background and target, the target pixel is mixed with the background according to the following equation [18].

$$f(x_1, x_2) = \alpha * T + (1-\alpha) * B + n \qquad (3.1)$$

where α is the fractional mixing level, T is the target signature, B is the background signature and *n* is the zero mean Gaussian noise. Images with targets of 1 pixel, 9 and 16 pixels are generated with several values of α. The same procedure will be developed with hyperspectral images capture for a remote sensor.

In the same way for unsupervised target detection is constituted a set of synthetic image captured by SOC700-VS camera, with distinct geometric figures on a background. The image size is 276 by 155 pixels with 120 bands. In addition some available hyperspectral images with target of several pixels will be taking into account for evaluating the performance of the proposed algorithms. The targets

compose of pure pixels are named as large targets, whereas the targets mixed with background information are named as small targets or subpixels [39], therefore different methodologies are developed for resolving these issues.

3.2 Unsupervised target detection methodology

The unsupervised target detection algorithm is presented as a block diagram in Figure 3.1.

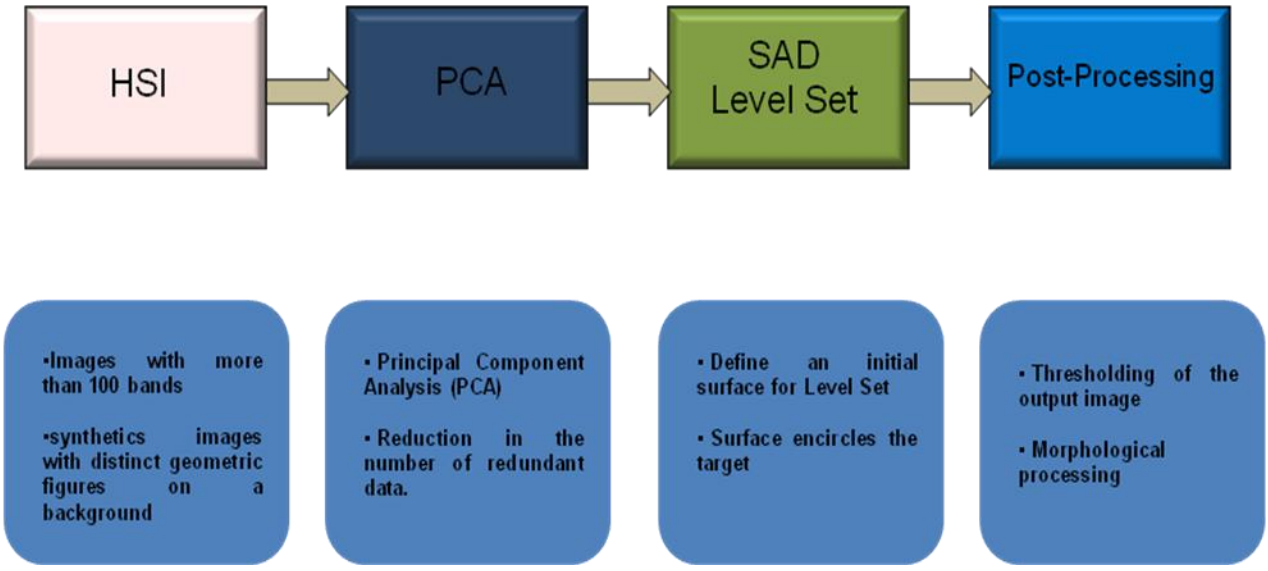

Figure 3.1 Block diagram for unsupervised target detection algorithm

The algorithm for automatic target detection is composed of three steps. In the first one the dimensionality of the input hyperspectral image is reduced by a technique of band subset selection like principal component analysis which transforms the original data to other subspace of less dimensionality, where the data is more uncorrelated.

In the second step, the level set technique is applied to the reduced data with the idea of encircling the target of interest. The spectral angle distance (SAD) is used instead of the Mahalanobis distance

in the level set evolution equation (2.19). The SAD between two vectors (r_i, rj) is defined by the following equation,

$$SAD(r_i, r_j) = \cos^{-1}\left(\frac{r_i . r_j}{|r_i| * |r_j|}\right) = \cos^{-1}\left(\sum_{t=1}^{N} r_{it} * r_{jt} \Big/ \left(\sum_{t=1}^{N} r_{it}\right)^{1/2} \left(\sum_{t=1}^{N} r_{jt}\right)^{1/2}\right) \quad (3.2)$$

where *N* represents the size of the vector. Introducing Equation (3.2) into Equation (2.19), we get the following equation,

$$\frac{\partial \phi}{\partial t} = \left\{\delta_{\varepsilon}(\phi(x,y))\left[\nu * div\left(\frac{\nabla \phi}{|\nabla \phi|}\right) - \beta\left\{\cos^{-1}\left(\frac{I(x,y,z).u_2}{|I(x,y,z).| * |u_2|}\right) - \cos^{-1}\left(\frac{I(x,y,z).u_1}{|I(x,y,z).| * |u_1|}\right)\right\}\right]\right\} \quad (3.3)$$

where, u_2 represents the mean vector of the pixels inside of the region defined by ϕ (*t*, *x*, *y*) is 0, u_1 represents the mean vector of the pixels outside of the region defined by ϕ (*t*, *x*, *y*) is 0, β is a constant that defined the speed of convergence of the surface ϕ (*t*, *x*, *y*). The new differential equation avoids calculating the inverse matrix that is necessary in Equation (2.19) and also allows the coupling of the information present in the different bands more efficiently.

3.2.1 Unsupervised target detection using texture and spectral information.

Texture features are calculated from the hyperspectral image with the purpose of improving the performance of the algorithm, and then replacing in the Equation (3.3) every pixel of the image *I(x,y)* by the set of features calculated for every pixel. The SAD can be calculated directly on the image using its spectral information; however a set of features which are extracted from the original image are used in Equation (3.3) with the purpose of recovering not only spectral but also texture information, in that way the original image is replaced by feature images.

Several texture features are widely used in segmentation and classification task [35] [36], in this work 15 features are selected, 3 of which are of edges detection, and the remainder of texture. The features selected are the followings:

Entropy: It measures the information content in a probability distribution. The data is modeled as a Gaussian distribution such that it is normalized with a mean of 0 and a standard deviation of 1.

$$Entropy = -\sum_i \sum_j M(i, j) * \log(M(i, j)) \tag{3.4}$$

where *M(i,j)* represents the norm of the pixel in (x,y) coordinates.

Inverse Difference Moment: IDM is the measure of local homogeneity.

$$IDM = \sum_i \sum_j \frac{M(i, j)}{1 + (i - j)^2} \tag{3.5}$$

Skewness: It measures the asymmetry of a probability distribution.

$$\gamma_3 = \frac{\sum_i \sum_j (X(i,j) - \bar{X})^3}{(N-1)\sigma^3} \tag{3.6}$$

Where $\bar{X}$ represents the mean vector, N is the number of pixels in the windows to be considered.

The former equation was modified to be used in Hyperspectral image:

$$\gamma_{HSI\_3} = \frac{\sum_i \sum_j SAD(X(i,j), \bar{X})^3}{(N-1)\sigma_{SAD}^3} \tag{3.7}$$

where SAD represents the spectral angle distance between two vectors, and σ_{SAD} is given by:

$$\sigma_{SAD} = \sqrt{\frac{\sum_i \sum_j SAD(X(i,j), \bar{X})^2}{N}} \tag{3.8}$$

Kurtosis: It is the normalized fourth order moment and is a measure of the heaviness of the tails in a distribution.

$$\gamma_4 = \frac{\sum_i \sum_j (X(i,j) - \bar{X})^4}{(N-1)\sigma^4} - 3 \tag{3.9}$$

The SAD was incorporated in Equation (3.9) to be used in Hyperspectral Images, as shown in the following equation:

$$\gamma_{4\_SAD} = \frac{\sum_i \sum_j SAD(X(i,j), \bar{X})^4}{(N-1)\sigma_{SAD}^3} - 3 \tag{3.10}$$

Eighth moments is given by:

$$m_{pq} = \sum_i \sum_j M(i,j) * i^p * j^q \tag{3.11}$$

Where $0 \le p \le 2$ and $0 \le q \le 2$, *M(i,j)* represents the norm of the pixel in (x,y) coordinates.

The features used for edge detection are listed in the following table.

Table 3.1 Edge feature calculated in Hyperspectral images.

Feature for edge detection	Features to be used in Hyperspectral Images
Average deviation of gradient magnitude: $f_1 = \left[\frac{1}{n_1 n_2} \sum_{i=1}^{n1} \sum_{j=1}^{n2} \lvert X(i,j) - X(i+1,j) \rvert + \lvert X(i,j) - X(i,j+1) \rvert \right]$	Average deviation of gradient magnitude for HSI: $f_{SAD\_1} = \left[\frac{1}{n_1 n_2} \sum_{i=1}^{n1} \sum_{j=1}^{n2} SAD\big(X(i,j), X(i+1,j)\big) + SAD\big(X(i,j), X(i,j+1)\big) \right]$
Average deviation of the vertical directional	Average deviation of the vertical directional residual

residual: $f_2 = \left[\frac{1}{n_1 n_2} \sum_{i=1}^{n1-1} \sum_{j=1}^{n2} \left| X(i,j) - \begin{pmatrix} X(i-1,j)+ \\ X(i+1,j)/2 \end{pmatrix} \right| \right]$	for HSI: $f_{SAD\_2} = \left[\frac{1}{n_1 n_2} \sum_{i=1}^{n1-1} \sum_{j=1}^{n2} SAD\left(X(i,j), \begin{pmatrix} X(i-1,j)+ \\ X(i+1,j)/2 \end{pmatrix} \right) \right]$
Average deviation of the horizontal directional residual: $f_3 = \left[\frac{1}{n_1 n_2} \sum_{i=1}^{n1} \sum_{j=1}^{n2-1} \left| X(i,j) - \begin{pmatrix} X(i,j-1)+ \\ X(i,j-1)/2 \end{pmatrix} \right| \right]$	Average deviation of the horizontal directional residual for HSI: $f_{SAD\_3} = \left[\frac{1}{n_1 n_2} \sum_{i=1}^{n1} \sum_{j=1}^{n2-1} SAD\left(X(i,j), \begin{pmatrix} X(i,j-1)+ \\ X(i,j-1)/2 \end{pmatrix} \right) \right]$

The spectral information of every pixel is replaced by 15 features which are calculated by masks of sizes 3x3 that are moved through the image, the block diagram can be seen in the following image.

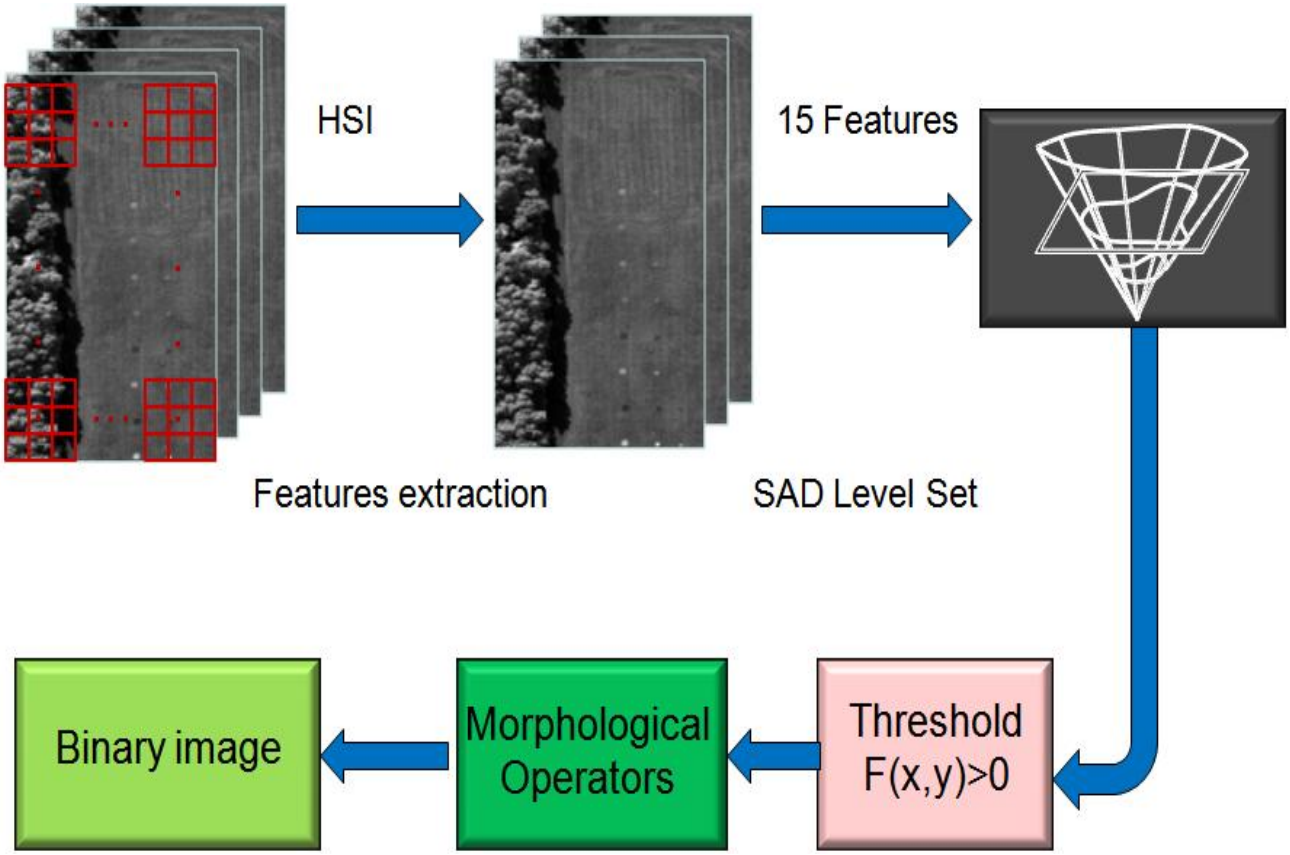

Figure 3.2 Block diagram for unsupervised target detection algorithm using texture information

Level Set is applied to the new images to generate a binary image where the target is extracted from the background, firstly a threshold to zero is applied to the matrix defined by ϕ (t, x, y), where the negative values determine the background and the positive ones the target, the zero positions define the borders between the target and the background.

Additionally, morphological operations are used to eliminate small regions that are wrongly detected by the level set technique. There are two basic morphological operators: dilation and erosion. A

function ***f*** represents the image; *N* is the structuring element, and *N*z the translation of the set *N* by a point **z**. The morphological erosion of ***f*** by *N* and dilation is defined by the following equation,

$$Erosion = \{z : N_z \subseteq f\} = \bigcap_{y \in N} f_{-y}$$

$$Dilatation = \{z : (N_z \cap f) \neq \phi\} = \bigcup_{y \in N} f_{-y} \quad (3.12)$$

The combination of erosion and dilation constitute opening (erosion followed by dilatation) and closing (dilation followed by erosion) which are applied for eliminating false detections.

The proposed algorithm can be summarized by the followings steps:

Step 1) Calculate the texture and spatial features on HSI. A set of Masks of 3x3 are move through the image for calculating texture information. The hyperspectral information is transformed to a new data set where the bands of the image are replaced by 15 texture features.

Step 2) Applying SAD-Level set to the image of features. The level set surface encircles the objects present in the new data set; it evolves through time by using the equation 3.3.

Step 3) Creating a binary image for extracting the positions in level set surface with negative values. The positions where the matrix that represents the level set surface are negative will be set zero, whereas the positions with positive values will be set one.

Step 4) applying morphological operator to the binary image generated in the former step. Apply the erosion operator followed by a dilation operation in the binary image to eliminate small artifacts.

3.2.2 Algorithm for anomalies detection

Automatic target detection can be seen as anomalies detection in some applications where the targets occupy a few pixels in an image, in this work a new methodology which incorporate Level Set and others techniques to extract automatically small targets in an image is proposed. This methodology can be seen in the following image.

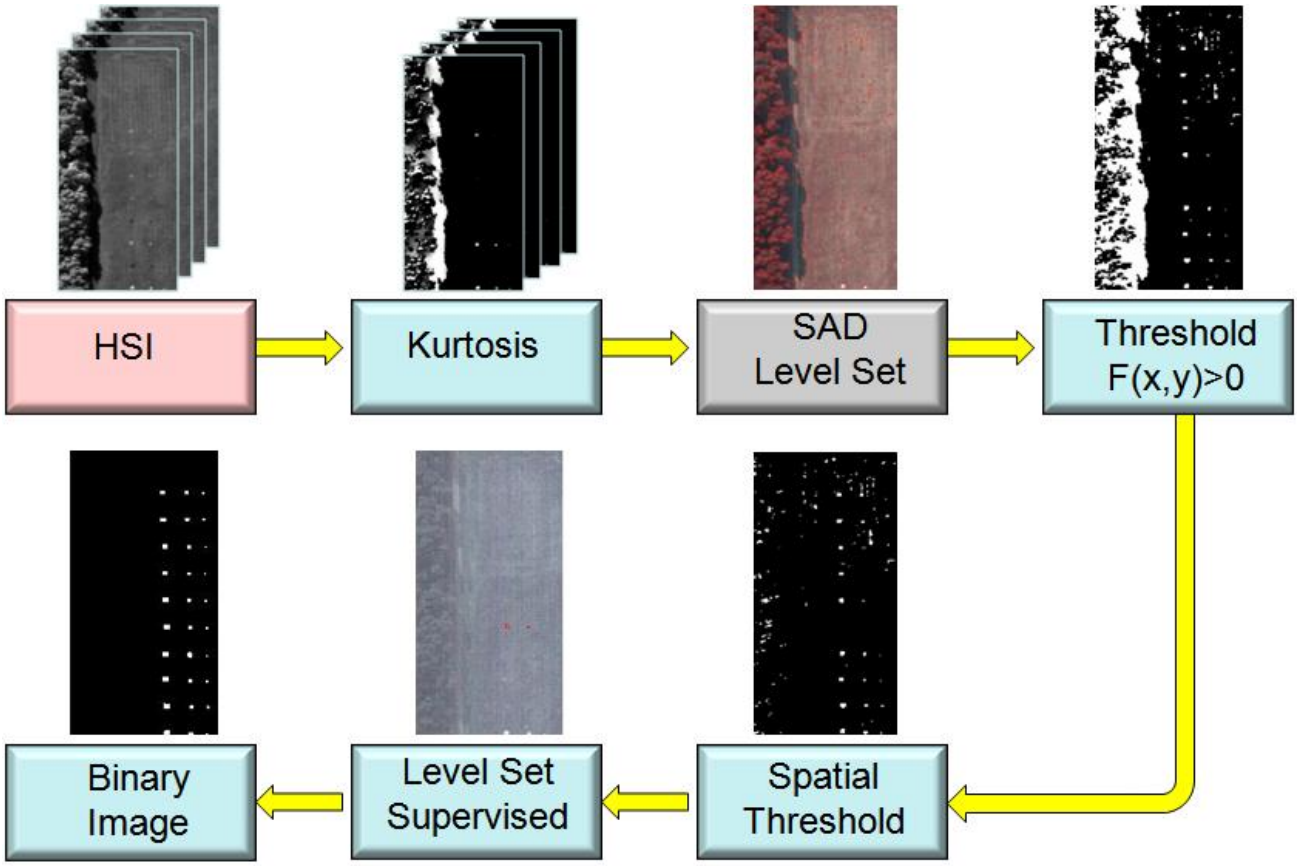

Figure 3.3 Block diagram for unsupervised algorithm of small targets

Kurtosis has been used widely in target detection [3][25], mainly because of its properties to enhance pixels whose values are far from the mean value of all pixels belonging to the image.

Kurtosis is calculated on HSI to generate a new image of the same size as the original image but with the characteristics previously mentioned.

SAD-Level Set is used to extract the targets in the new image that is produced by applying the Kurtosis operator. Then the pixels whose positions on the Level set surface ϕ (t, x, y) have negative values are labeled as background whereas the pixels with positive values are recovered in a new binary image as possible targets. The extracted pixels are grouped with all possible pixels recovered that are connected by their nearest eight-neighbors.

In the groups of pixels recovered not only are the targets but also some objects of small and large size that belong to the background (false positives), that is presented mainly in images whose background is not uniform and where there are distinct materials. Therefore a post-processing step is necessary to eliminate false positives. The objects of large size are eliminated by thresholding the number of pixels that constitute the distinct groups recovered, due to the fact that the size of targets generally are of a few pixels.

The small objects that are not targets are eliminated by using level set in its supervised manner. The average spectral signature of all the pixels that constitute a specific group is passed to level set. For each group level set on the image is applied to recover the pixels that are spectrally closer to the spectral signature of a particular group. Then a binary image with the objects extracted is generated. Only the groups whose binary images have objects of small size are recovered and labeled as targets. The proposed algorithm can be summarized by the followings steps:

Step 1) Set ε and β. The parameter ε is an integer that represents the larger target (number of pixels) that can be detected by proposed algorithm, in the same way the parameter β is an estimation of the amount of pixels that belong to a particular type of target.

Step 2) Calculate Kurtosis on HSI using (16). The hyperspectral information is transformed to a new data set where the targets are highlighted. Kurtosis is a feature used widely for enhancing the outliers in a data set.

Step 3) Applying SAD-Level set to the image generated after applying kurtosis operator. The level set surface encircles the targets present in the new data set; it evolves through time by using the equation 3.3.

Step 4) Generating a binary image by extracting the position in level set surface with negative values. The positions where the matrix that represents the level set surface are negative will be set zero, whereas the positions with positive values will be set one.

Step 5) Grouping pixels in the binary image by using their nearest eight-neighbors. The positions in the binary image with values of zero are discarded; whereas the pixels with values of one are grouped with those pixels that are especially connected in the binary image.

Step 6) for each group do, if the size of group> ε, discard group, otherwise recover it in another binary image. The groups that fulfill the former condition are recovered in a binary image, whereas the others are discarded.

Step 7) For each group recovered in the former step, calculate its average spectral signature, and passing it to level set to be applied on HIS in a supervised manner. The supervised level set

algorithm is applied to the whole hyperspectral image for generating a binary image, in that way for each groups of pixels previously extracted a binary image is generated.

Step 8) if the number of pixels extracted in the former step is larger than β, discard pixels, otherwise label them as targets.

3.3 Supervised target detection methodology

The supervised target detection algorithm is presented as a block diagram in Figure 3.4.

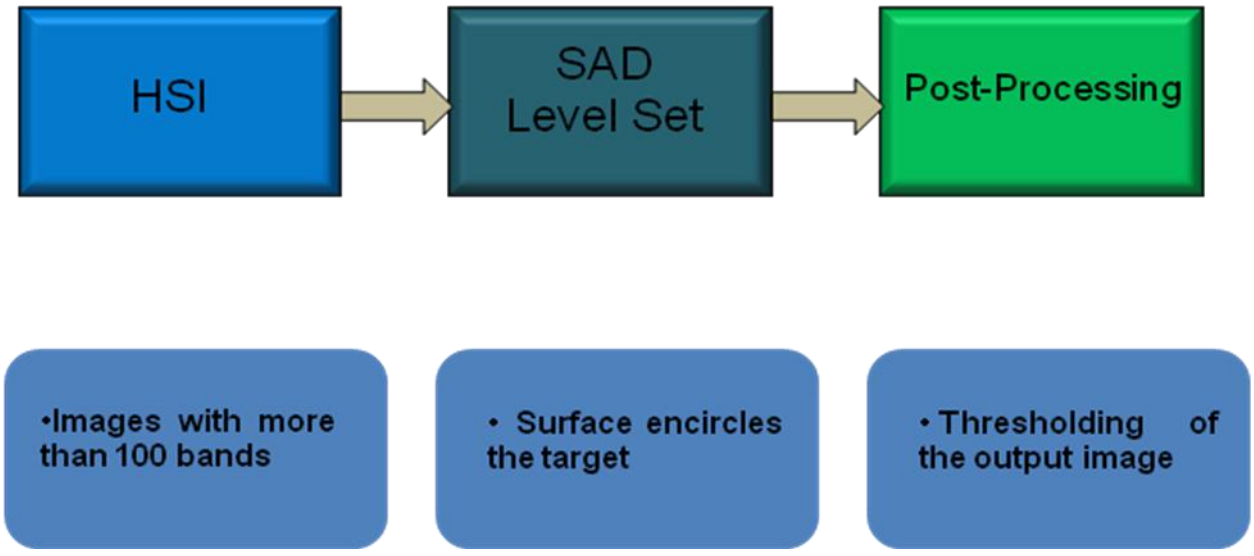

Figure 3.4 Block diagram for supervised target detection algorithm

The algorithm is composed by two steps, in the first step the level set technique is applied to the hyperspectral image constitutes by a background and a target which generally has a few pixels. The level set evolution equation almost follows the same structure used in unsupervised target detection with the difference that additional information of the target is required.

According to [14] the tasks of extracting an object placed in an image can be seen as the minimization of the following "fitting" energy functional with a length regularization term:

$$E(c_1, c_2, \phi) = \int_{\Omega} \left\{ (u - c_1)^2 * H(\phi) + (u - c_2)^2 * (1 - H(\phi)) + \mu * |\nabla H(\phi)| \right\} dxdy \tag{3.13}$$

where ϕ represents the level set surface given by Equation (2.6), μ is a constant and u is the image to be processed. H(ϕ) is the regularized function defined as:

$$H_{\varepsilon}(z) = \frac{1}{2}\left(1 + \frac{2}{\pi}\arctan\left(\frac{z}{\varepsilon}\right)\right) \tag{3.14}$$

The term ε is a constant, and when ε→0, the regularized version of Heaviside converge to its standard form. On another hand the Heaviside function allows to separate the pixels which are placed inside and outside the zeros loop defined by the level set surface. The graphical representation of Heaviside function is shown in the following image.

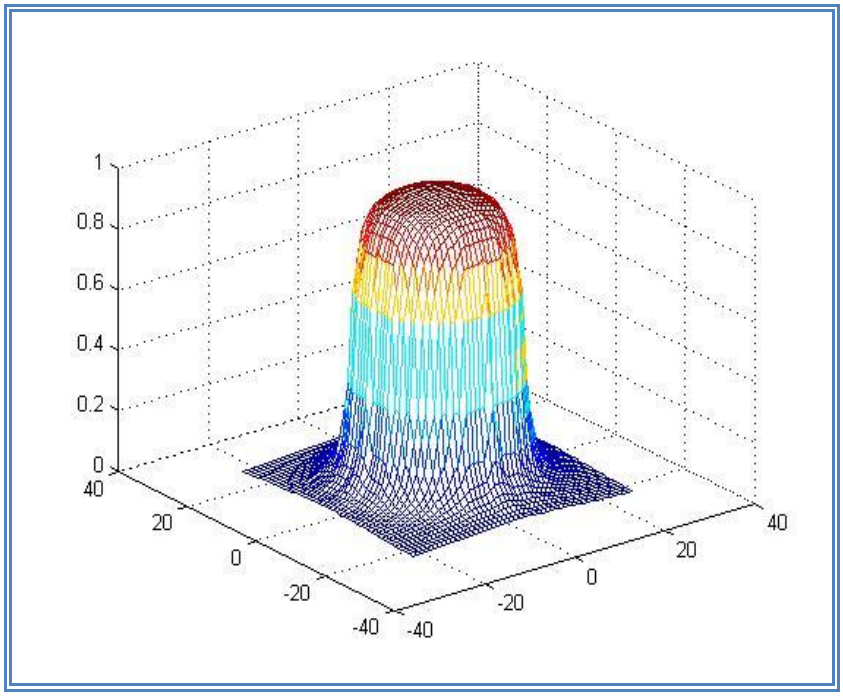

Figure 3.5 Graphical representation of the Heavise function

The first term in Equation (2.16) allows that the pixels inside the region where $\phi < 0$ conserve a homogeneity, in the same way the second term guarantee this property for the pixel where $\phi > 0$. The last parameter in (2.16) smoothes the level set function and avoids abrupt change around the objects detected in the image. Using the fundamental lemma of calculus of variations, E is minimized with respect to ø, getting the corresponding Euler-Lagrange equation:

$$\frac{\partial E(c_1, c_2, \phi)}{\partial \phi} = \left\{ (u - c_1)^2 - (u - c_2)^2 + \mu * \nabla . \left(\frac{\nabla \phi}{|\nabla \phi|} \right) \right\} * \delta(\phi) \tag{3.15}$$

where $\delta(\phi)$ is the Dirac function given by Equation (2.14) and it is got by deriving the Heaviside function with respect to ø.

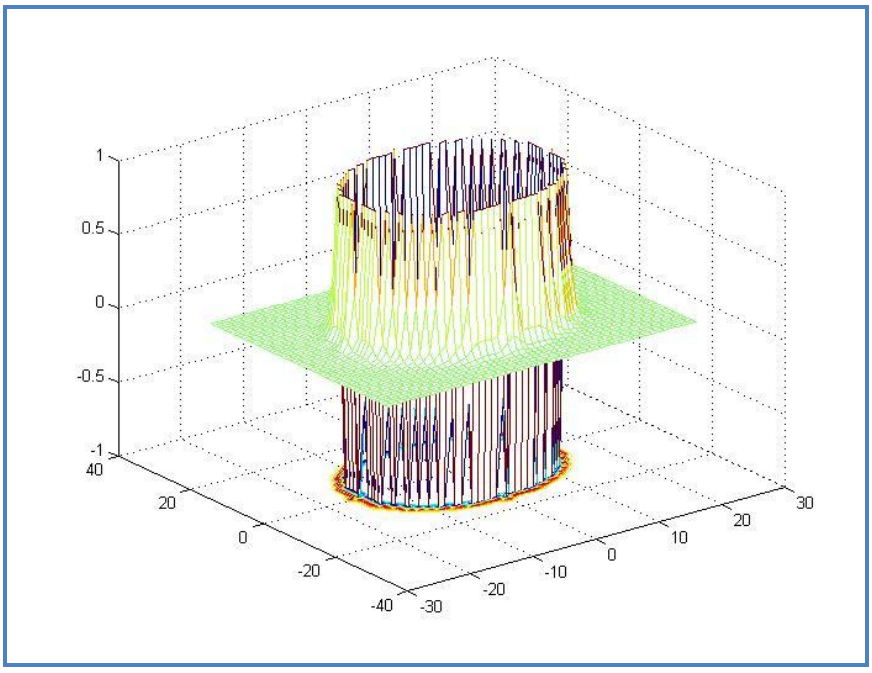

Figure 3.6 Graphical representation of the Delta Dirac function

Next using the steepest descent method, we get the evolution equation as follows:

$$\frac{\partial \phi}{\partial t} = -\left\{ (u - c_1)^2 - (u - c_2)^2 + \mu * \nabla . \left(\frac{\nabla \phi}{|\nabla \phi|} \right) \right\} * \delta(\phi) \tag{3.16}$$

In the same way the derivative of the energy with respect to C_1 is taken:

$$\frac{\partial E(c_1, c_2, \phi)}{\partial c_1} = \int_{\Omega} \{2(u - c_1) * H(\phi)\} dxdy = 0$$

Working out the value of C_1 we get:

$$c_1 = \frac{\int_{\Omega} \{u * H(\phi)\} dxdy}{\int_{\Omega} H(\phi) dxdy} \tag{3.17}$$

In the same way the derivative of the energy with respect to C_2 is taken:

$$\frac{\partial E(c_1, c_2, \phi)}{\partial c_2} = \int_{\Omega} \{2(u - c_2) * (1 - H(\phi))\} dxdy = 0$$

Working out the value of C_2 we get:

$$c_2 = \frac{\int_{\Omega} \{u * (1 - H(\phi))\} dxdy}{\int_{\Omega} 1 - H(\phi) dxdy} \tag{3.18}$$

The term C_1 is calculated continually during the evolution of the level set equation as the mean value of the pixels of the region where ϕ (t, x, y) is positive, whereas C_2 is with respect to the pixels where ϕ (t, x, y) is negative.

Supervised target detection knows beforehand some characteristics of the target of interest, generally the spectral signature of the targets is available and it is used to ease their detection. In this work a new energy functional is proposed whose main idea is to minimize the difference between pixel value of the target and mean value of the pixels which belong to the region where ϕ (t, x, y) is positive. The proposed functional is as follows:

$$E(c_1,c_2,\phi)=\int_{\Omega}\left\{(u-c_1)^2*H(\phi)+(u-c_2)^2*(1-H(\phi))+(u-c_3)^2*H(\phi)+\mu*|\nabla H(\phi)|\right\}dxdy \tag{3.19}$$

where C_3 corresponds to the pixel value of the target or anomaly of interest. This new term allows that the level set surface encircle pixels whose values are very close to the value of the target. Minimizing E with respect to ø, getting the corresponding Euler-Lagrange equation:

$$\frac{\partial E(c_1,c_2,\phi)}{\partial \phi}=-\delta(\phi)\left\{(u-c_1)^2-(u-c_2)^2+(u-c_3)^2+\mu*\nabla.\left(\frac{\nabla\phi}{|\nabla\phi|}\right)\right\} \tag{3.20}$$

Next using the steepest descent method, we get the evolution equation as follows:

$$\frac{\partial \phi}{\partial t}=-\delta(\phi)\left\{(u-c_1)^2-(u-c_2)^2+(u-c_3)^2+\mu*\nabla.\left(\frac{\nabla\phi}{|\nabla\phi|}\right)\right\} \tag{3.21}$$

The variables C_1 and C_2 are updated in every iteration and their values are given by (3.17) and (3.18) respectively. On another hand these equations are useful in gray scale images and it is necessary to do some modifications to be implemented for hyperspectral images. *SAD* is incorporated into (3.17), (3.18) and (3.19) generating the following equation.

$$\frac{\partial \phi}{\partial t}=-\delta(\phi)\left\{(SAD(u,c_1))^2-(SAD(u,c_2))^2+(SAD(u,c_3))^2+\mu*\nabla.\left(\frac{\nabla\phi}{|\nabla\phi|}\right)\right\} \tag{3.22}$$

where *SAD(x1,x2)* is the spectral angle distance and is given by Equation (3.2).

In the same way for unsupervised target detection a post-processing step is necessary to extract the target from the background, for which a threshold to zero is used to determine the presence or absence of the target.

The proposed supervised algorithm receives as input parameters the hyperspectral signature of the target to be detected and the hyperspectral image to be processed. The proposed algorithm can be summarized by the followings steps:

Step 1) Applying the supervised Level set to the HSI. The level set surface encircles the targets present in hyperspectral image; it evolves through time by using the equation 3.22.

Step 2) Generating a binary image. The positions of the matrix that represents the level set surface that take negative values are set to zero whereas the remainder are set to one. In that way a binary image is generated with the extracted targets.

3.4 Practical considerations in the implementation of the proposed algorithms.

The proposed algorithms were implemented as a computer program in Matlab 7.0; the level set surface is represented as a matrix with the same number of rows and columns of the image to be processed. The matrix of level set is initialized by using Equation (1.2). The surface *S* (see Equation (1.3)) is defined as a set of circles with radius 1 and separated by 1 position in the level set matrix;

for instance, if the number of columns and rows of an image are 10, the level set surface is initialized as follow:

$$\begin{pmatrix}
0.5000 & -0.5000 & 0.5000 & 0.9142 & 0.5000 & -0.5000 & 0.5000 & 0.9142 & 1.7361 & 2.6623 \\
-0.5000 & -0.9142 & -0.5000 & 0.5000 & -0.5000 & -0.9142 & -0.5000 & 0.5000 & 1.5000 & 2.500 \\
0.5000 & -0.5000 & 0.5000 & 0.9142 & 0.5000 & -0.5000 & 0.5000 & 0.9142 & 1.7361 & 2.6623 \\
0.9142 & 0.5000 & 0.9142 & 1.7361 & 0.9142 & 0.5000 & 0.9142 & 1.7361 & 2.3284 & 3.1056 \\
0.5000 & -0.5000 & 0.5000 & 0.9142 & 0.5000 & -0.5000 & 0.5000 & 0.9142 & 1.7361 & 2.6623 \\
-0.5000 & -0.9142 & -0.5000 & 0.5000 & -0.5000 & -0.9142 & -0.5000 & 0.5000 & 1.5000 & 2.5000 \\
0.5000 & -0.5000 & 0.5000 & 0.9142 & 0.5000 & -0.5000 & 0.5000 & 0.9142 & 1.7361 & 2.6623 \\
0.9142 & 0.5000 & 0.9142 & 1.7361 & 0.9142 & 0.5000 & 0.9142 & 1.7361 & 2.3284 & 3.1056 \\
1.7361 & 1.5000 & 1.7361 & 2.3284 & 1.7361 & 1.5000 & 1.7361 & 2.3284 & 3.1056 & 3.7426 \\
2.6623 & 2.5000 & 2.6623 & 3.1056 & 2.6623 & 2.5000 & 2.6623 & 3.1056 & 3.7426 & 4.5000
\end{pmatrix}$$

The level set matrix is updated 30 times (the number of iterations was found experimentally) by using Equation (2.10), the term Δt is defined as a constant of value 0.3, the term $\partial\phi/\partial t$ corresponds to a matrix that is updated at each iteration by using either Equation (3.3) or (3.22) depending on case (supervised or unsupervised target detection). In the case of supervised target detection, the spectral signature of the target that corresponds to a vector of real values is used as input parameter by Equation (3.22).

The term $\partial\phi/\partial t$ depends mainly on three parameters (see either Equation (3.3) or (3.22)), the first one is the curvature [9], it corresponds to a matrix defined by Equation (2.9). The second term ($SAD(u,c_i)$) is represented as a matrix of real values obtained for calculating the Spectral Angel Distance (see Equation (3.2)) between each of the pixels of an image 'u' and the vector 'c_i'. The term c_1 is calculated as the mean pixel of all pixels of image corresponding to the position where

level set matrix takes negative values; in the same way c_2 is the mean vector of all the pixels in the image where the level set matrix takes positive values. The last term is the delta Dirac function '$\delta(x)$' that is updated by using Equation (2.14).

The output level set matrix contains the positions of the targets detected, the elements of the matrix that take negative values correspond to the positions in the image where the targets are placed, the reminder elements (positive values) are associated to the background of image.

The experiments were carried out on a PC DELL INSPIRON 640m with a processor Intel Centrino Duo of 2GHz and 2GB of *RAM*.

4 ALGORITHMS VALIDATION AND PERFORMANCE EVALUATION

In this section, the results obtained with the proposed target detection algorithms are presented. The testing of the distinct proposed algorithms was done using synthetic and real remote sensing images and their performance were evaluated using ROC diagrams.

4.1 Unsupervised detection results for large targets

The proposed target detection algorithm is tested with real and synthetic images; the SOC-700 hyperspectral camera is used for capturing texture images of distinct materials. This camera acquires a 640 pixel by 640 pixel image with a spectral resolution of 4 nm which ranges from 400 to 900 nm, for a total of about 120 bands. It is available at the Laboratory for Applied Remote Sensing and Image Processing (LARSIP). The different textures captured from the camera are showed in the following images.

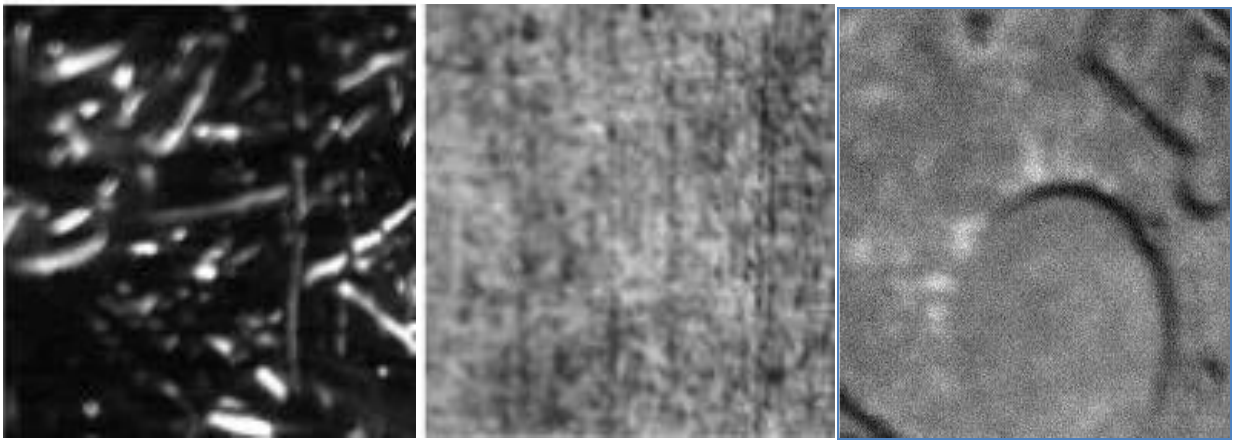

(a) (b) (c)

Figure 4.1 Different texture images for testing the proposed algorithm. (a) mango leaves texture, (b) concrete texture, (c) iron texture

Two images are generated with textures of concrete, iron and mango leaves. These images have dimensions of 120x120x120 and they are characterized by a circular-shaped target in a background. The targets are constituted by iron whereas the background corresponds to mango leaves in the first image and both concrete and mango leave in the second one.

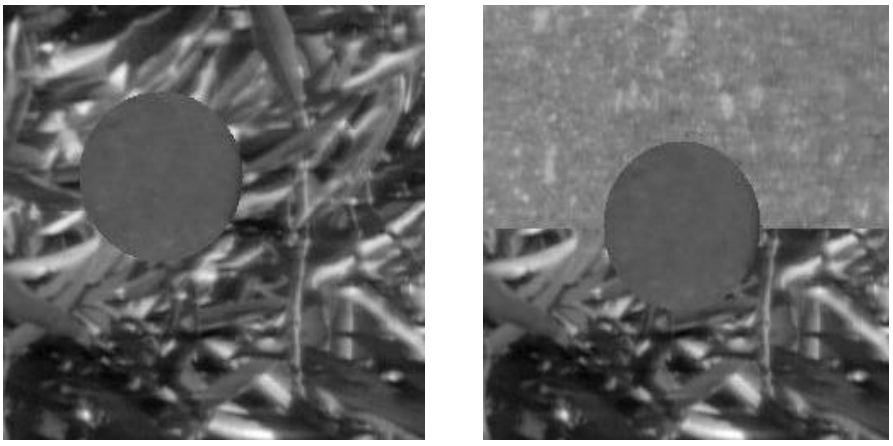

Figure 4.2 Synthetic images generated for testing the proposed algorithm

Another synthetic image was created with two targets of concrete placed in a background of asphalt. The image is constituted by 640 lines, 640 samples and 120 bands. The synthetic image is showed in the following Figure.

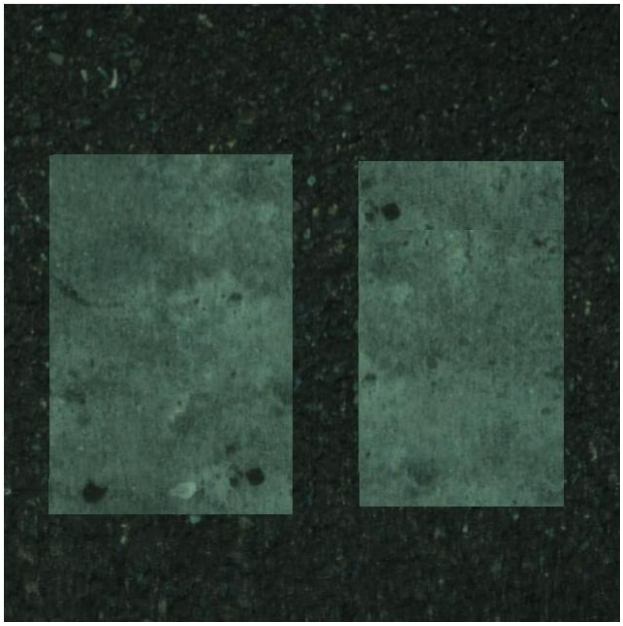

Figure 4.3 Regions selected from Fake leaves hyperspectral image.

Three synthetic hyperspectral images are generated with a subset of the fake leaves image, this one was also captured by SOC-700 and it is available in [36]. The regions used as targets and background are showed in the following Figure.

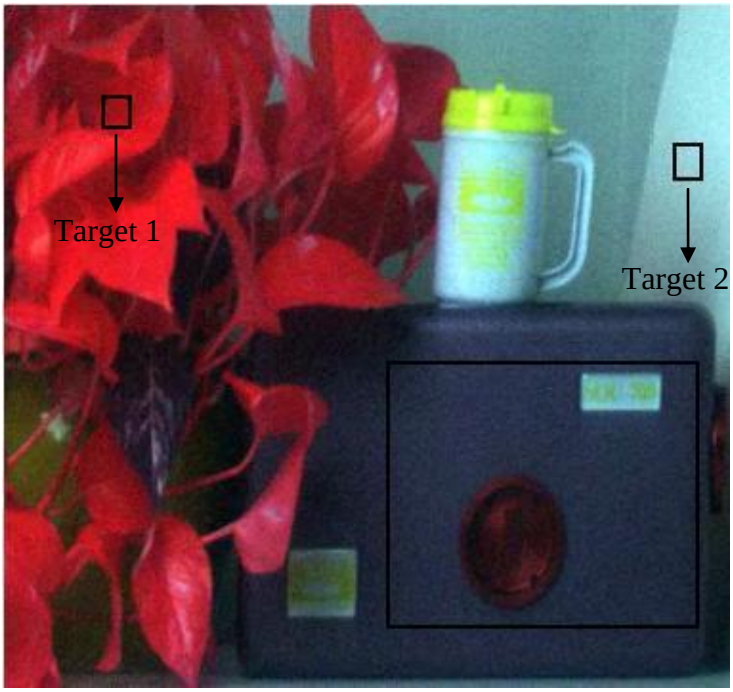

Figure 4.4 Regions selected from Fake leaves hyperspectral image.

The new images have targets with distinct shapes embedded in a background; they have 246 lines, 145 columns and 120 bands. They are show in the Figure 4.5.

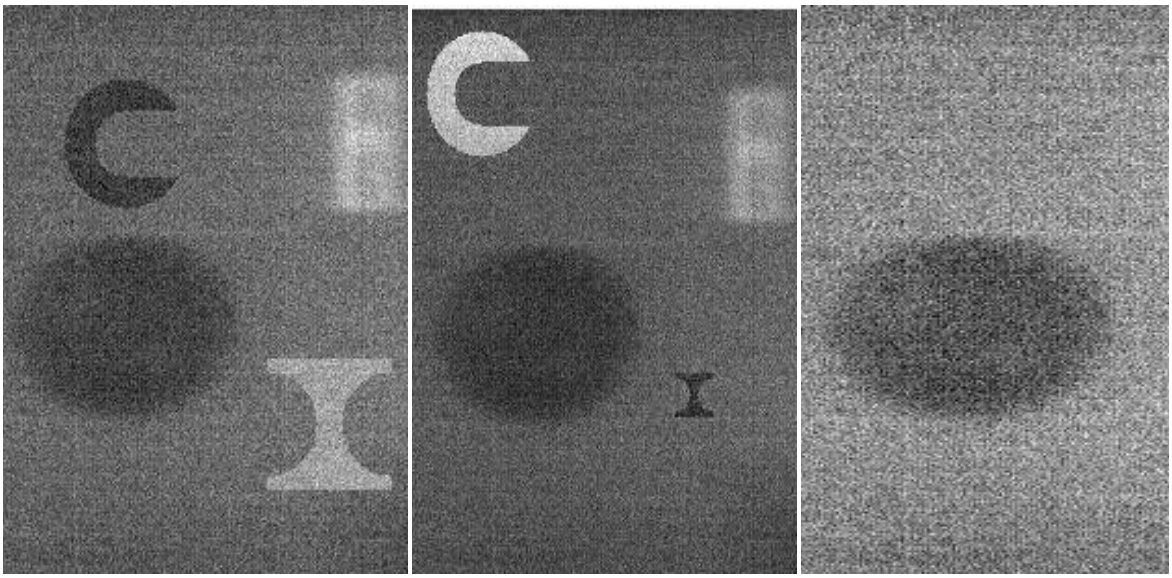

Figure 4.5 Synthetic images generated for testing the proposed algorithm

4.1.1 Unsupervised target detection results for SOC-700 camera data sets using spectral information

The method proposed by Chan and Vese [11] was implemented and tested in a set of synthetic images with distinct geometric figures on a background. The image has a dimension of 276 by 155 pixels with 120 bands. The method was combined with band subset selection algorithms such as Bhattacharya distance and information divergence to determine a set of bands with highest information. The PCA has the advantage of reducing the data dimensionality without having prior knowledge of the objects present in the image. The results with Chan algorithm are show in Figure 4.6.

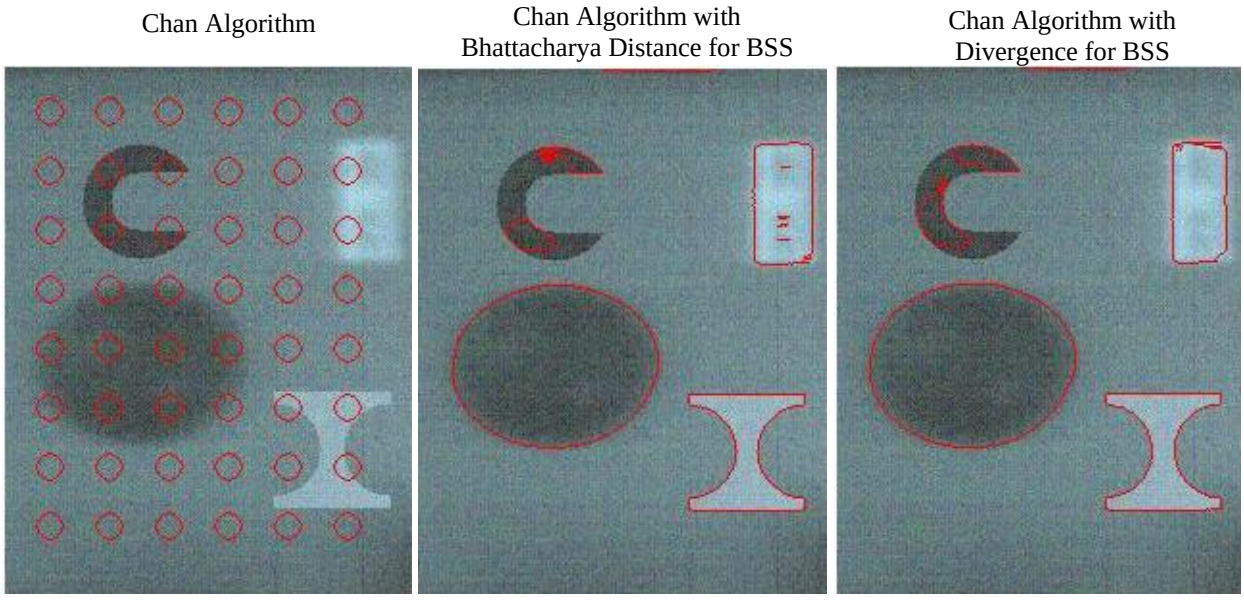

Figure 4.6 Segmentation with Chan algorithm .

The segmentation with all bands caused the surface of level sets to shrink and disappear. There is a lot of redundant information in the original set of bands; hence the desired targets are not detected by direct extension of Chan's algorithm to hyperspectral images. The incorporation of Bhattacharya distance and information divergence improved the performance of the algorithm. Bhattacharya distance and information divergence used 250 and 1600 iterations respectively, however the time required to select the 10 best bands is very high and needs computational recourse.

Comparison results of the proposed algorithm with the algorithm proposed by Chan [11] are given below. Chan's algorithm is applied to 10 bands selected by Bhattacharya distance. The proposed algorithm using Spectral Angle Distance (SAD level set) using only spectral information is applied with all 120 bands and bands obtained with PCA. Additionally Morphological operators are used to improve the results obtained with level set and SAD. These results are showed in Figure 4.7.

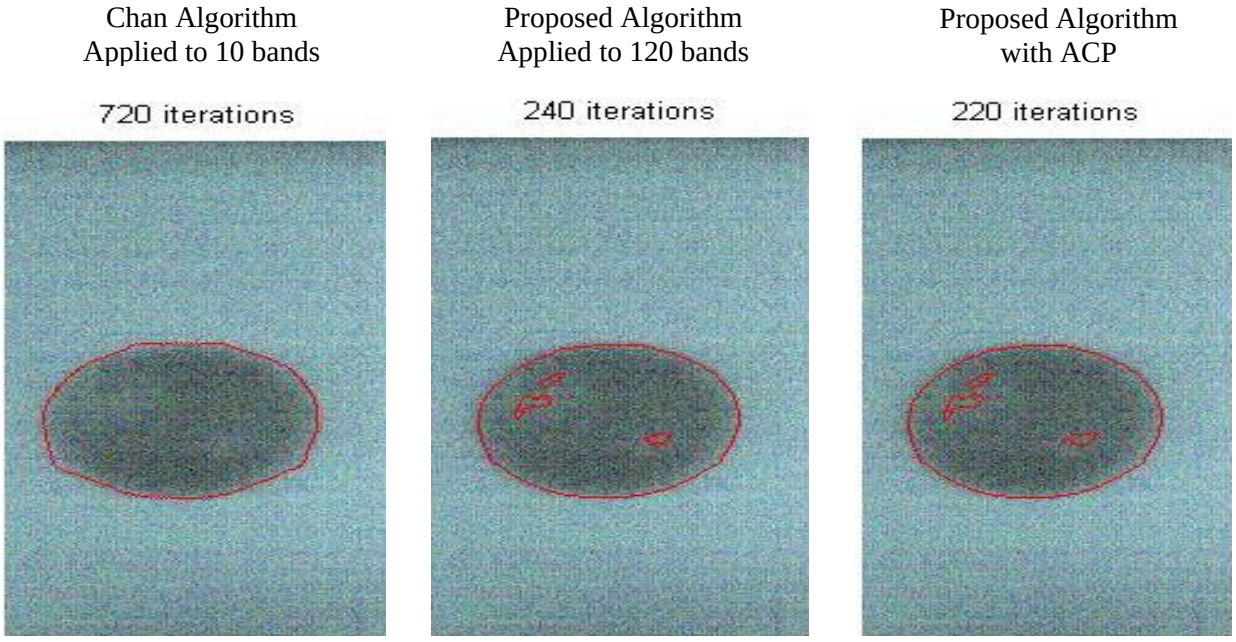

Image 1

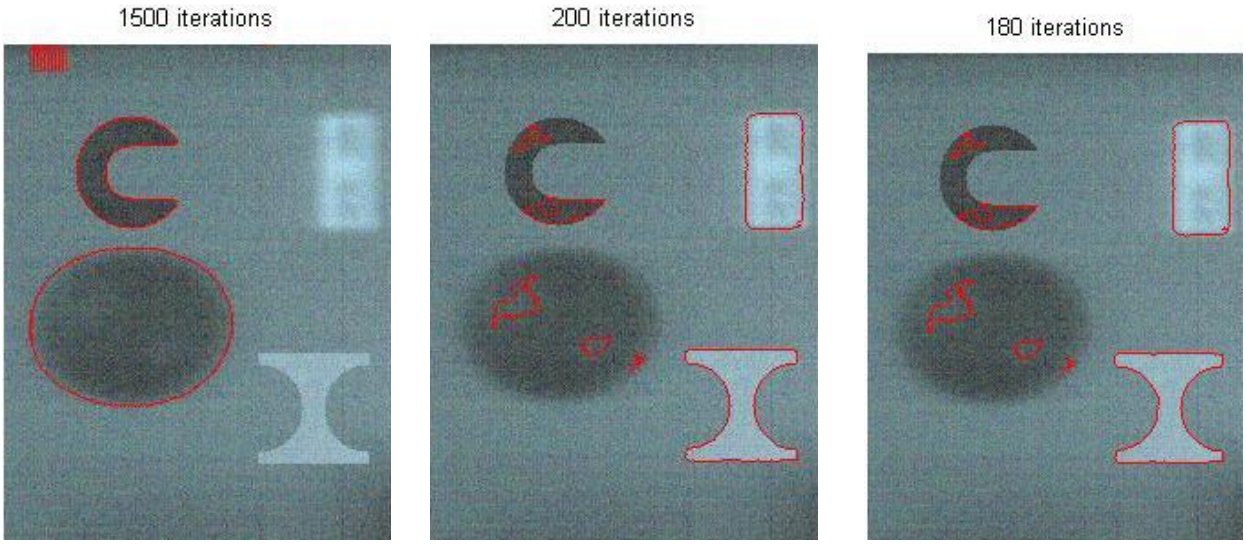

Image 2

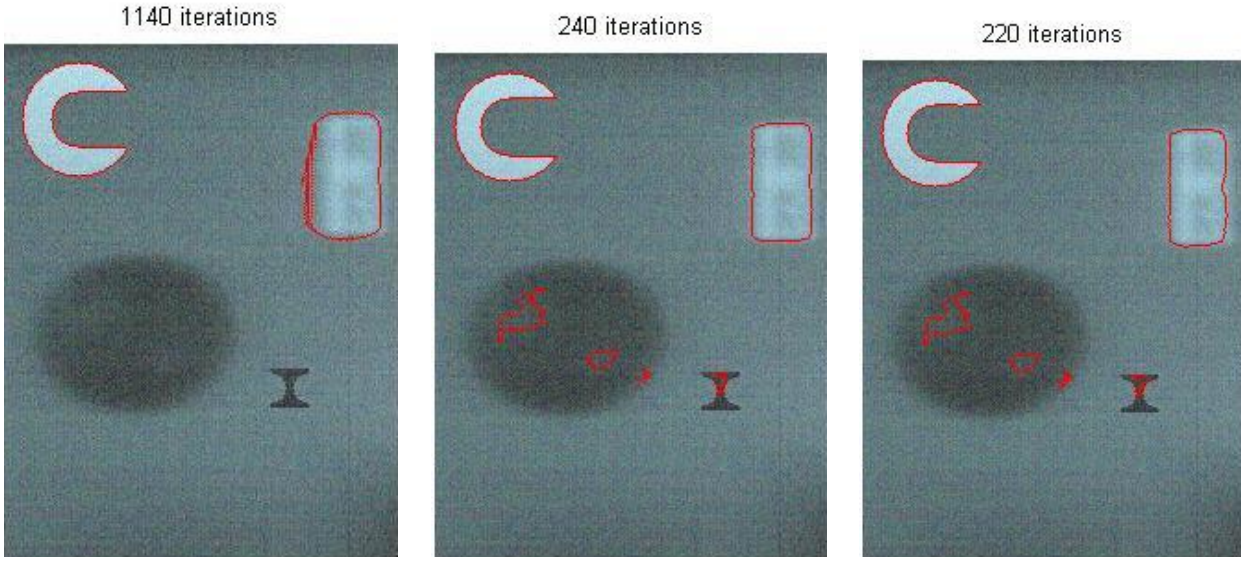

Image 3

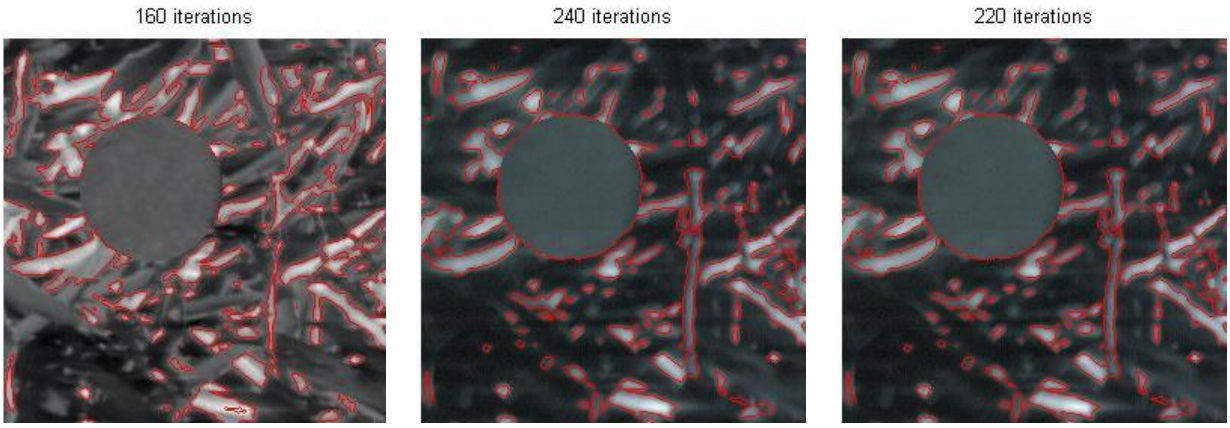

Image 4

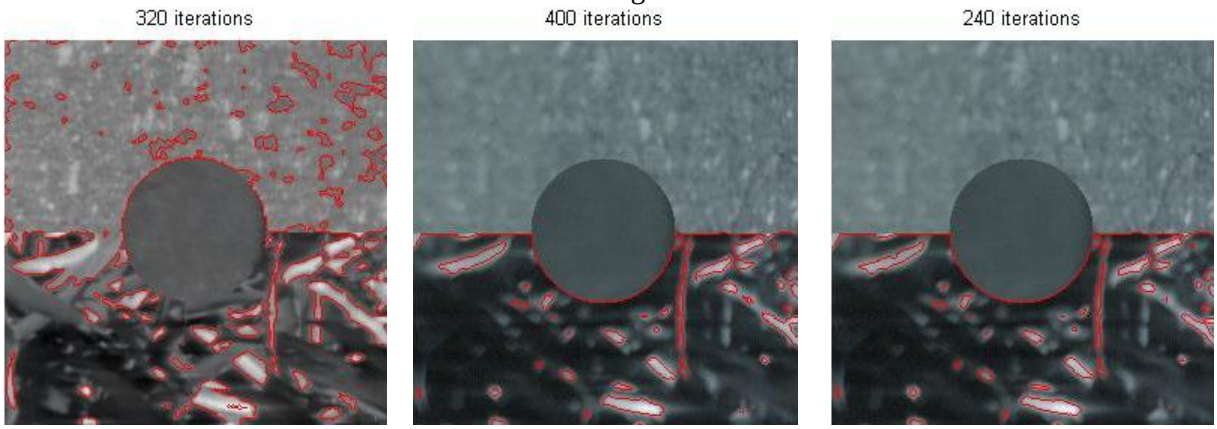

Image 5

Incorporation of Morphological

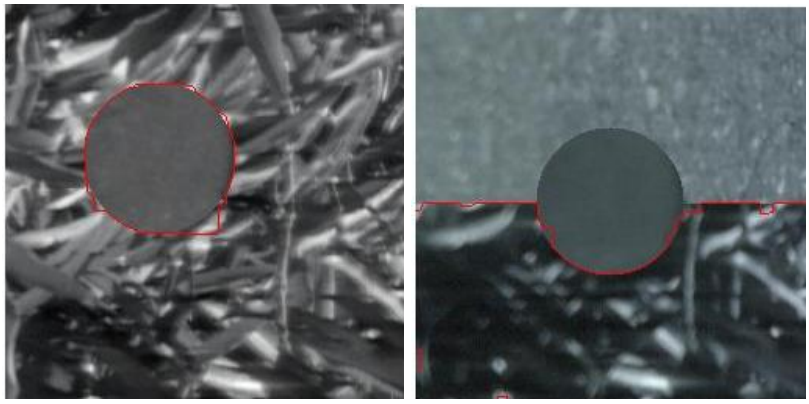

Image 6

Figure 4.7 Results got with Level Set + SAD algorithm

The Figure 4.7 shows that the proposed method results in better detection and lesser number of iterations and time of convergence. The Table 4.1 summarizes the results.

Table 4.1 Comparison of time of convergence and number iterations.

Method	Time of convergence (*seconds*)			Number of iterations		
	Image 1	Image 2	Image 3	Image 1	Image 2	Image 3
Chan Algorithm	249.76	42.68	83.21	1140	160	320
Proposed Algorithm applied to 120 bands	400.78	621.77	623.95	240	240	400
Proposed Algorithm with ACP	60.41	52.21	76.61	220	220	240

The timing required for Chan's algorithm [11] using 10 bands is close to the timing of the proposed algorithm using 120 bands. This shows that the proposed methodology contributes considerably to the time of convergence and at the same time efficiently couples the information in all bands.

4.1.2 Unsupervised target detection results for SOC-700 camera data sets using texture information

The method proposed for large target detection using texture information was tested in the set of synthetic images with distinct geometric figures on a background. The results are shown in the following Figure.

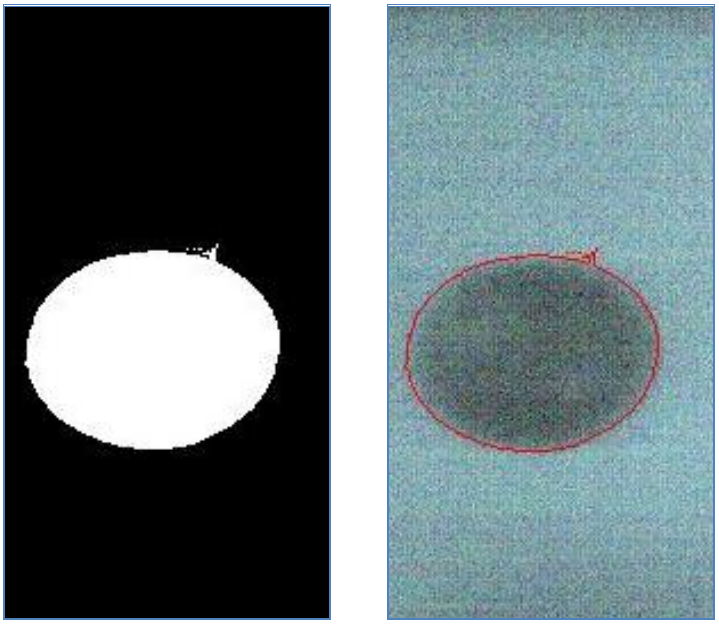

Image 1

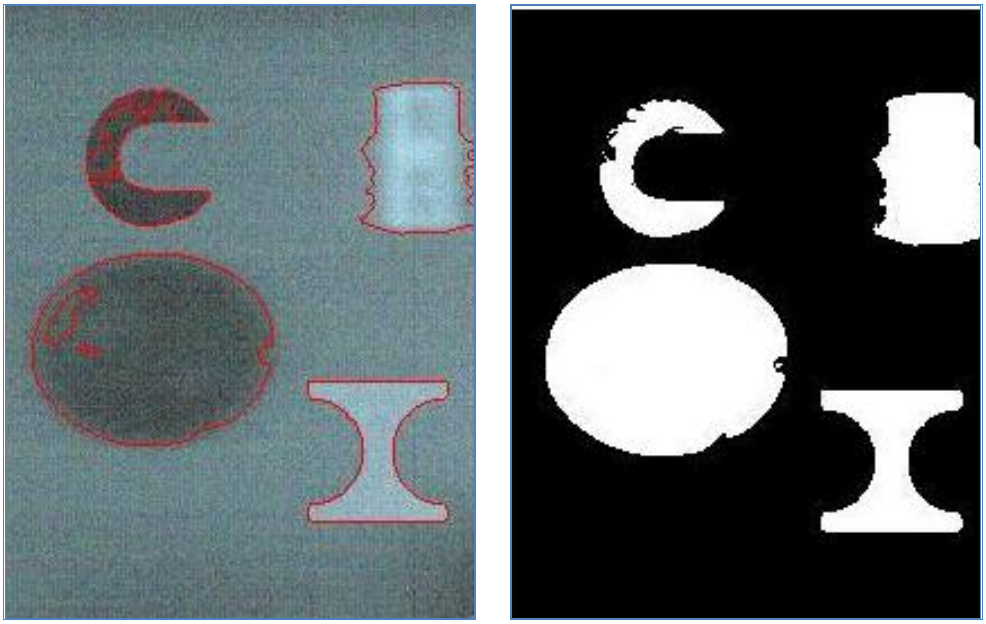

Image 2

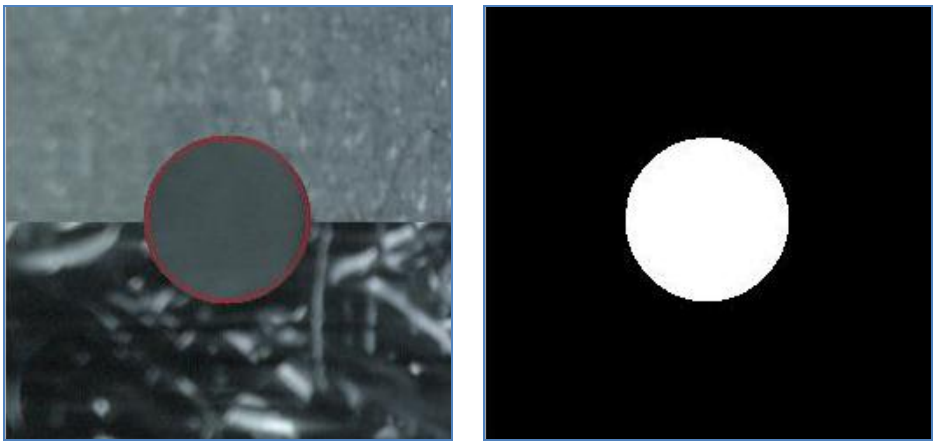

Image 3

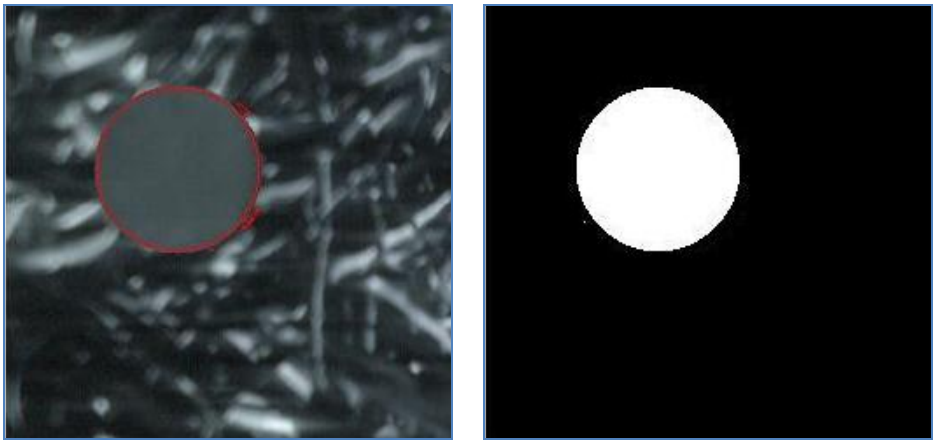

Image 4

Figure 4.8 Results for large target detection using texture information.

The results show that all objects placed in the images were successfully extracted. The level set technique encircles the objects while the post-processing step generates a binary image which discards the background and recovers the objects in the images.

The results were also compared with the algorithms proposed by Chan [11] and SAD-level set using only spectral information [21]. The time of execution, number of iterations and number of targets recovered are shown in Table 4.2.

Table 4.2 Comparison of time of convergence and number iterations.

Method	Time of convergence (*seconds*)				Number of iterations				Number of Targets Recovery			
	Image 1	**Image 2**	**Image 3**	**Image 4**	**Image 1**	**Image 2**	**Image 3**	**Image 4**	**Image 1**	**Image 2**	**Image 3**	**Image 4**
Chan Algorithm	249.76	42.68	83.21	92.14	1140	160	320	240	0	0	1	2
SAD-Level Set (Hyperspectral information)	60.41	52.21	76.61	67.2	220	220	240	182	1	0	1	2
SAD-Level Set (Texture information)	124.62	71.13	83.4	76.4	245	238	320	195	1	1	1	4

The experiments were carried out on a PC DELL INSPIRON 640m with a processor Intel Centrino Duo of 2GHz and 2GB of *RAM*. The results in the Table 3 shows that the time of execution of SAD-Level Set using hyperspectral information is lesser than the time of execution of others algorithms, however only the proposed algorithm (level set using texture information) recovered all targets in images.

Other results obtained with the proposed algorithm for large target detection are shown in the following Figure.

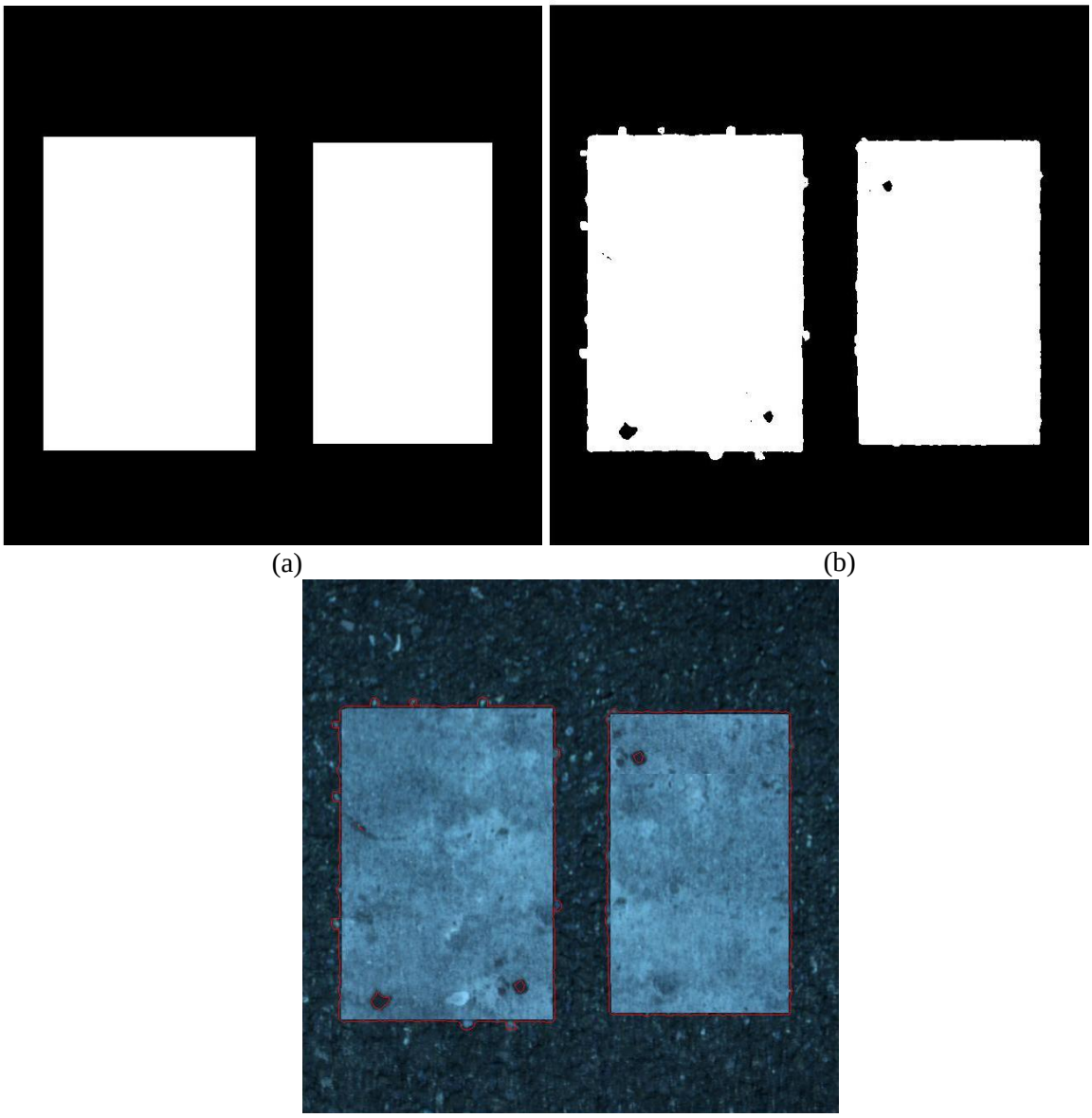

(a) (b)

(c)

Figure 4.9 Results for large target detection using texture information. (a) Ground truth, (b) Targets extracted, (c) Targets encircled by Level Set.

The results obtained show that the two targets were recovered successfully, additionally 97.4% of the pixels that belong to the targets were extracted properly and 0.43% of the pixels of the background were erroneously identified as targets.

4.1.3 Unsupervised target detection results for Hydice Desert Image using texture information

The HYDICE Desert image was used for testing the proposed algorithm in supervised target detection tasks. It was collected in Arizona in 1995 at altitude of 20,000 feet. It is constituted by 3000 rows, 120 columns, 210 bands and a spectral resolution that ranges from 0.35 μm to 2.5 μm.

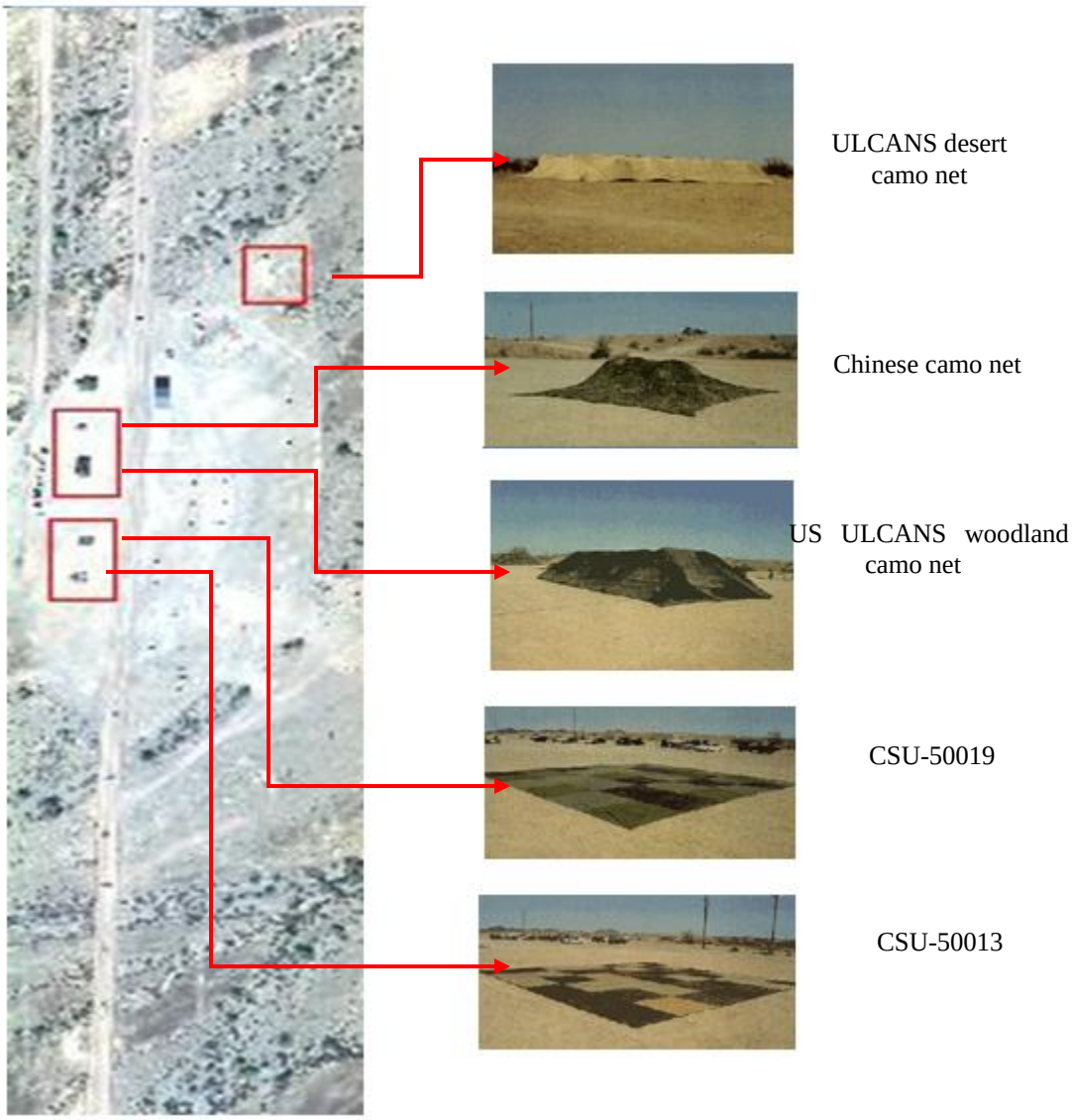

Figure 4.10 Scenes selected from HYDICE desert image.

Three scenes were extracted from the Hydice desert image; the first scene has dimensions of 45x43 pixels and 210 bands, it is constituted by two targets, the first target is an ULCANS desert camo net, whereas the second target is an US ULCANS woodland camo net. The

second scene has a size of 70x51 pixels and 210 bands and it is composed of two targets, the last scene has a target of ULCANS desert camo net, and the image has a size of 51x36 pixels and 210 bands. The results obtained are shown in the following image.

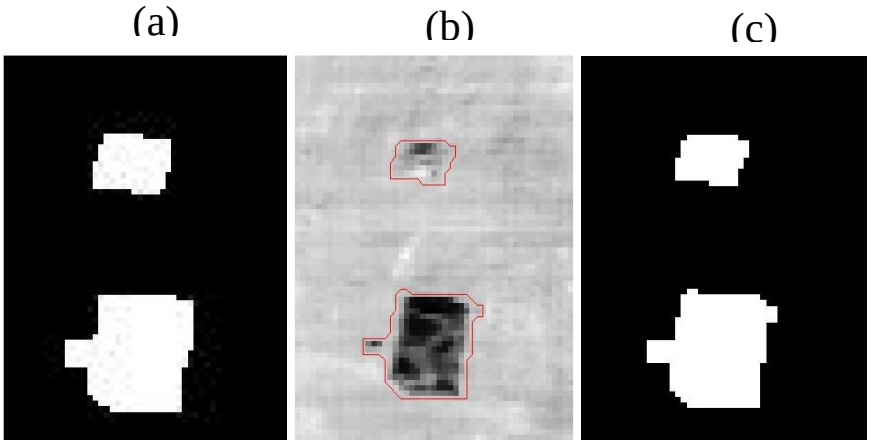

Scene 1

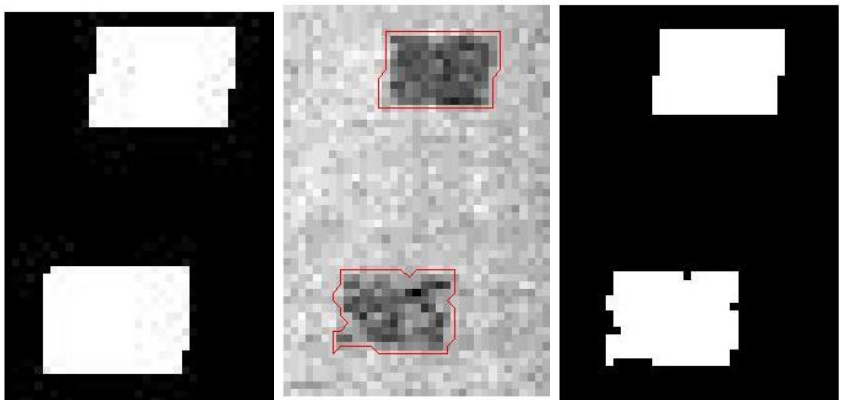

Scene 2

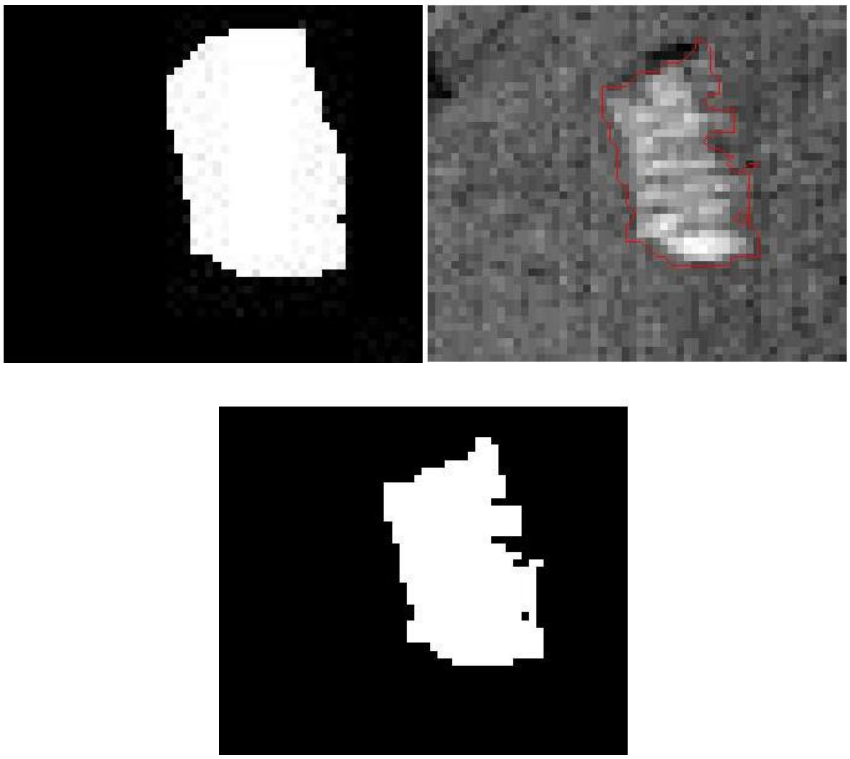

Scene 3

Figure 4.11 Reults for Automatic target detection algorithm. (a) Ground truth, (b) Targets encircled by Level Set, (c) Targets extracted.

The results show that the proposed algorithm for large target detection extracted successfully the objects in the images. For the first image the algorithm recovered 98.5% of the pixels that belong to the targets, similarly 97.5% and 95.2% of the pixels that constitute the targets were extracted successfully, in the second and third scene, respectively.

4.1.4 Unsupervised target detection results for Indian pine data sets using texture information

In the second experiment the Indian Pine image acquired by the AVIRIS sensor is used. The Indian Pine image has 145 lines, 145 samples and 220 bands; it also has a spectral resolution of 10nm from 400nm to 2500nm. Only 185 bands are used as the remaining corresponds to the water adsorption bands and band 220 which is noisy. Also, the bands with strong artifacts were eliminated.

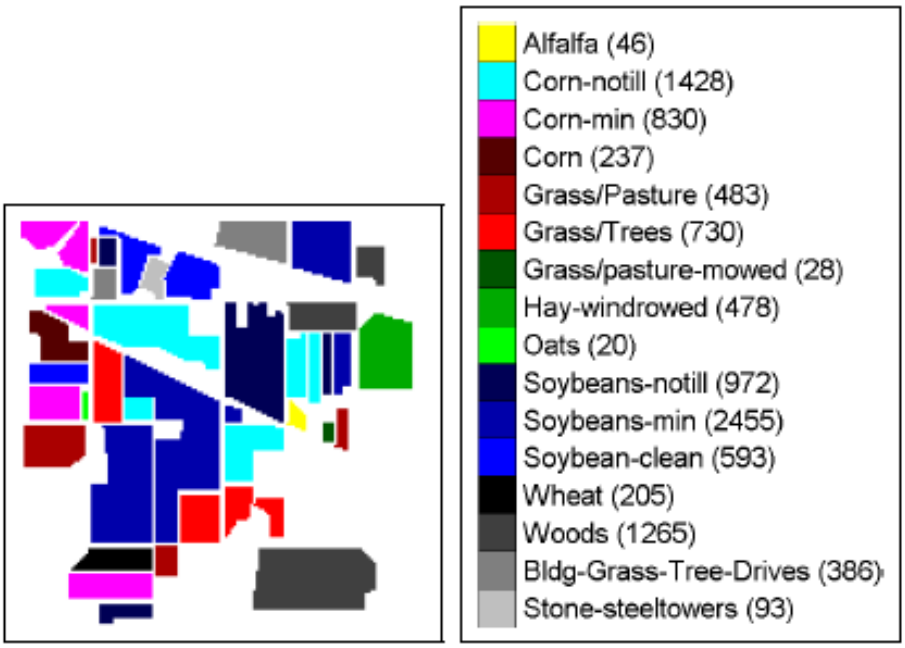

Figure 4.12 Indian Pine ground truth for 16 classes. Image Courtesy of [38].

The whole image of Indian Pine was used for testing. In addition, 2 new images with targets are synthesized from it. The first image has 71 lines, 128 samples and 185 bands; it was generated from a region of grass/trees, soybean min-till, corn-notill, corn-min and corn. The

second one corresponds to a region of 28x35 pixels of soybean min-till in which an artificial object constituted by wood was embedded. The regions selected are shown in the following image.

Figure 4.13 Regions selected for target detection experiments

The results obtained with the proposed algorithm are shown in Figure 4.14.

(a) 10 iterations

(b) 220 iterations

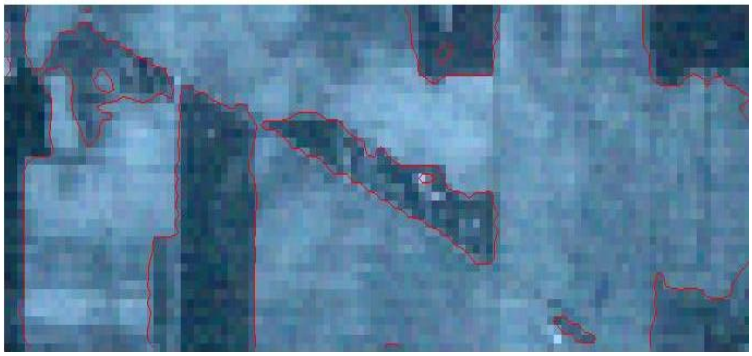

(C) 2000 iterations

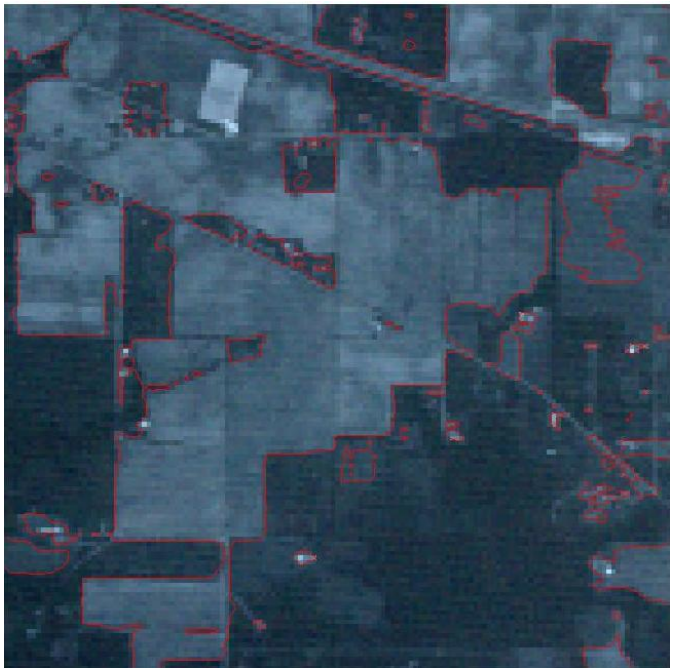

Figure 4.14 Results got with Level Set + SAD algorithm

The results show that the algorithm detected successfully the object in the first image. In the second image, the fields of grass/trees, soybean min-till, corn-notill, corn-min and corn were extracted from the background. For the whole image the number of iterations is 2000. While the sub-images in (a) and (b) converged in 10 and 220 iterations, respectively.

4.2 Unsupervised target detection results for small targets

The testing of the proposed target detection algorithm for small targets is done with synthetic and real hyperspectral images. The synthetic images are composed of background and distinct targets, the pixels that constitute the targets are mixed with the background according to the following equation [15]:

$$f(x_1, x_2) = \alpha * T + (1-\alpha) * B + n \qquad (4.1)$$

where α is the fractional mixing level, *T* is the target signature, *B* is the background signature and *n* is the zero mean Gaussian noise.

4.2.1 Unsupervised target detection results for HYDICE sensor data sets

A set of images with targets of 9 and 16 pixels are generated with several values of α. The background and the targets are extracted from the Washington D.C. mall hyperspectral image. This image contains 307 lines, 282 samples and 191 bands collected from 0.4 to 2.4 μm of the visible and infrared spectrum. A water region marked with '1' (see Fig. 4.15) is selected to constitute the background.

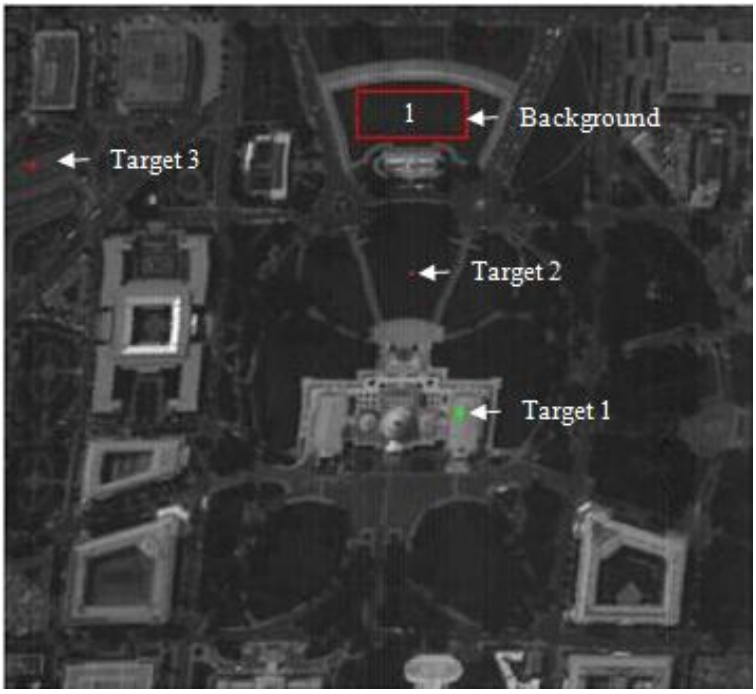

Figure 4.15 Washington D.C. mall image

The algorithm is tested with a grass target of 24 pixels, an asphalt target of 9 pixels and a concrete target of 16 pixels. The results of the proposed algorithm are shown in Figure 4.16.

(a)

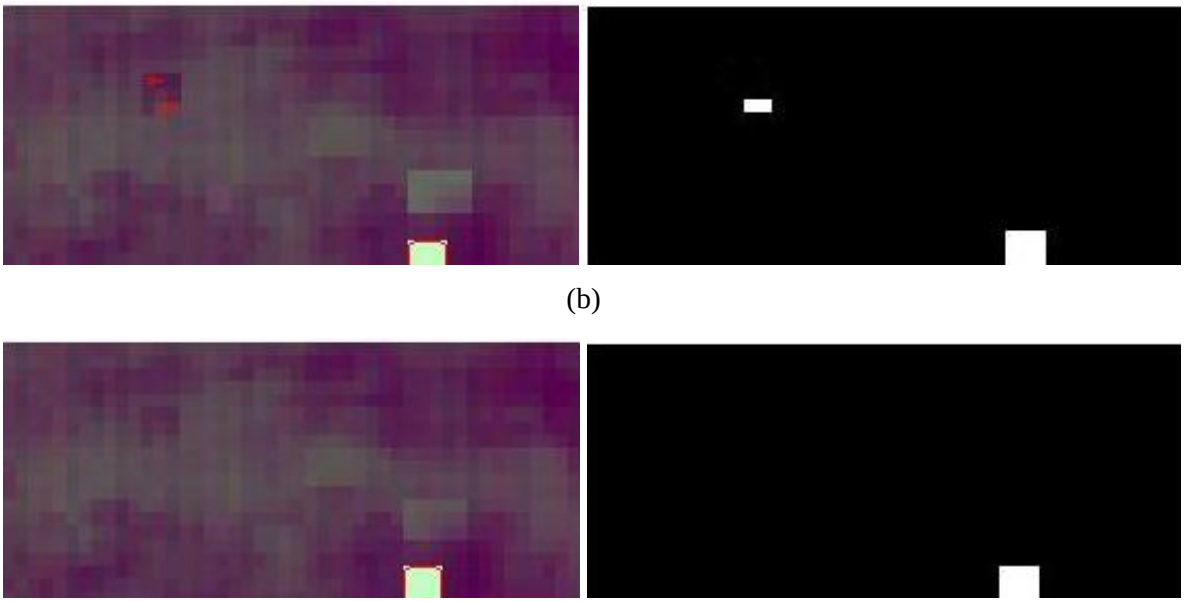

(b)

(c)

Figure 4.16 (a)Targets extracted with α=0.6, (b)Targets extracted with α=0.5,(c)Targets extracted for α=0.4

The results show that the targets with a fractional mixing level of 0.6 were all extracted by the proposed algorithm, for α=0.5 the asphalt and concrete targets were extracted successfully, whereas for α=0.4 only the concrete target was recovered.

The HYDICE Forest image is also used for testing the proposed algorithm, it was collected in Maryland in 1995 from a flight altitude of 10,000 ft, contains 1228 lines, 320 samples and 210 bands. It has about 1.5-m spatial resolution and 0.4–2.5 μm spectral coverage. Two scenes of the original images are selected for testing the proposed algorithm; the first scene has 249 x 128 pixels and 120 bands, additionally it has 30 panels organizes in three columns

of ten panels, the panels in the same row were made from the same material of sizes 3 × 3 m, 2 × 2 m, and 1 × 1 m, respectively, and are considered as one class.

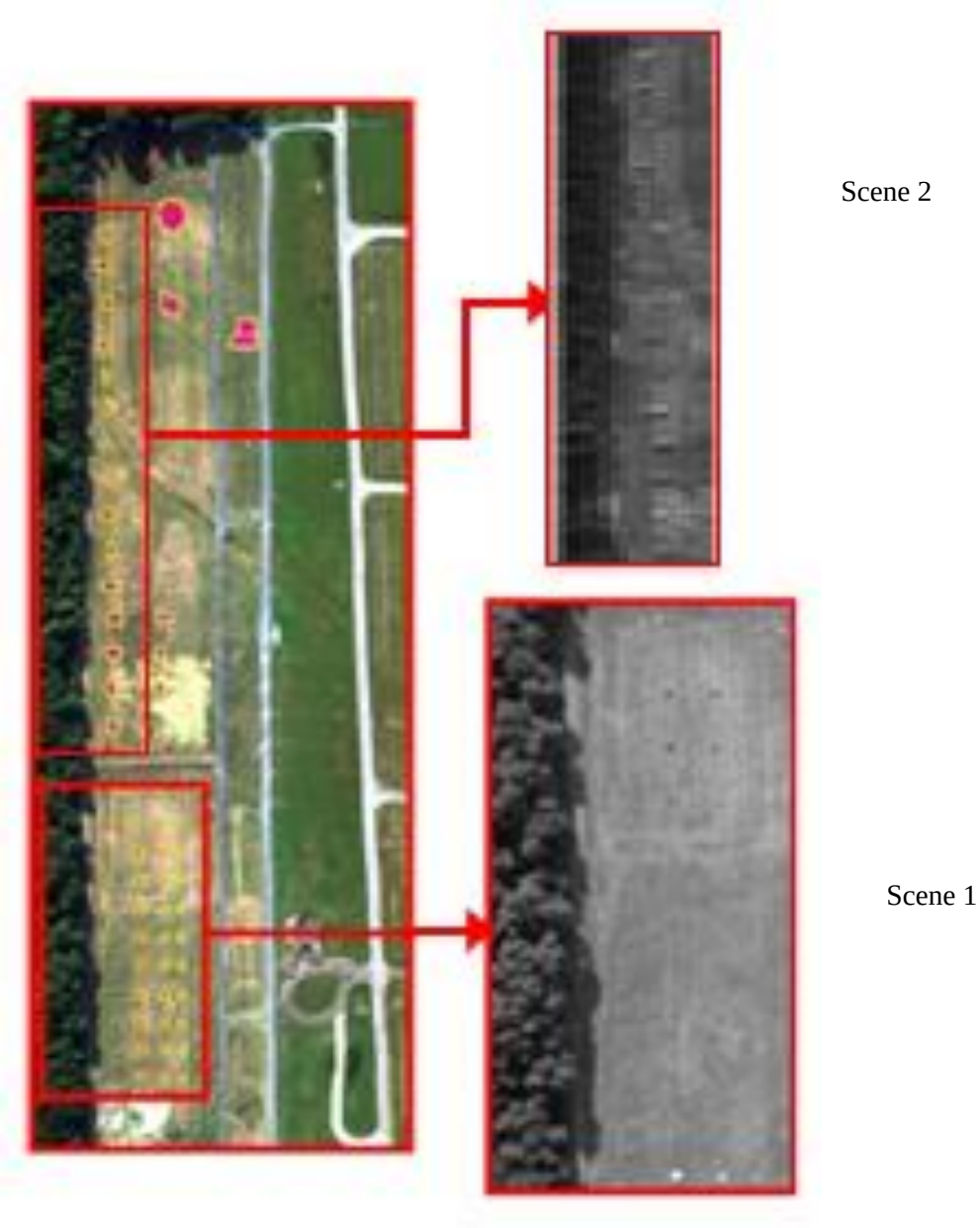

Figure 4.17 The HYDICE Forest image together with the scenes used for testing the algorithm.

The second scene has 428 x 71 pixels and 120 bands; it is constituted by 14 objects aligned vertically. The objects have a size of about 5 x 5 m. The two scenes and the original image are shown in Figure 4.17.

The ROC diagram is used for measuring the performance of the proposed algorithm [20], for calculating the ROC diagram the fact that the level set surface defined by Equation (2.6) evolves until encircling the pixels that belong to the targets is used. The final level set surface can be seen as an image that enhances the pixels marked as targets from the pixels identified as background. The proposed algorithm recovers sequentially the targets of the same class; in consequence as many level set surface are generated as types of targets present in the image. The images generated by the proposed algorithm and their corresponding ground truth are shown below.

(a) (b)

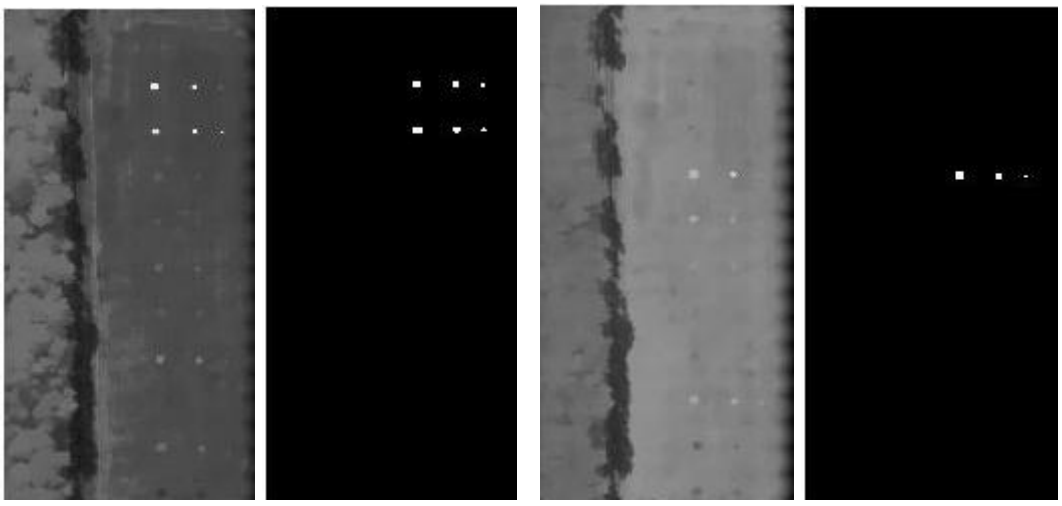

(c)

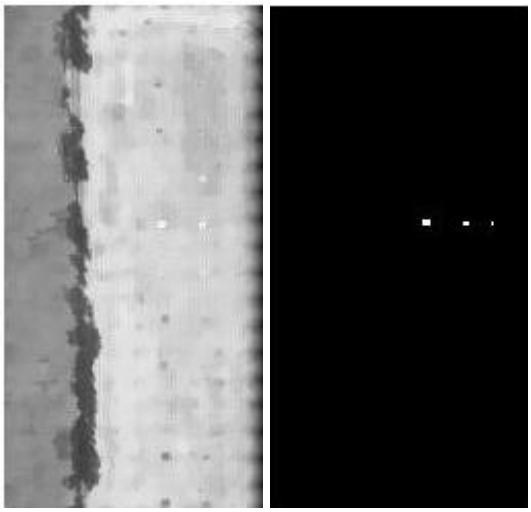

(d)

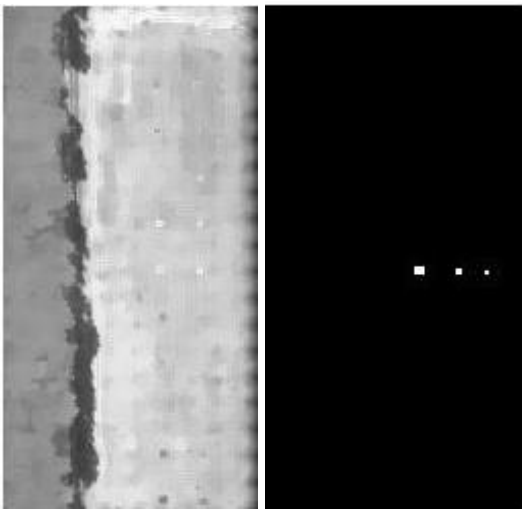

(e)

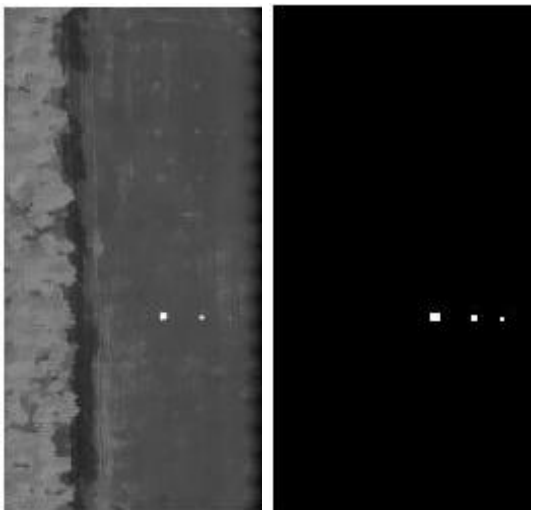

(f)

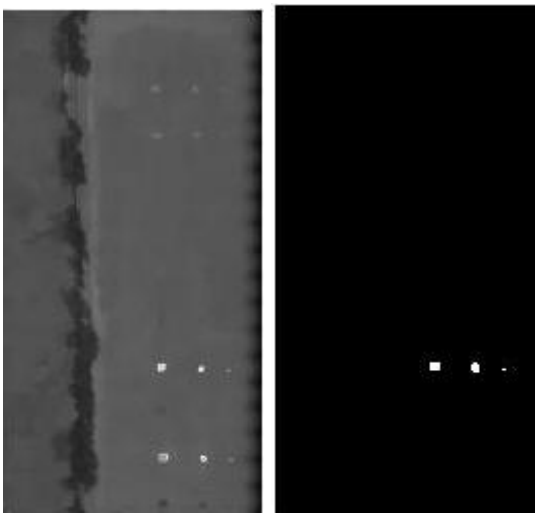

(g) (h)

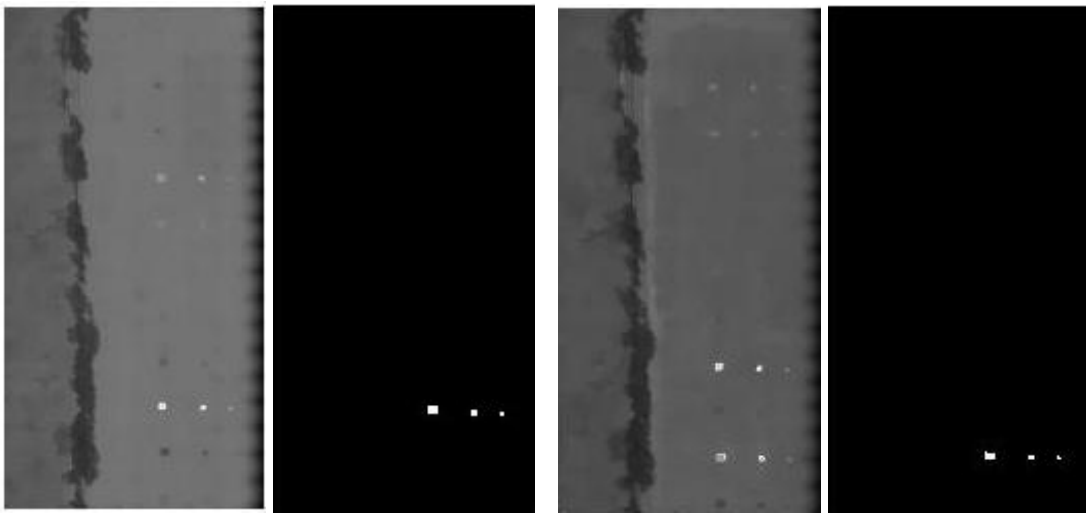

(i)

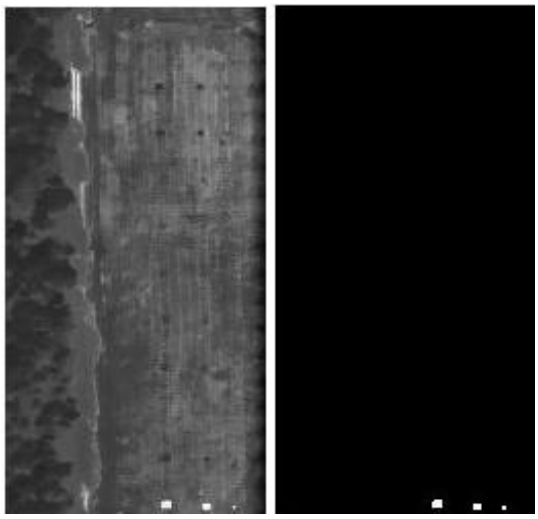

Figure 4.18 Targets enhanced and ground truth ,(a)Targets of Green fabric-untagged over asphalt, (b) Targets of dark olive parachute, (c) Targets of light olive parachute , (d) Nomex/Kevlar woodland fabric, (e)Targets of Green tenting fabric, (f) Targets of Woodland cotton/nylon fabric, (g)Targets of Woodland poncho , (h) Targets of green cotton fabric, (i) Targets of khaki/tan fabric

The results show that the pixels that belong to the target are enhanced from the pixels of the background, however in some cases where the mixture between the targets and background are more appreciable, for instance the cases of targets of light olive parachute and Nomex/Kevlar woodland fabric the target is not enhanced. For each of the generated images the histograms that plots the pixels of targets (red color) and background (blue color) is created, they are shown in the following image.

(a)

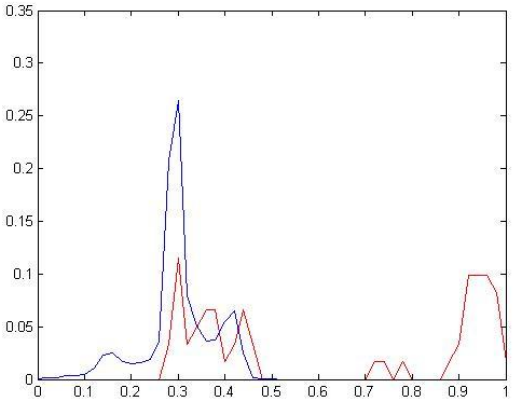

(b)

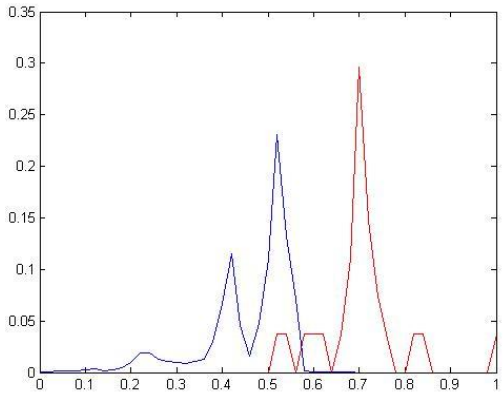

(c)

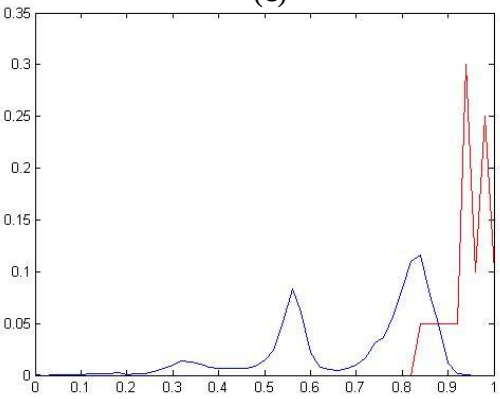

(d)

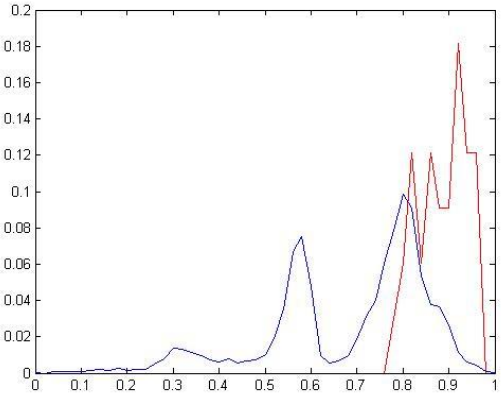

(e)

(f)

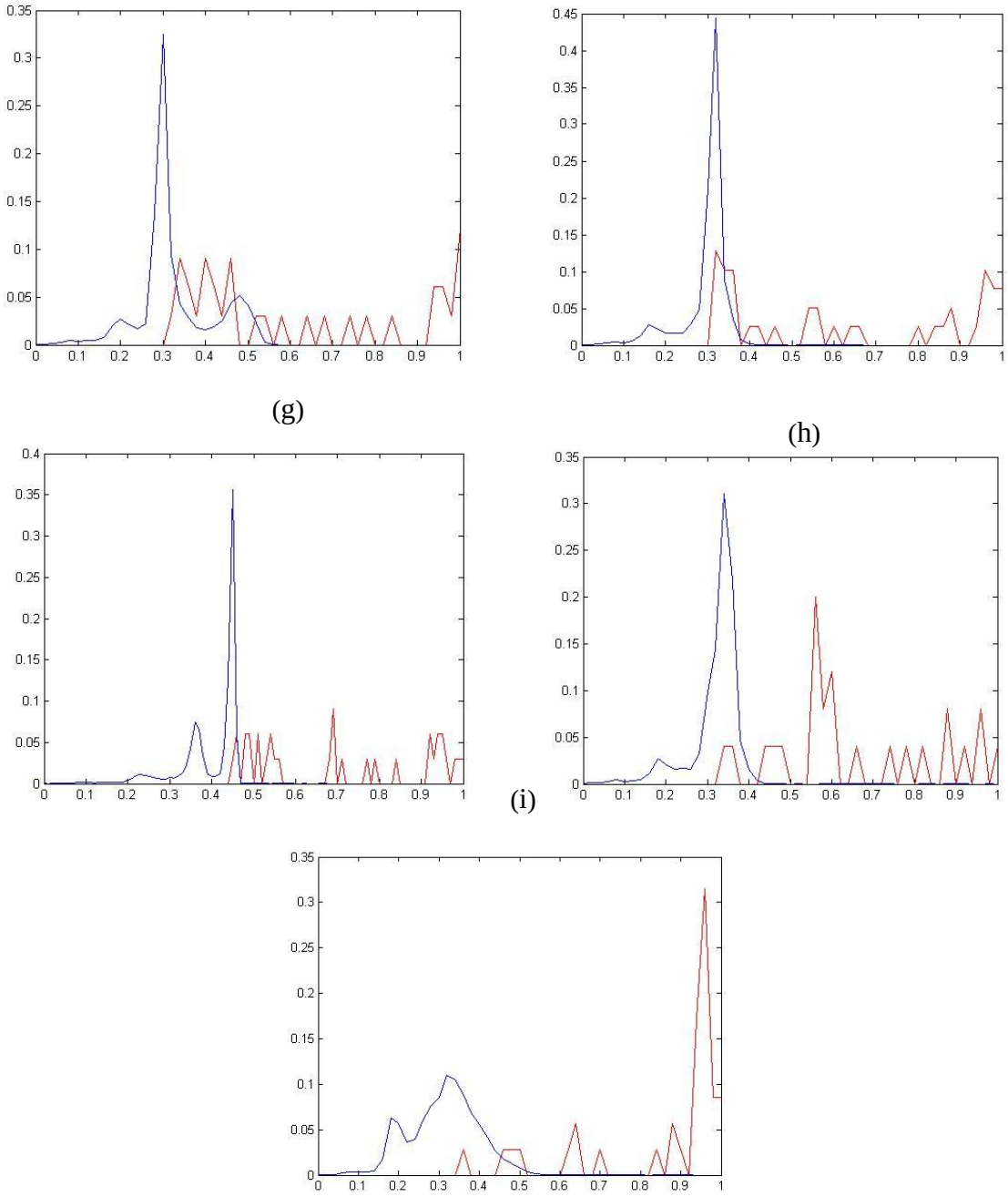

Figure 4.19 Histogram of Background and targets, (a) Targets of Green fabric-untagged over asphalt, (b) Targets of dark olive parachute, (c) Targets of light olive parachute, (d) Nomex/Kevlar woodland fabric, (e)Targets of Green tenting fabric, (f) Targets of Woodland cotton/nylon fabric, (g)Targets of Woodland poncho , (h) Targets of green cotton fabric, (i) Targets of khaki/tan fabric

The ROC diagrams are generated for each of the histograms obtained as results of the proposed algorithm. The threshold that separates the pixels of the targets and background is moved for all possible values through the histogram and then the pixels successfully identified as targets (true positive) versus the pixels of background identified as targets (false alarm) are plotted, then all ROC diagrams are averaged for generating a final ROC diagram. The binary image generated by the proposed algorithm for the scene 1 is shown in Figure 4.20.

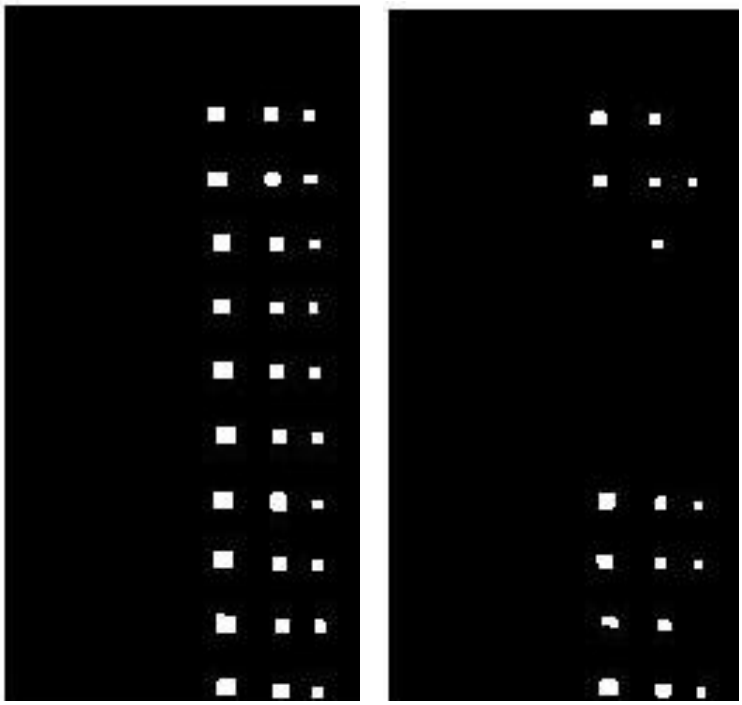

(a) (b)

Figure 4.20 (a) Ground truth, (b) Targets recovered by the proposed algorithm

The results show that the algorithm recovered 7 of the 10 kind of targets placed in the image with zero false positive. The binary image generated by the proposed algorithm for the scene 2 is shown in Figure 4.21.

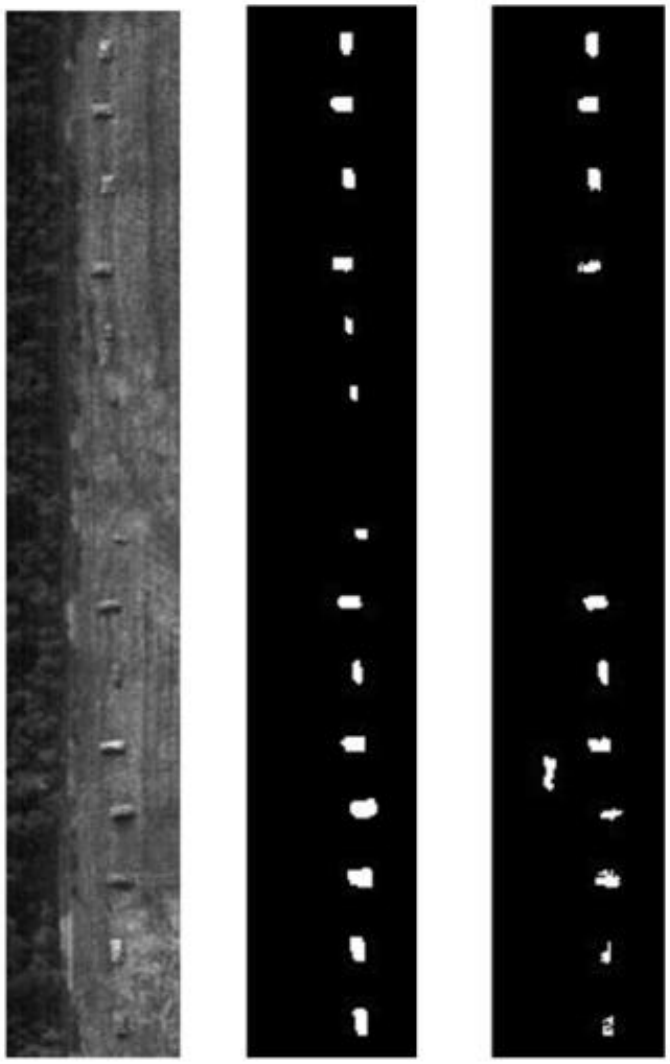

(a) (b) (c)

Figure 4.21 (a) Band 110 of the HYDICE Forest image, (b) Ground truth, (c) Targets recovered by proposed algorithm.

The results show that the algorithm recovered 11 of the 14 targets placed in the image with only one false positive. In addition the proposed algorithm has the property of distinguishing the different kind of targets recovered due that all targets of a specific type are extracted at time.

The ROC diagram that plots the probability of target detection versus the probability of false alarm is generated with the images available for testing the proposed algorithm, the diagram is shown in the following image.

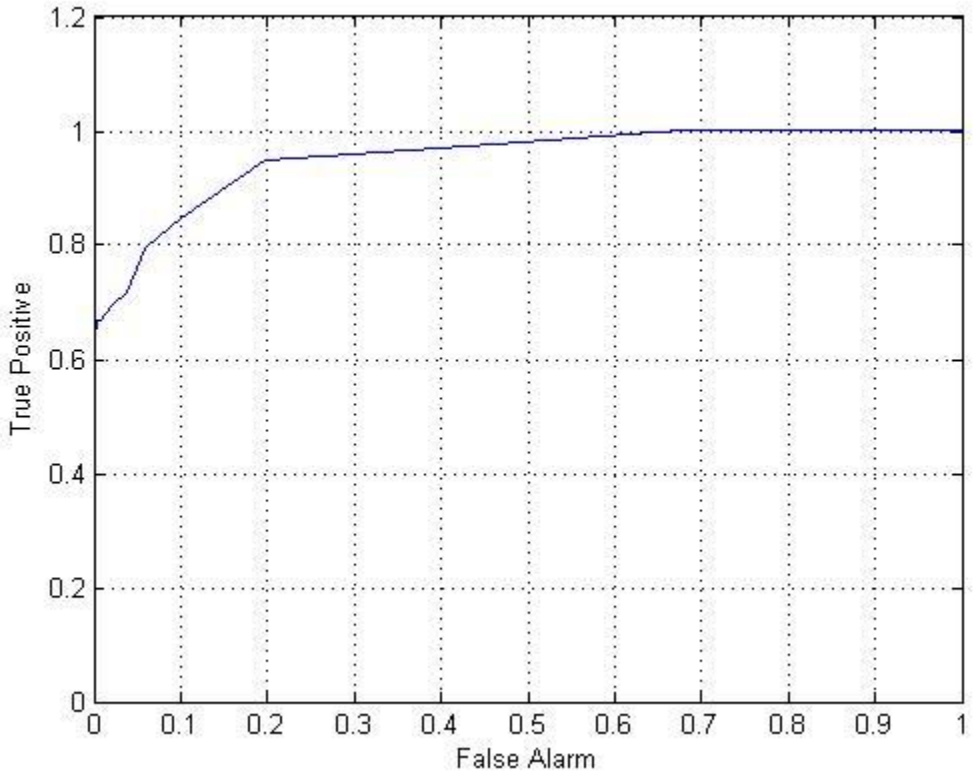

Figure 4.22 ROC Diagram for proposed algorithm.

The ROC diagram shows that the proposed algorithm obtained a target detection probability of 76.5% with only a 5% for false alarms. Additionally for a false alarm of 10%, the algorithm obtained an 84.6% for target detection probability. For false positive probabilities higher than 15.1%, the proposed algorithm obtained target detection probabilities over 90%.

4.3 Supervised target detection results

For testing the supervised version of the proposed algorithm, both synthetic and real hyperspectral images were used.

The synthetic images were generated with backgrounds of real hyperspectral images and some pixels of different material in the scene as targets, the background and the targets are mixed according with [15]. The parameter α is the fractional mixing level and represents the percentage of mixing between the targets and the background. The algorithm is applied to the group of images generated, and the results are compared with both OSP and CSD methods.

4.3.1 Supervised target detection results for SOC-700 camera data sets using spectral information

The Fake Leaves image is used for testing the supervised target detection algorithm, the image was collected by the Surface Optics Company using the SOC-700 hyperspectral camera. Three synthetic images were created selecting a subset of the Fake Leaves image, additionally targets of 1, 9 and 16 pixels, were inserted into them; the new scenes have dimensions of 35x40 x120 and they are shown in the following Figure.

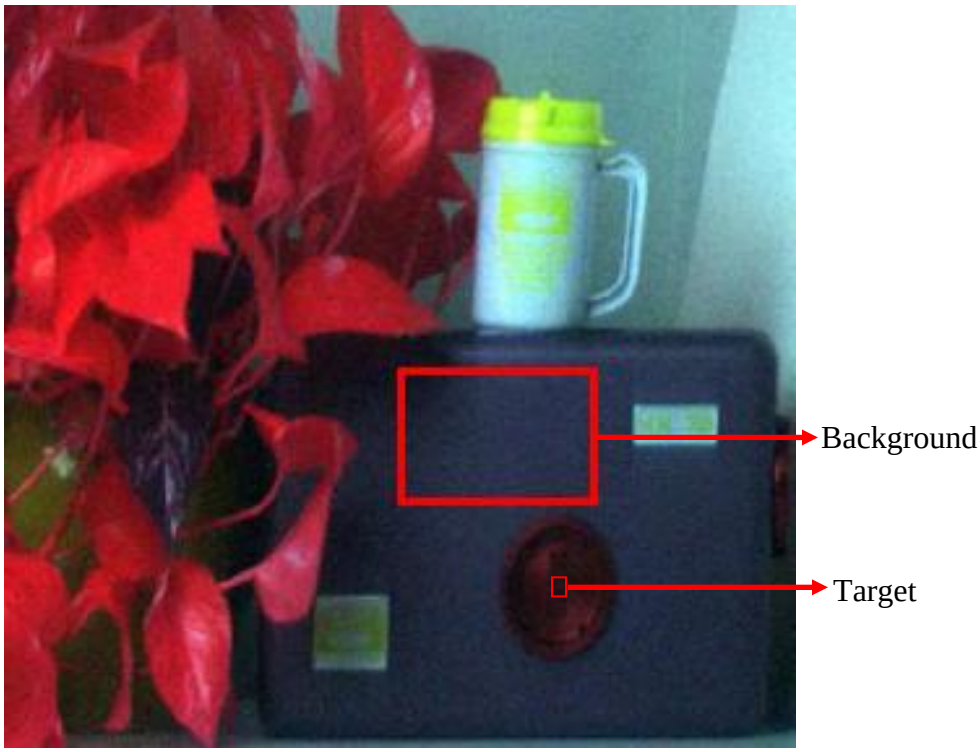

Figure 4.23 Scene extracted from Fake leaves hyperspectral image.

Several values of α was used in Equation (4.1) for mixing the spectral signal of background and the targets. The results are shown in Figure 4.24.

Image with 1 pixel
α=0.8

Image with 9 pixels
α=0.8

Image with 16 pixels
α=0.8

Level Set+ SAD

OSP

CSD

115 iterations

Target of 1 pixel, α=0.67

112 iterations

Target of 9 pixels, α=0.63

112 iterations

Target of 9 pixels, α=0.62

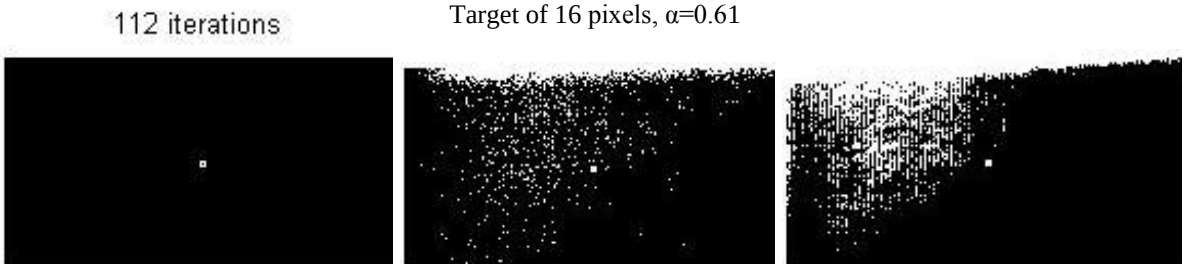

Figure 4.24 Results applying supervised level set, OSP and CSD methods.

The results obtained with level set shows that targets of 1 pixel are detected for values of α> 0.66, for targets of 9 pixels α > 0.62, whereas for targets of 16 pixels, α>0.61 to detect it. OSP and CSD detect the targets but have a high false alarm rate, detecting background pixels as targets, as well. The variation of α does not affect the results obtained with OSP and CSD.

4.3.2 Supervised target detection results for Indian pine data sets using spectral information

A second experiment is done with some regions of the Indian Pine image. This image has 16 land cover classes of which corn no-till, grass/pasture, woods, hay windrowed, corn min and soybean min-till are selected to simulate a set of images with targets constituted by 1, 9 and 16 pixels, respectively. The value of the target is determined by Equation (4.1). The regions selected are shown in Figure 4.25.

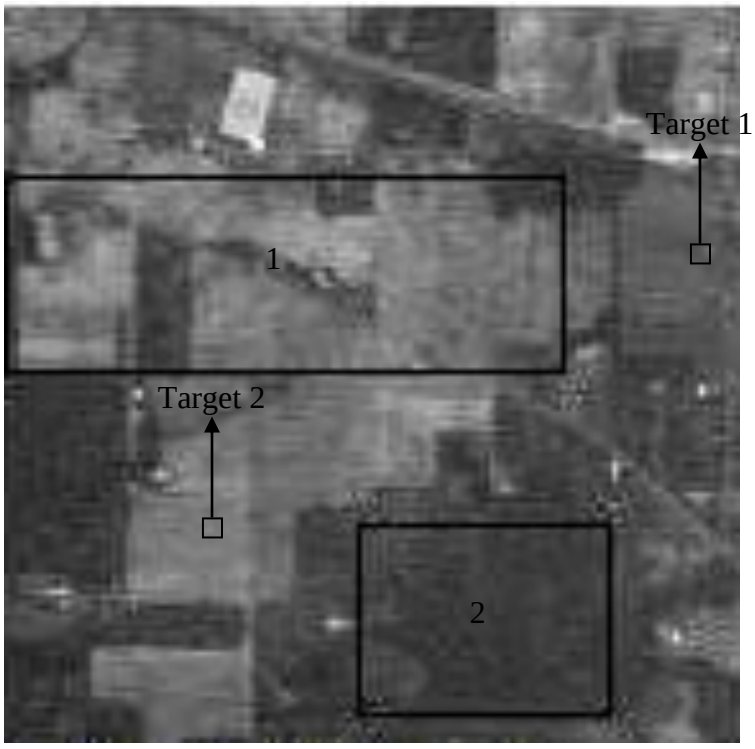

Figure 4.25 Regions selected for target detection experiments

Region 1 is constituted by Corn no-till, Soybean min-till and Grass/Trees whereas the target corresponds to a crop of Hay. Region 2 image presents a crop of Woods and has a target constituted by Soybean min-till. The results obtained with the proposed algorithm and with OSP and CSD are shown in Figure 4.26.

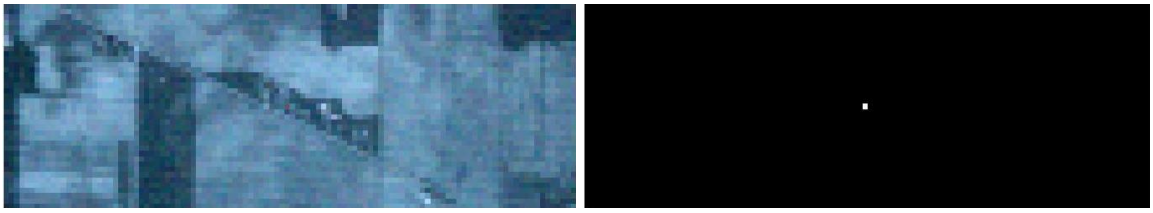

Target of 1 pixel detected by Level Set

Target detected by Level Set , α=0.7

Target detected by OSP, α=0.7 Target detected by CSD, α=0.7

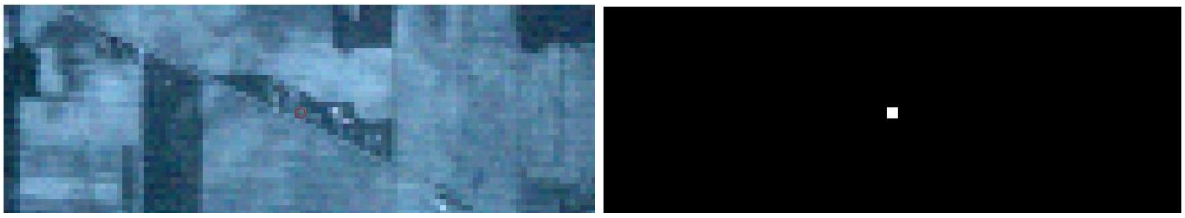

Target of 9 pixels detected by Level Set Target detected by Level Set , α=0.6

Target detected by OSP, α=0.6 Target detected by CSD, α=0.6

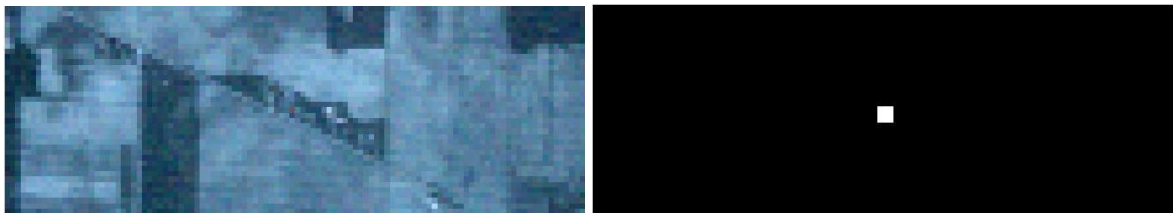

Target of 16 pixel detected by Level Set Target detected by Level Set , α=0.6

Target detected by OSP, α=0.6 Target detected by CSD, α=0.6

Figure 4.26 Results obtained with the region 1 of Indian Pine Image

Figure 4.26 shows the results of applying the techniques of level set, OSP and CSD to detect targets of 1, 9 and 16 pixels, respectively. For targets of 1 pixel, the minimum value of α (fractional mixing level) with level set method is 0.6, for targets of 9 and 16 pixels the value of α is 0.6 in both cases. Both OSP and CSD have high false detection rates. The same experiment is done for the second region; these results are shown in Figure 4.27.

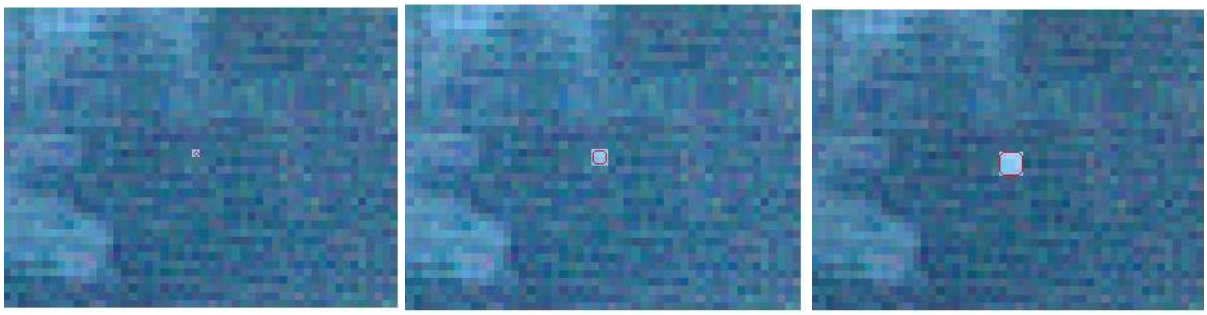

Target of 1 pixel detected by Level Set

Target of 9 pixels detected by Level Set

Target of 16 pixels detected by Level Set

Target detected by OSP, α=0.6

Target detected by OSP, α=0.5

Target detected by OSP, α=0.5

Target detected by CSD, α=0.6 | Target detected by CSD, α=0.5 | Target detected by CSD, α=0.5

Figure 4.27 Results obtained with image simulated from Indian Pine data.

Figure 4.27 shows the results for the region 2 image of Indian pine image. The minimum value for α for detecting the target of 1 pixel with the technique of level set is 0.6. For targets of 9 and 16 pixels the value is 0.5. Again both OSP and CSD methods detect many background pixels as targets. In general the results with Supervised Level Set give better results in target detection than OSP or CSD methods.

4.3.3 Supervised target detection results for HYDICE sensor data sets

Another experiment is conducted with Washington D.C. mall hyperspectral image. A water region marked with '1' (see Fig. 4.28) is selected to constitute the background of a new scene, additionally pixels of concrete, asphalt, grass and roof are used for targets in the new image.

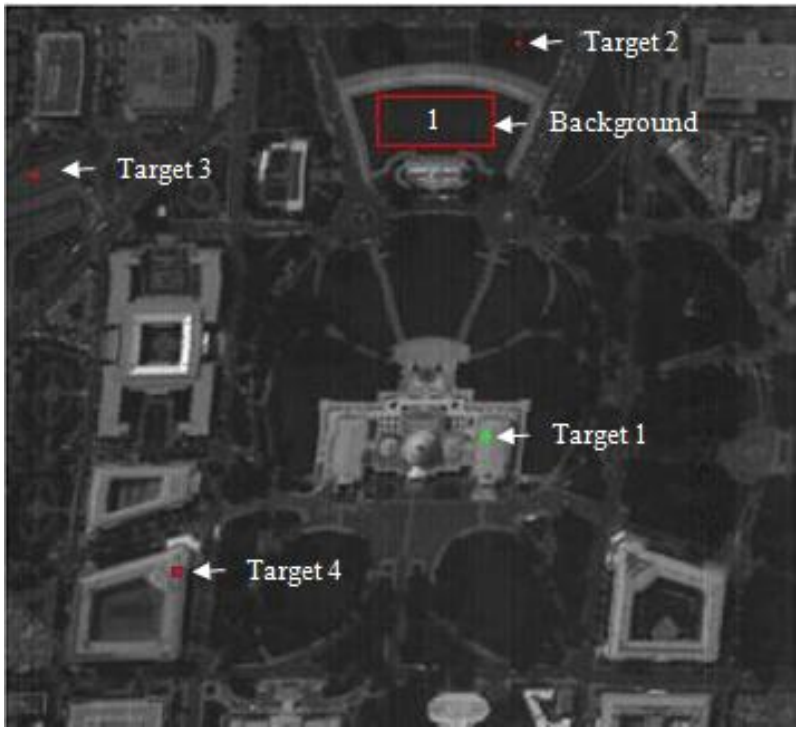

Figure 4.28 Background and targets selected from Washington D.C. Mall hyperspectral image

The proposed algorithm is tested with concrete targets of 1,9,16 pixels, Grass Targets of 1 pixel, Roof targets of 9 pixels and Asphalt targets of 16 pixels. The results of the detection are shown in Figure 4.29.

Target detected by Level Set , α=0.6

Target detected by Level Set , α=0.6

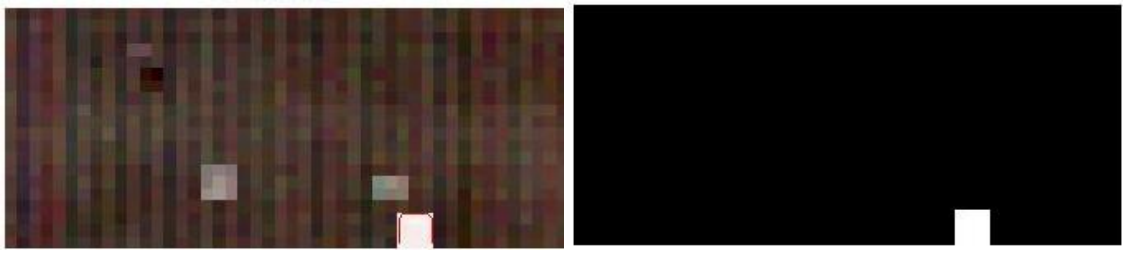

Target detected by Level Set , α=0.5

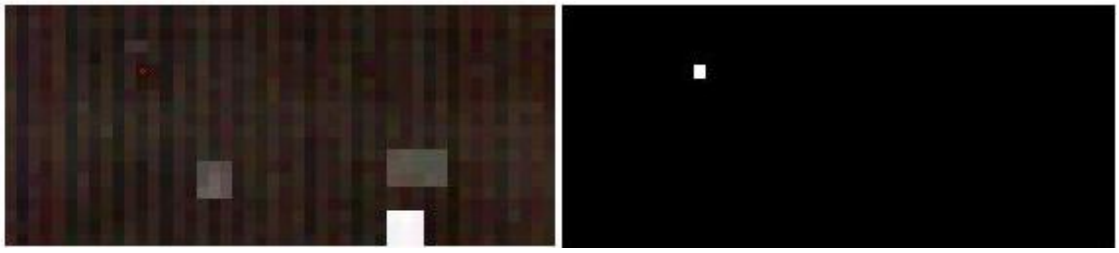

Target detected by Level Set , α=0.4

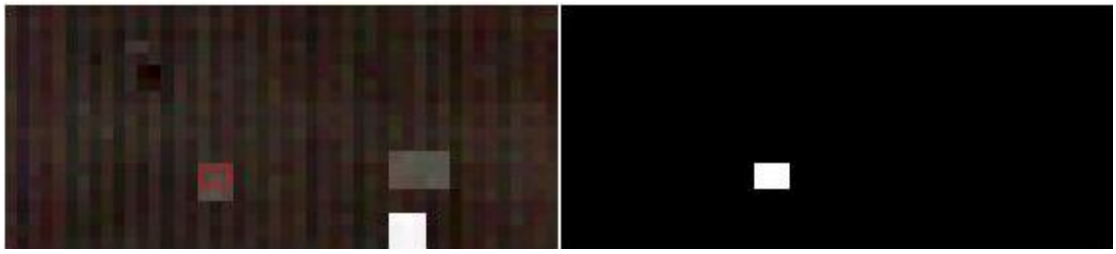

Target detected by Level Set , α=0.6

Target detected by Level Set , α=0.6

Target detected by Level Set , α=0.7

Figure 4.29 Results obtained with image simulated from Washington data.

The minimum value of α (Fractional Mixing Level) for detecting concrete targets of 16 pixels using level sets is 0.4, whereas for targets of 1 and 9 pixels the value of α is 0.6 in both cases. For grass targets the minimum value of α is 0.4, whereas for roof and asphalt targets the value of α is 0.6. The results show that the algorithm is capable of detecting different types and sizes of targets in a scene.

A subset of the HYDICE Forest image was used for testing the proposed algorithm, the new image has 249 lines, 128 samples and 120 bands were used after bad bands were removed. In addition there are ten panel classes that have close spectral signatures and are difficult to discriminate.

The HYDICE Forest image in Fig. 4.30 shows the precise locations of pure panel pixels (pink centers); a subset image that was selected from the original image for testing is shown.

Figure 4.30 Image extracted from HYDICE Forest image

For testing 7 distinct types of targets: green fabric-untagged over asphalt, dark olive parature, Green tenting fabric, Woodland cotton/nylon fabric, woodland poncho, green cotton fabric and khaki/tan fabric were included. The results are shown in Figure 4.31.

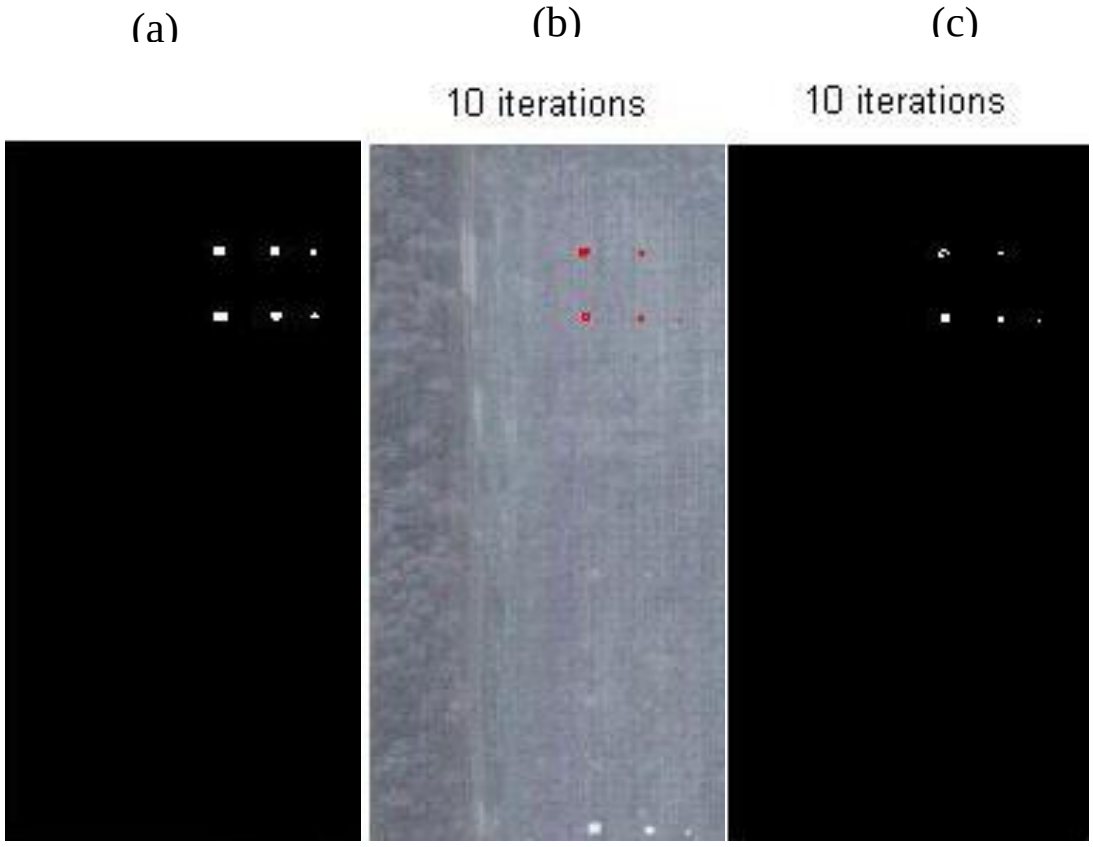

Targets of Green fabric-untagged over asphalt.

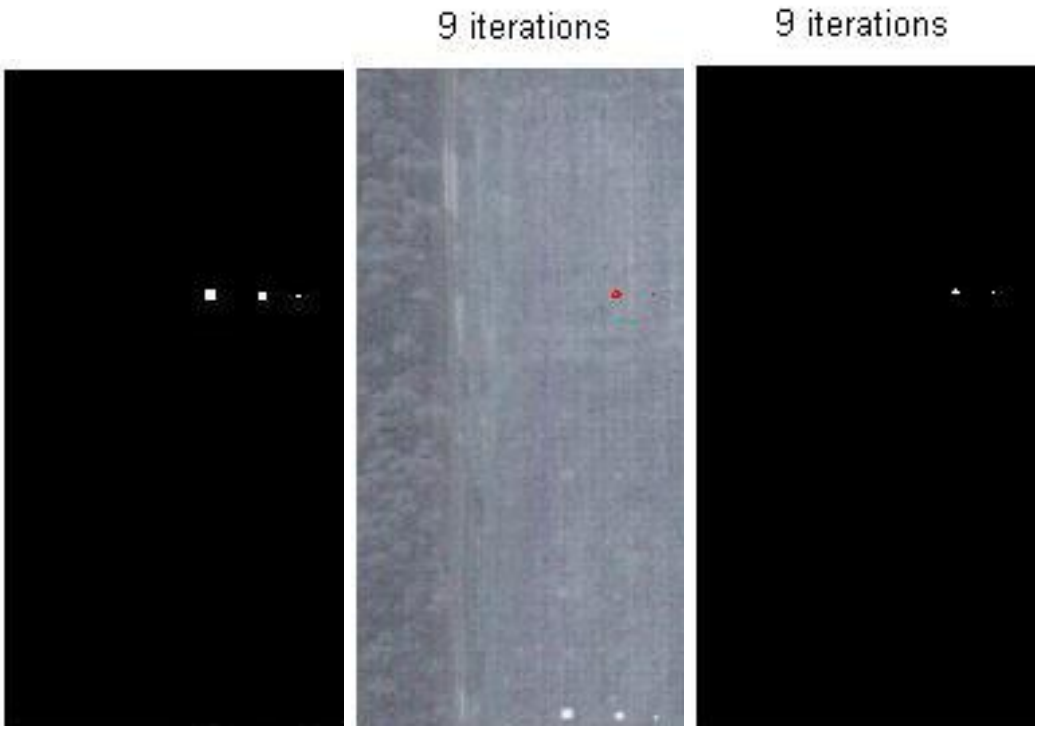

Targets of dark olive parachute.

Green tenting fabric

Woodland cotton/nylon fabric

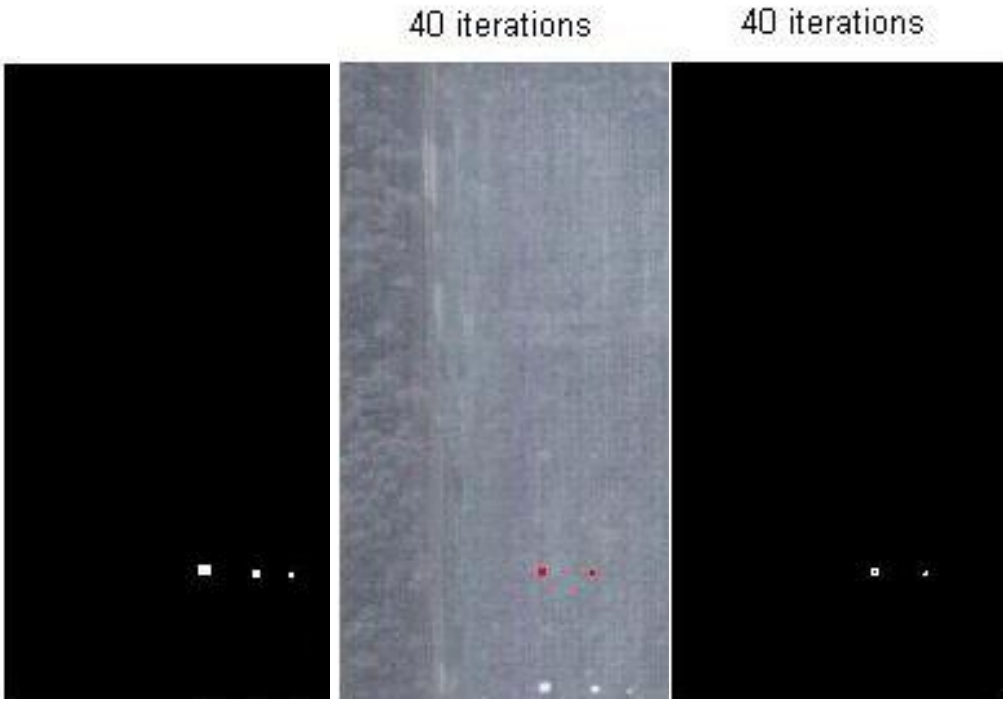

Woodland poncho target

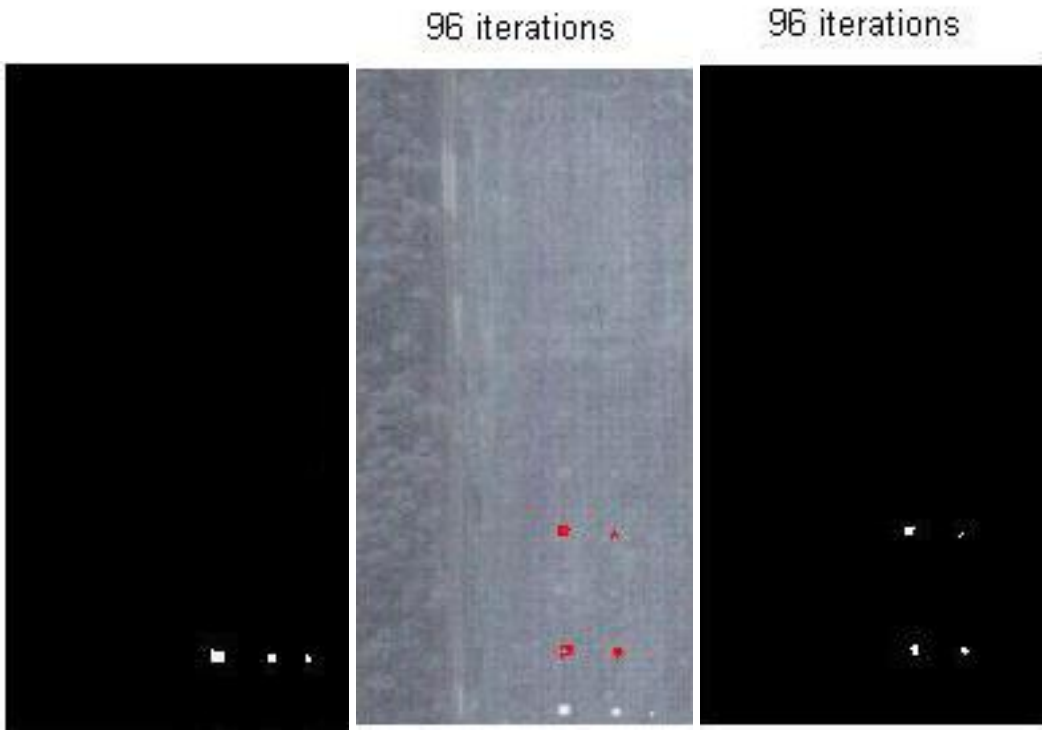

Targets of green cotton fabric.

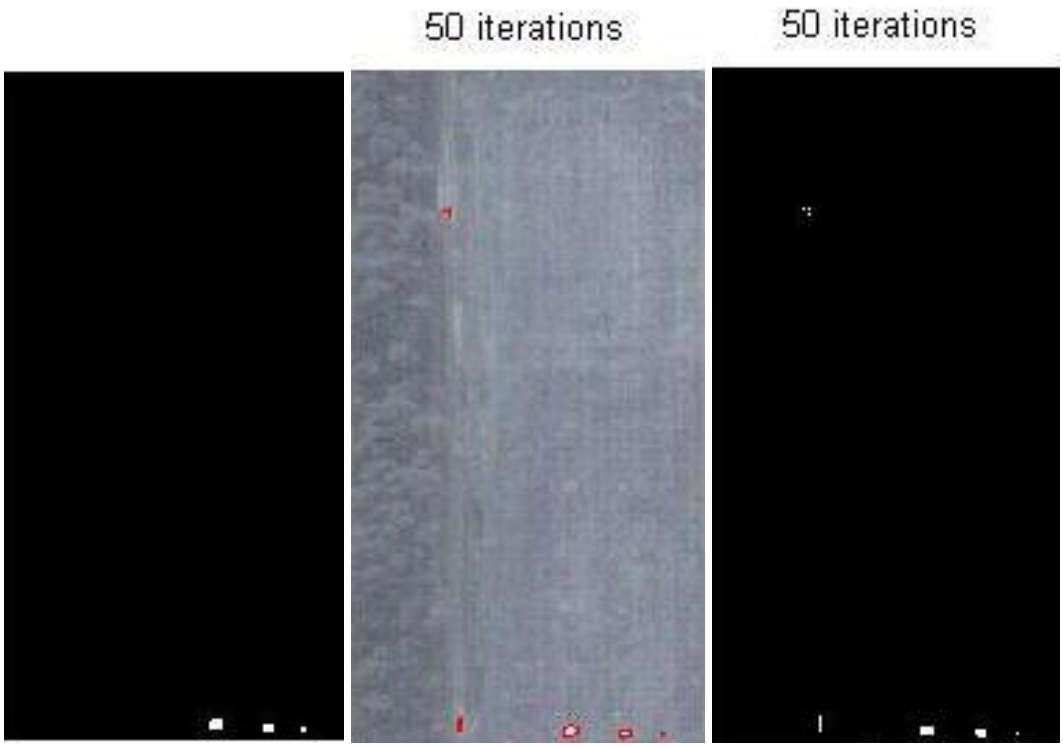

Targets of khaki/tan fabric.

Figure 4.31 Target detection results for HYDICE image. ; (a) Ground truth, (b) Targets encircled by Level Set, (c) Targets extracted.

The experiments were carried out on a PC DELL INSPIRON 640m with 2GB of RAM, processor Intel Centrino Duo of 2GHz. The time of convergence, number of iterations, targets recovered and the number of false positive got by the proposed algorithm are shown in Table 3.

Table 4.3 Quantitative Target detection results for HYDICE image. (1) green fabric-untagged over asphalt, (2) dark olive parature, (3) Green tenting fabric, (4) Woodland cotton/nylon fabric, (5) woodland poncho, (6) green cotton fabric, (7) khaki/tan fabric.

Target	Time of convergence (*seconds*)	Iterations	Targets Available	Targets Recovered	False Positive
1	47.74	10	6	5	0
2	47.12	9	3	2	0
3	60.91	16	3	2	0
4	47.46	10	3	3	0
5	109.04	40	3	2	0
6	196.21	96	3	2	2
7	134.72	50	3	3	3

The proposed algorithm could recover an 85.71% of targets of 16 pixels, 100% of targets of 9 pixels, and a 57.14% of targets of 1 pixel. In addition 100% of different types of targets were recovered successfully, on the another hand for 5 of the 7 types of targets the algorithm got zero false positive, for detecting woodland targets the algorithm recovered erroneously 2 objects, and for detecting the green tenting fabric 3 false positives was obtained.

In the same way three scenes were selected from the HYDICE desert image for testing the proposed algorithm, the first image has 291 lines, 171 samples and 210 bands; it is constituted by 4 targets placed in a road. The second scene has a size of 287x181 pixels and 210 bands and it is constituted by an array of 27 targets that corresponds to panels of distinct classes and sizes, they are organized in three columns of nine targets, additionally the targets in the same row were made from the same material. The last scene consists of 6 targets aligned vertically; the image has a size of 310x186 pixels and 210 bands. The three images generated from HYDICE desert image are shown in the following Figure.

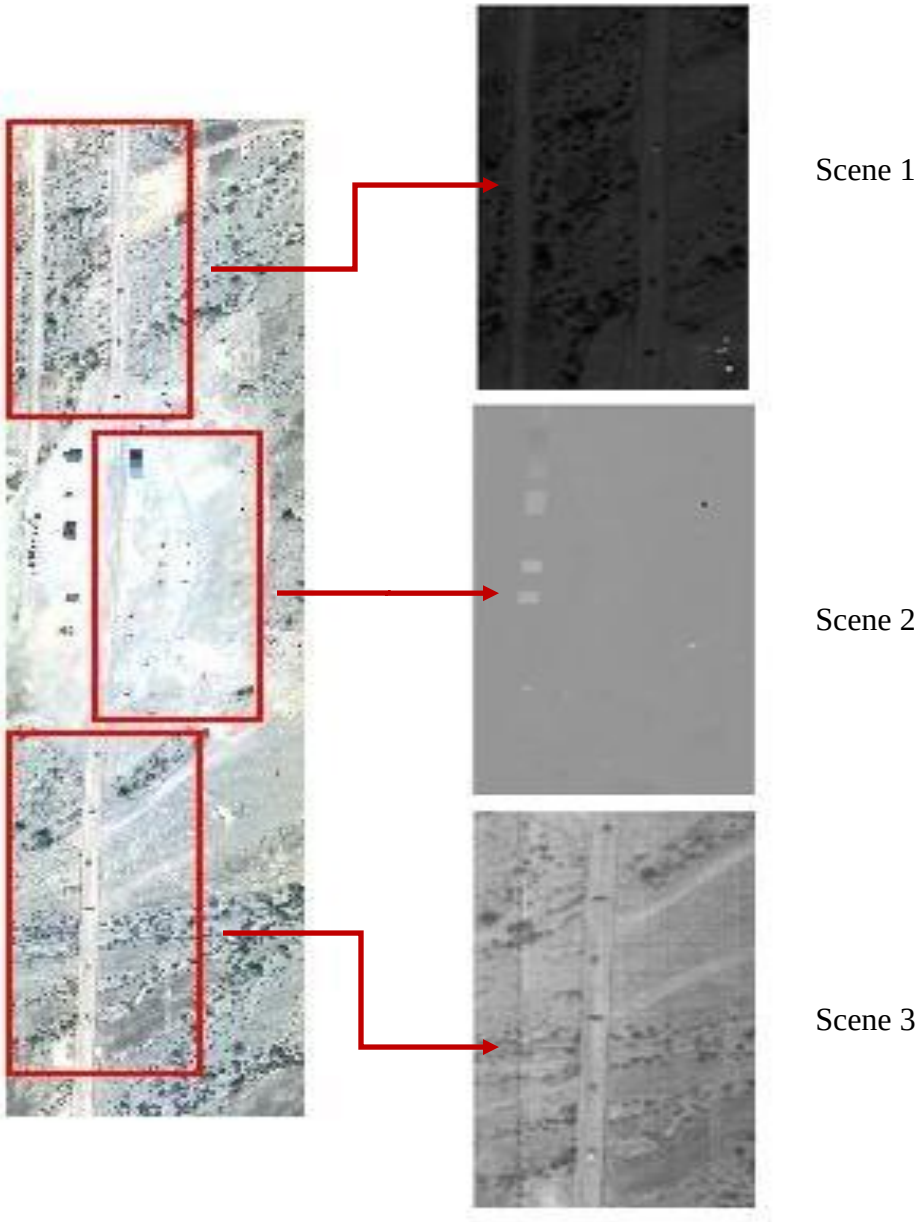

Figure 4.32 Images extracted from HYDICE Desert

The results obtained in the first scene are shown in the following figure.

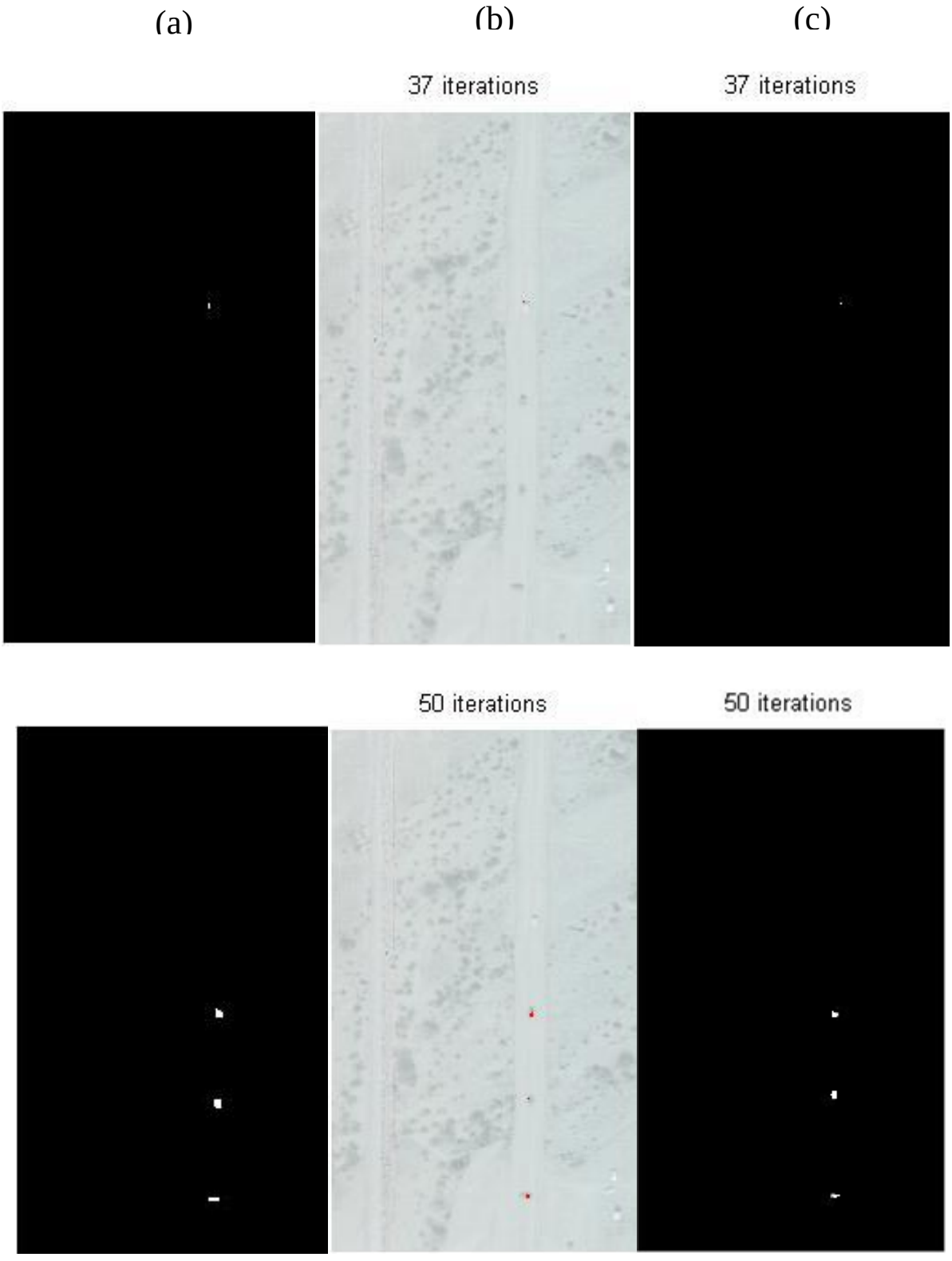

Figure 4.33 Results for first scene of HYDICE Desert image. ; (a) Ground truth, (b) Targets encircled by Level Set, (c) Targets extracted.

The results obtained with the second scene are shown in the following image.

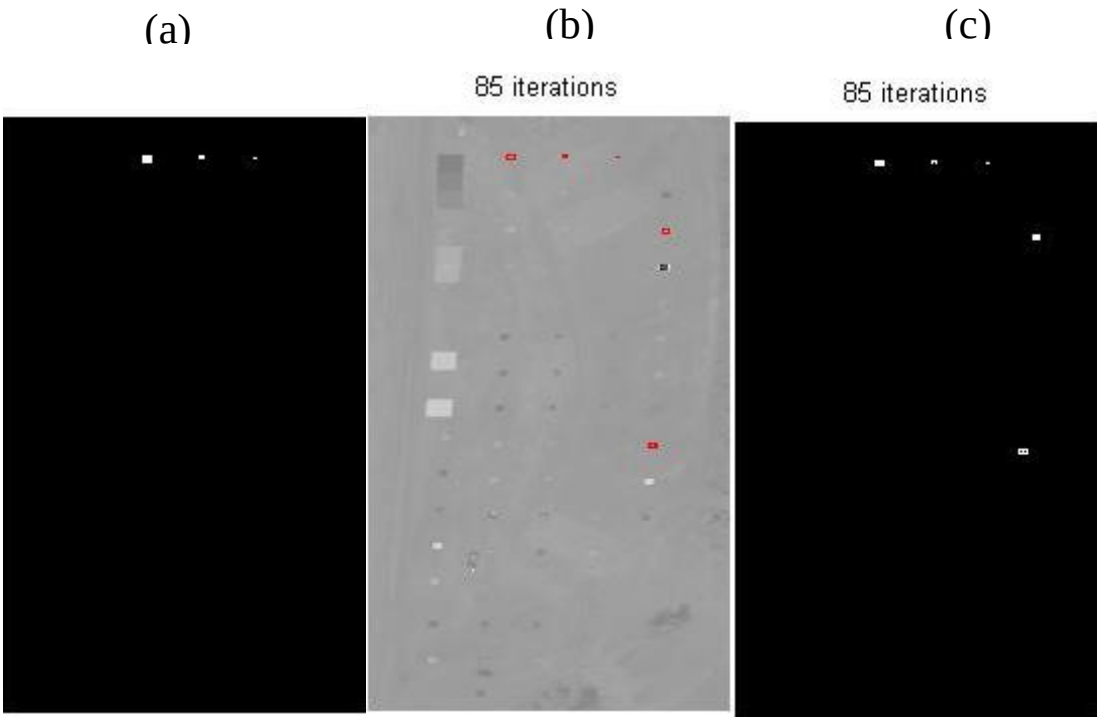

Targets of unpainted wood.

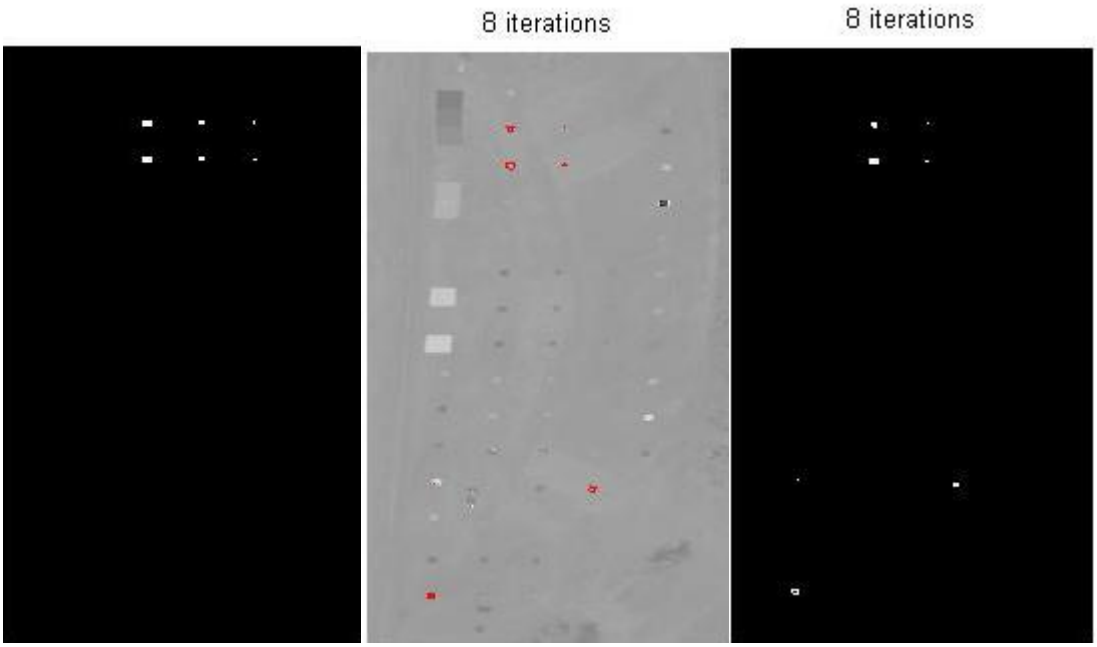

Targets of heavily and lightly painted tan wood.

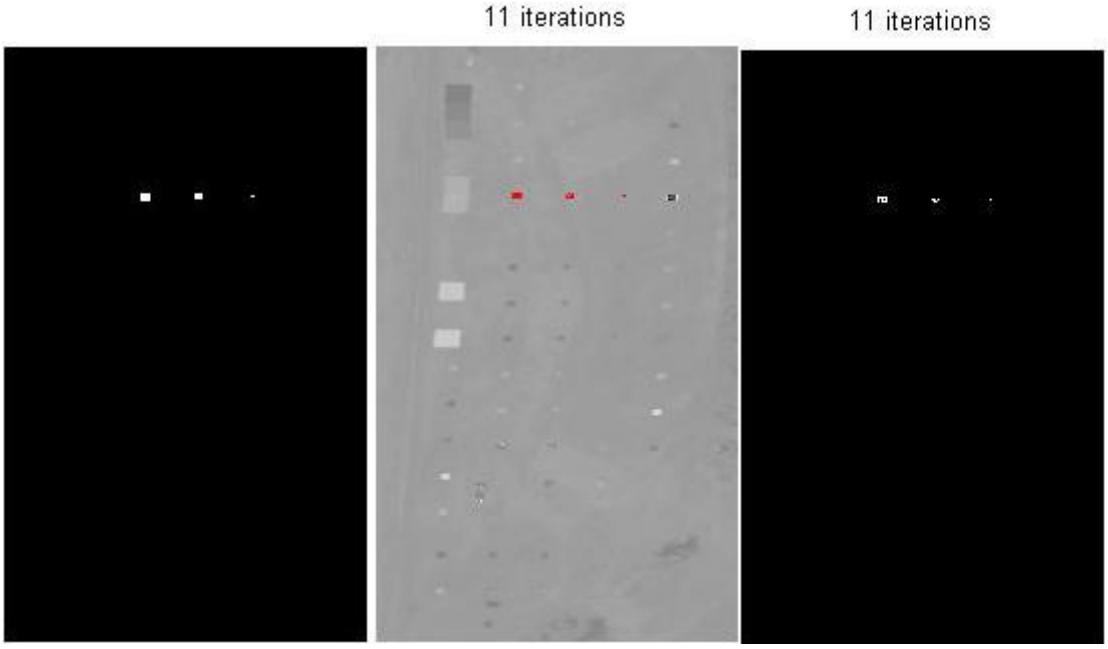

Targets of nylon/cotton light-weight desert BDU

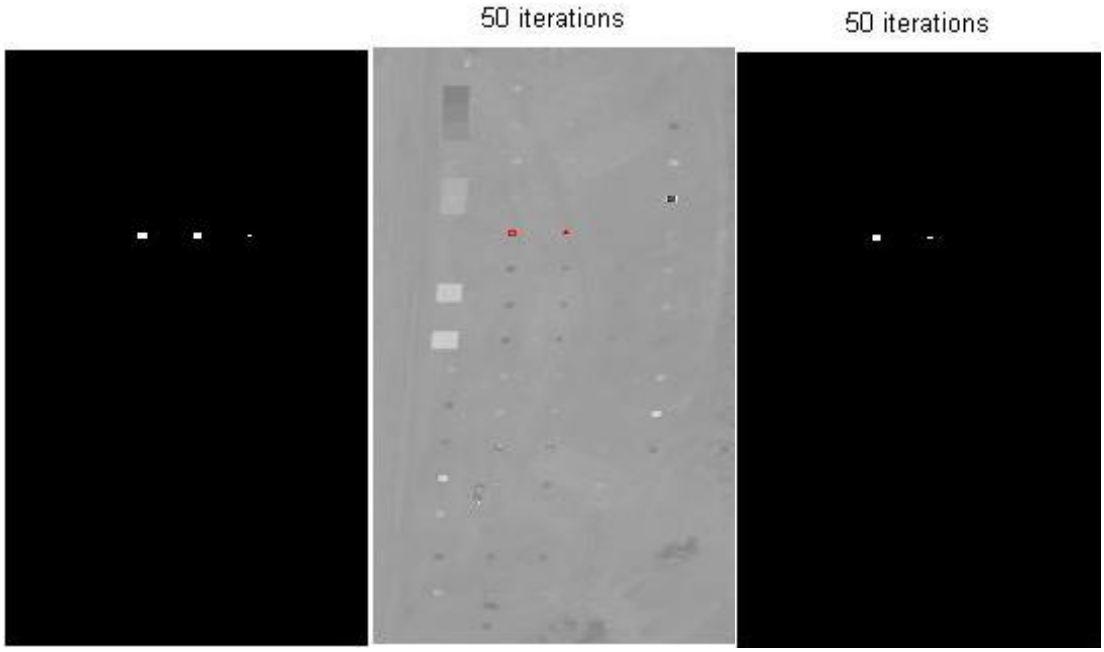

Targets of cotton, desert BDU

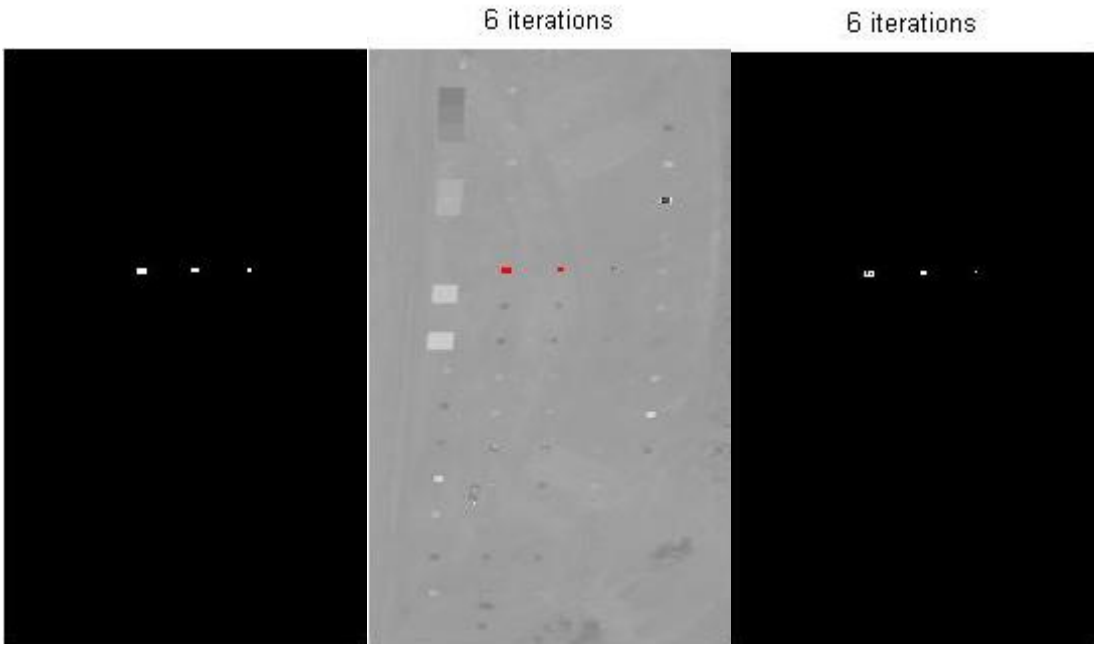

Targets of Cotton, green oxford

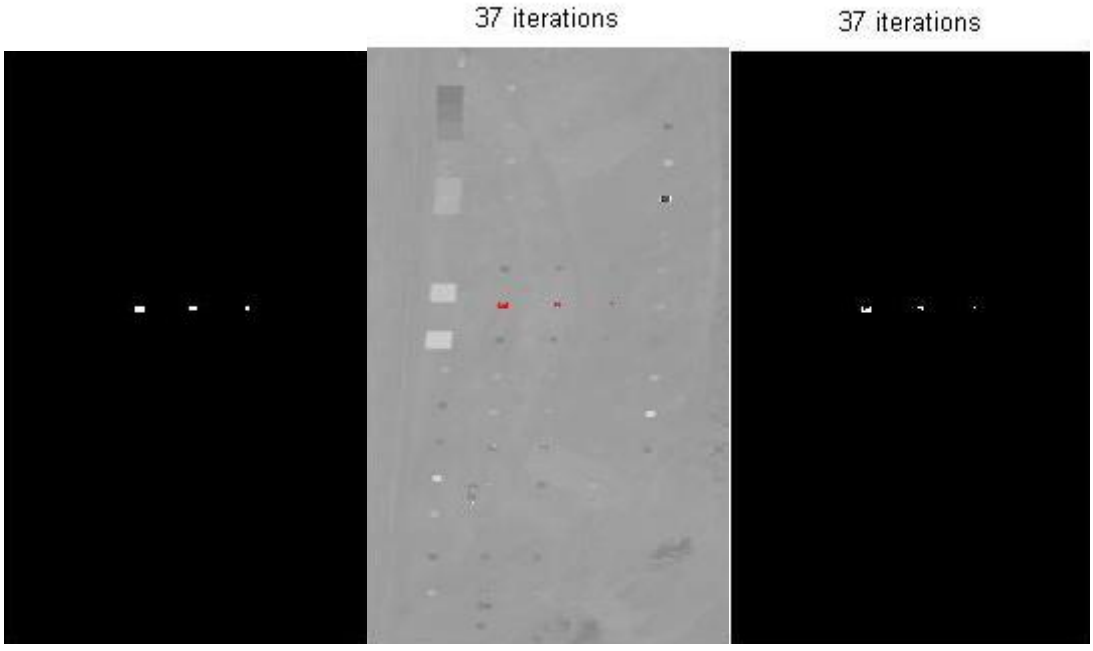

Targets of nylon, woodland camo poncho

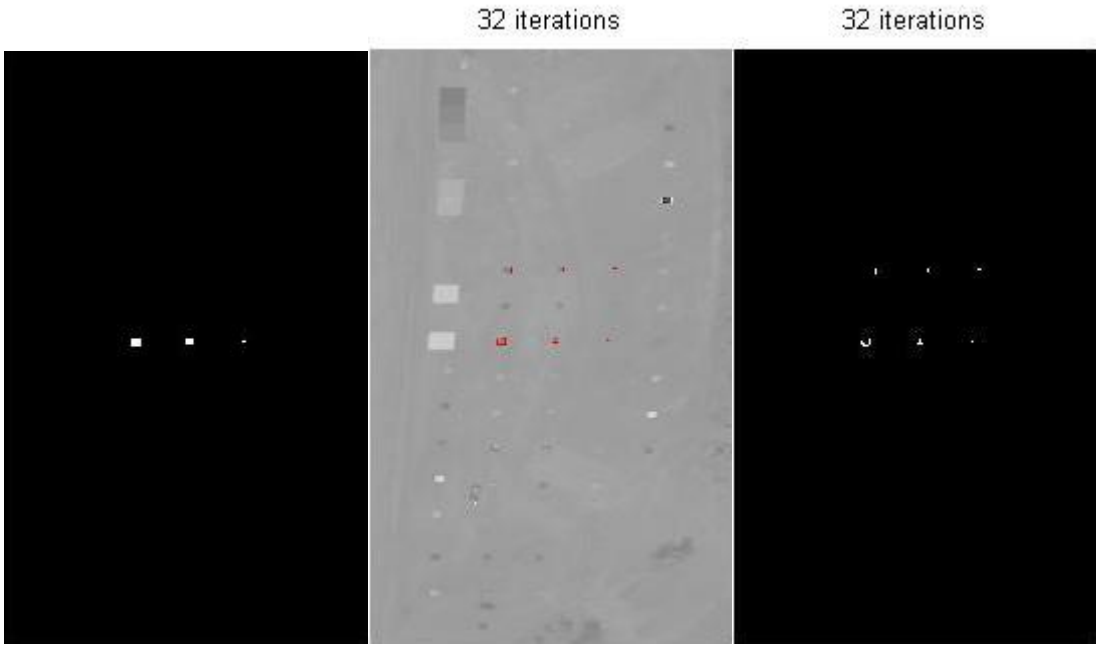

Targets of cotton/nylon woodland BDU

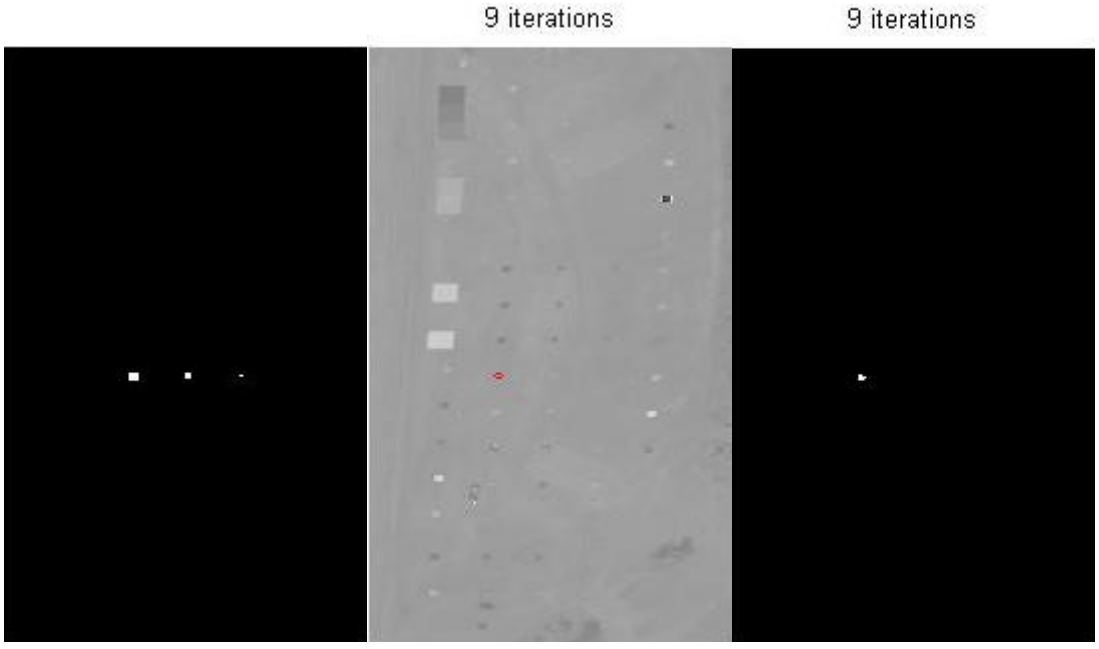

Targets of tan painted plywood with taggant

Figure 4.34 Results for second scene of HYDICE Desert image. ; (a) Ground truth, (b) Targets encircled by Level Set, (c) Targets extracted.

The results obtained with the last scene extracted from HYDICE desert image is shown in the following Figure.

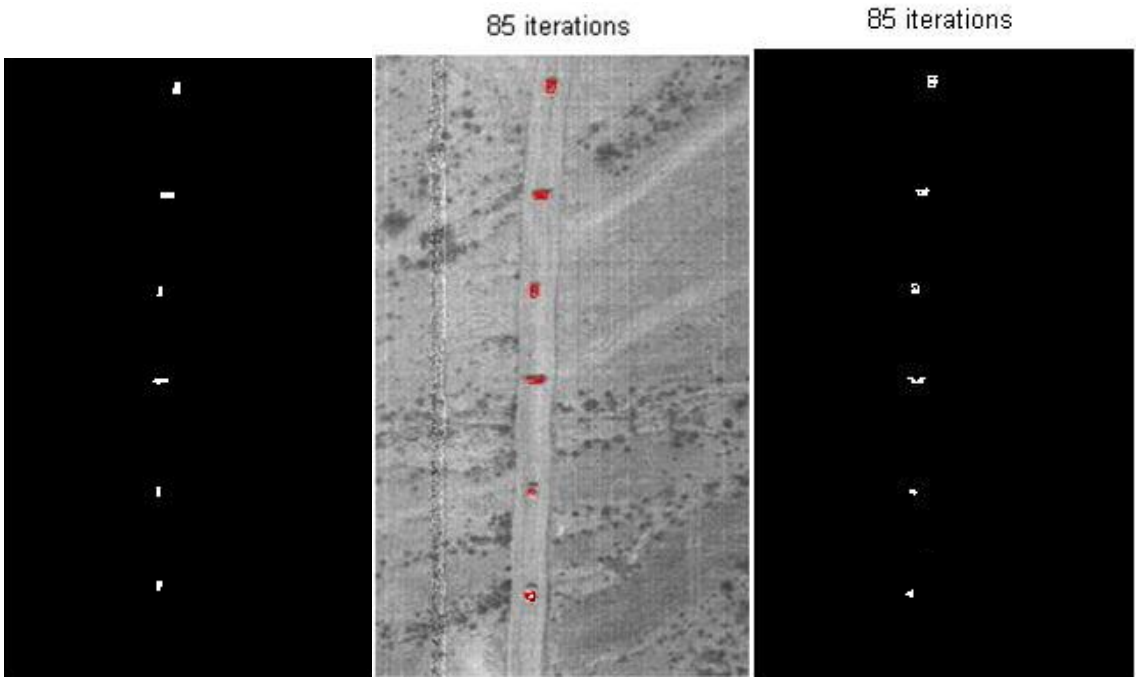

Figure 4.35 Results for scene three of HYDICE desert image; (a) Ground truth, (b) Targets encircled by Level Set, (c) Targets extracted.

The results obtained for the first scene show that 100% of different types of targets were recovered successfully, additionally 91.3% of the pixels that belong to the targets were classified properly and 100% of the pixels of the background were identified as background. For the second scene, 81% of different types of targets were extracted successfully, whereas 76.5% of pixels that belong to the targets were recognized as targets, and a 0.16% of pixels that belong to the background were recovered erroneously as targets. The results for the last

scene show that all targets were recovered successfully; moreover 94.2% of the pixels that belong to the targets were recovered properly and only a 0.09% of pixels that belong to the background were assigned as targets.

The performance of the proposed algorithm for supervised target detection, OSP and CSD were compared over the set of images available, as result show in the ROC diagram that plots the probability of target detection versus probability of false alarm for the three methods used.

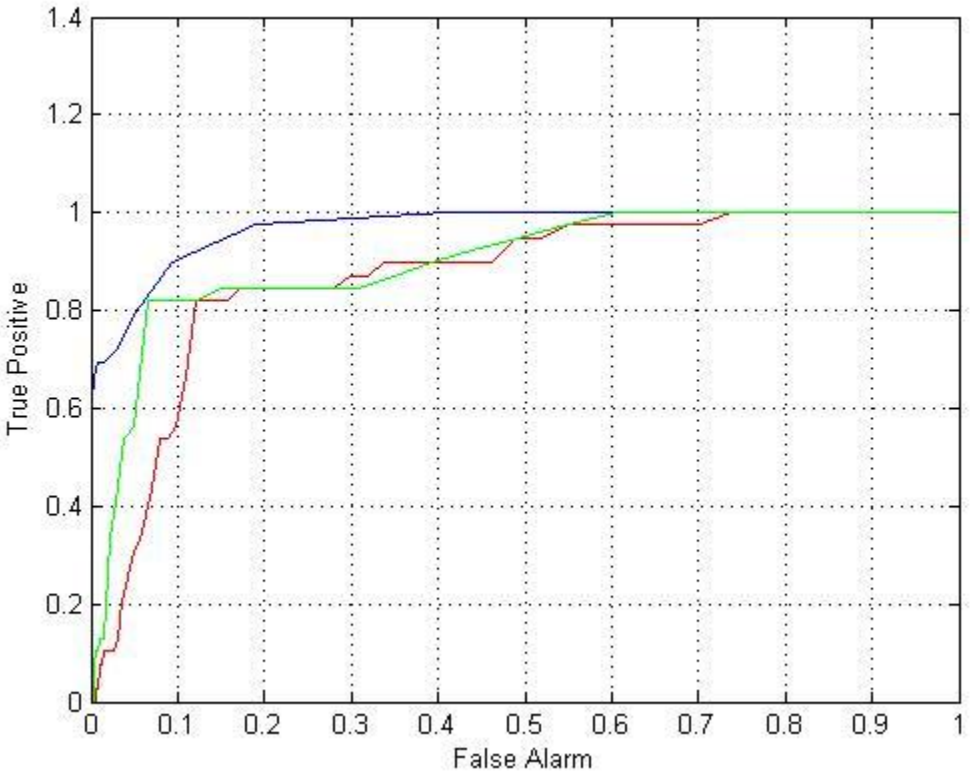

Figure 4.36 ROC Diagram, (blue) proposed algorithm, (green) CSD, (red) OSP.

The ROC diagram shows that the probability of target detection for the proposed algorithm is much higher than that obtained for OSP and CSD for a specific false alarm rate, in the same

way the results obtained with CSD were better than the ones for OSP. For a false alarm rate of 0.1, the proposed algorithm obtained a target detection rate of 0.902 whereas OSP and CSD obtained only 0.572 and 0.820 respectively.

5 CONCLUSIONS AND FUTURE WORK

The conclusions obtained from experimental results are presented in this chapter, additionally some recommendations for future work are mentioned.

5.1 Conclusions

In this work we developed a new methodology for unsupervised and supervised target detection using level set. The new methodology can be applied to hyperspectral image by incorporating spectral angle distance into the partial differential equation that determines the evolution of the level set function. The proposed algorithm for unsupervised target detection was used in the detection of large and small targets, in the first case spectral and texture information was used, and for small targets only spectral information was used. On another hand the supervised target detection algorithm were implemented for detecting target of small size (a few pixels) in hyperspectral images by incorporating the spectral signature of the target into the partial differential equation of level set.

The unsupervised target detection algorithm that only uses spectral information in level set technique obtained good results in images where the targets and background have a uniform texture. The incorporation of PCA as a technique for decorrelating and reducing the data

dimensionality were included in a pre-processing step, it allows to reduce the time of execution of the algorithm, in the same way morphological operations like dilation and erosion were used in a post-processing step and it helped considerably to eliminate objects erroneously extracted by the algorithm. These results were compared with the ones obtained with another level set technique developed by Chan [11], and they showed that the performance of the proposed algorithm recovered the targets faster.

The unsupervised target detection algorithm that incorporates texture information in the level set function obtained better result in tasks of extracting objects of images where the background was not uniform, different size of windows were used for calculating texture information (3x3, 5x5, 7x7, 9x9, 12x12), however the results obtained with different size of windows were similar with exception that the time of convergence increased with the raising of the size of window. The unsupervised target detection algorithm that uses only spectral information, the algorithm developed by Chan and the proposed algorithm that uses texture information were compared, the results shows that only the algorithm that take into account texture information could recover all the targets placed in four synthetic images.

Incorporation of texture information for detecting targets of size less than the mask size used for extracting texture features is not recommended due to the fact that the mixing between target and background is more predominant.

The results for supervised target detection were much better than the ones obtained with techniques widely used for target detection as OSP and CSD. The ROC diagram shows that the proposed algorithm obtained higher targets detection probabilities with smaller false alarm probabilities than OSP and CSD. In addition the algorithm was tested with distinct scenarios that prove its functionality.

PCA was applied as a preprocessing step to reduce the number of bands for detection of large targets. It was not applied for detection of target less than a pixel in size or when the pixel is a mixing between the spectral signature of the target and background because it tends to eliminate the information of target.

5.2 Future Work

- Shape information have been incorporated lately in level set for recovery objects with an specific geometric shape, as a future work this information can be incorporated to help the algorithm to extract targets with a specific shape.
- Implementing the proposed algorithms in C++ for easing the portability of code to others platform like linux, UNIX and macintosh. That would allow integration of the proposed algorithm with others existing packages developed for target detection and hyperspectral image processing.
- Implementation in GPU architectures using jackets and other software available to port codes from Matlab environment to parallel and distributed systems.

References List

[1] Ball John E., Mann Bruce Lori, “Level Set Hyperspectral Image classification Using Best Band Analysis”, IEEE TRANSACTIONS ON GEOSCIENCE AND REMOTE SENSING, VOL. 45, NO. 10, OCTOBER 2007.

[2] J. E. Ball and L. M. Bruce, “Level set hyperspectral segmentation: Nearoptimal speed functions using band selection and scaled spectral angle mapper,” in *Proc. IEEE Int. Geosci. Remote Sens. Symp.*, Jul. 2006, pp. 2596–2600.

[3] Shao-Shan Chiang, Chein-I Chang, Irving W. Ginsberg, “Unsupervised Target Detection in Hyperspectral Images Using Projection Pursuit”, *IEEE* Transactions on Geoscience and Remote Sensing, Vol. 39, NO. 7, JULY 2001.

[4] Robila, Stefan A.; Varshney, Pramod K, “Target detection in hyperspectral images based on independent component analysis”, Proc. SPIE Vol. 4726, p. 173-182, Automatic Target Recognition XII, Firooz A. Sadjadi; Ed., July 2002.

[5] S. Johnson, “The relationship between the matched filter operator and the target signature space orthogonal projection classifier,” *IEEE Trans. Geosci. Remote Sens.*, vol. 38, no. 1, pp. 283–286, Jan. 2000.

[6] C.-I Chang, “Orthogonal subspace projection (OSP) revisited: A comprehensive study and analysis,” *IEEE Trans. Geosci. Remote Sens.*, vol. 43, no. 3, pp. 502–518, Mar. 2005.

[7] R. Malladi and J. A. Sethian, “A unified approach for shape segmentation, representation, and recognition,” Report LBL -36069, Lawrence Berkeley Laboratory, university of California, Berkely, August 1994.

[8] Hongchuan Yu, chin-seng chua ,“Image Enhancement and Denoising under max/min flow framework,” 2002.

[9] S. Osher, J. A. Sethian, “Fronts propagating with curvaturedependent speed: algorithms based on Hamilton-Jacobi formulations”, *J. Comp. Phys.*, vol. 79, pp. 12-49, 1988.

[10] R. Malladi, J. Sethian, and C. Vemuri, “Shape modeling with front propagation: a level set approach,” IEEE Transactions on Pattern Analysis and Machine Intelligence, no. 2, pp. 158–175, 1995.

[11] V. Caselles, F. Catte, T. Coll, and F. Dibos, “A geometric model for active contours,” Numerische Mathematik, p. 19, 1993.

[12] Chunming Li, Chenyang Xu, Changfeng Gui, “Level Set Evolution Without Re-initialization: A New Variational Formulation”, IEEE Computer Society Conference on Computer Vision and Pattern Recognition, 2005.

[13] Kwon Heesung, Nasrabadi Nasser M. , “Hyperspectral Target Detection Using Kernel Spectral Matched Filter”, IEEE Computer Society Conference on Computer Vision and Pattern Recognition Workshops, 2004.

[14] T. Chan and L. Vese, “Active contours without edges,” IEEE Transactions on Image Processing, no. 2, pp. 266–277, 2001.

[15] S. Jehan-Besson, M. Barlaud, and G. Aubert, “Shape gradients for histogram segmentation using active contours,” in Proc. of IEEE International Conference on Computer Vision, 2003.

[16] M. Rousson and R. Deriche, Geometric Level Set Methods in Imaging, Vision, and Graphics, ch. Adaptive Segmentation of Vector Valued Images, pp. 195–206. New York: Springer-Verlog, 2003.

[17] M. Rousson and R. Deriche, “A variational framework for active and adaptive segmentation of vector valued images,” Tech. Rep. 4515, INRIA, 2002.

[18] Ayanna Howard, Curtis Padgett, Kenneth Brown, “Intelligent Target Detection in Hyperspectral Imagery”, Jet Propulsion Laboratory, California Institute of Technology.

[19] Jorgen Karlholm, Ingmar Renhorn “Wavelength band selection method for multispectral target detection” Optical Society of America, Vol. 41, No. 32, 10 November 2002.

[20] Dimitris Manolakis, David Marden, and Gary A. Shaw, “Hyperspectral Image Processing for Automatic Target Detection Applications”, Lincoln Laboratory Journal, Volume 14, Number 1, 2003

[21] John Kerekes, “Receiver Operating Characteristic Curve Confidence Intervals and Regions, IEEE Geoscience and Remote Sensing Letters”, volume. 5, no. 2, april 2008.

[22] Strickland Robin N., Peters Richard Alan, “Image Complexity Metrics for Automatic Target Recognizers”, Automatic Target Recognizer System and Technology Conference, Naval Surface Warfare Center, Silver Spring, MD, 30-31 October 1990.

[23] chen sagiv, nir a. sochen, and yehoshua y. zeevi, “Integrated active contours for texture segmentation”, ieee transactions on image processing, vol. 15, no. 6, june 2006

[24] Karoui, I.; Fablet, R.; Boucher, J.M.; Augustin, J.M.,”Unsupervised region-based image segmentation using texture statistics and level-set methods”; Intelligent Signal Processing, 2007. WISP 2007. IEEE International Symposium, Oct. 2007.

[25] Qian Du, Ivica Kopriva,”Automated Target Detection and Discrimination Using Constrained Kurtosis Maximization”, ieee geoscience and remote sensing letters, vol. 5, no. 1, january 2008

[26] N. M. Nasrabadi, “Regularized Spectral Matched Filter for Target Recognition in Hyperspectral Imagery”, ieee signal processing letters, vol. 15, 2008

[27] P. Tichavský, Z. Koldovský, and E. Oja, “Performance analysis of the FastICA algorithm and Cramér–Rao bounds for linear independent component analysis,” *IEEE Trans. Signal Process.*, vol. 54, no. 4, pp. 1189–1203, Apr. 2006.

[28] Joshua Broadwater, Rama Chellappa, “Hybrid Detectors for Subpixel Targets”, IEEE transactions on pattern analysis and machine intelligence, vol. 29, no. 11, november 2007.

[29] N. M. Nasrabadi, “Regularized Spectral Matched Filter for Target Recognition in Hyperspectral Imagery” , IEEE signal processing letters, vol. 15, 2008

[30] Heesung Kwon, Nasser M. Nasrabadi, ,”Kernel Matched Subspace Detectors for Hyperspectral Target Detection”, IEEE transactions on pattern analysis and machine intelligence, vol. 28, no. 2, february 2006.

[31] C.-I. Chang, H. Ren, and S.-S. Chiang, “Real-Time Processing Algorithms for Target Detection and Classification in Hyperspectral Imagery,” *IEEE Trans. Geosci. Remote Sensing, vol. 39, pp. 760–768,* Apr. 2001.

[32] Jean-Francois Aujol, Gilles Aubert, and Laure Blanc-Féraud, “Wavelet-Based Level Set Evolution for Classification of Textured Images”, IEEE transactions on image processing, vol. 12, no. 12, december 2003.

[33] John E. Ball,Lori Mann Bruce,“Level Set Hyperspectral Image Classification Using Best Band Analysis”, IEEE transactions on geoscience and remote sensing, vol. 45, no. 10, October 2007.

[34] M. Hanmandlu, V.K. Madasu and S. Vasikalra, “A Fuzzy Approach to Texture Segmentation”, Proc. International Conference on Information Technology: Coding and Computing, 2004.

[35] Y. Deng, and B.S. Manjunath, “Unsupervised segmentation of color–texture regions in images and video”, IEEE Trans. Pattern Anal. Mach. Intell. 238, pp. 800–810, 2001.

[36] http://www.surfaceoptics.com/Products/Hyperspectral/HyperspectralData.htm

[37] Alarcon Andres, Manian Vidya, “A variational level-set method for automatic target detection in hyperspectral images", SPIE conference: Automatic Target Recognition XVIII, Vol. 6967,March 19-20, 2008.

[38] Selim Aksoy, Gokhan Akcay, “Multi-resolution Segmentation and Shape Analysis for Remote Sensing Image Classification”, 2nd International Conference on Recent Advances in Space Technologies, June 2005.

[39] Chen-I Chang, Weiming Liu, Chein-Chi Chang “Discrimination and Identification for Subpixels Targets in Hyperspectral Images”, IEEE international conference for image processing, 2004.